MIT
International Center for
Air Transportation

MODELING THE EFFECTS OF AIRCRAFT FLIGHT TRACK VARIABILITY ON COMMUNITY NOISE EXPOSURE

Callen T. Brooks and R. John Hansman

This report is based on the Master's Thesis submitted to the Department of Aeronautics and Astronautics in partial fulfillment of the requirements for the degree of Master of Science at the Massachusetts Institute of Technology.

Report No. ICAT-2017-06
September 2017

MIT International Center for Air Transportation (ICAT)
Department of Aeronautics & Astronautics
Massachusetts Institute of Technology
Cambridge, MA 02139 USA

Technical Report Documentation Page

1. Report No.	2. Government Accession No.	3. Recipient's Catalog No.
23-ICAT-2017-06		

4. Title and Subtitle	5. Report Date
Modeling the Effects of Aircraft Flight Track Variability on Community Noise Exposure	July 2017
	6. Performing Organization Code

7. Author(s)	8. Performing Organization Report No.
Callen T. Brooks and R. John Hansman	

9. Performing Organization Name and Address	10. Work Unit No. (TRAIS)
Center of Excellence for: Alternative Jet Fuels and Environment Massachusetts Institute of Technology Department of Aeronautics & Astronautics Cambridge, MA 02139	11. Contract or Grant No. 13-C-AJFE-MIT-008

12. Sponsoring Agency Name and Address	13. Type of Report and Period Covered
Federal Aviation Administration Office of Environment and Energy	Technical Report
	14. Sponsoring Agency Code

15. Supplementary Notes

http://hdl.handle.net/1721.1/110790

16. Abstract

The implementation of Performance Based Navigation (PBN) routes across the National Airspace System (NAS) has caused a significant concentration of flight tracks. This flight track concentration also creates a concentration of noise impacts on the communities surrounding airports, which has led to an increase in noise complaints at many airports that have implemented these routes. In order to understand these changes in noise, and to design procedures that could help mitigate any negative effects, it is important to have modeling tools capable of capturing the noise impacts of flight track variability. This thesis develops a model for this purpose. First, twenty days of radar flight trajectory data from 2015 and 2016 at Boston Logan International Airport (KBOS) is used to quantify the observed distributions of variability in speed, altitude, and lateral track position. It is shown that altitude and speed variability have relatively small impacts on noise, but that the impacts of observed lateral variability are significant. Using this information, a physics-based model is developed to capture the noise impacts of lateral flight track variability. This tool is then used to model several example scenarios. First, the changes in noise due to pre- and post-PBN procedures are examined for KBOS Runway 33L departures. Next, a hypothetical procedure is designed to intentionally introduce lateral dispersion to KBOS Runway 33L departures. Finally, the tool is used to rapidly model noise impacts on due to both arrival and departure operations on all runways at KBOS. The model is shown to reduce computational expense by 1-2 order of magnitude relative to traditional methods. The results of these example analyses show that increased lateral dispersion causes a significant noise reduction at higher noise levels directly below the flight track at the cost of wider contours at lower noise levels. Because of this, any decision to add or remove flight track lateral dispersion has highly localized impacts that depend on the geometry of the route and the population of the surrounding area, and thus must be closely analyzed on an individual basis.

17. Key Words	18. Distribution Statement
Aircraft noise, Noise modeling, Dispersion, AEDT, Air Transportation, ASCENT	

19. Security Classif. (of this report)	20. Security Classif. (of this page)	21. No. of Pages	22. Price
Unclassified	Unclassified		

PAGE INTENTIONALLY LEFT BLANK

MODELING THE EFFECTS OF AIRCRAFT FLIGHT TRACK VARIABILITY ON COMMUNITY NOISE EXPOSURE

by

Callen T. Brooks

Submitted to the Department of Aeronautics and Astronautics
20 June 2017
In Partial Fulfillment of the Requirements for the Degree of
Master of Science in Aeronautics and Astronautics

ABSTRACT

The implementation of Performance Based Navigation (PBN) routes across the National Airspace System (NAS) has caused a significant concentration of flight tracks. This flight track concentration also creates a concentration of noise impacts on the communities surrounding airports, which has led to an increase in noise complaints at many airports that have implemented these routes. In order to understand these changes in noise, and to design procedures that could help mitigate any negative effects, it is important to have modeling tools capable of capturing the noise impacts of flight track variability. This thesis develops a model for this purpose. First, twenty days of radar flight trajectory data from 2015 and 2016 at Boston Logan International Airport (KBOS) is used to quantify the observed distributions of variability in speed, altitude, and lateral track position. It is shown that altitude and speed variability have relatively small impacts on noise, but that the impacts of observed lateral variability are significant. Using this information, a physics-based model is developed to capture the noise impacts of lateral flight track variability. This tool is then used to model several example scenarios. First, the changes in noise due to pre- and post-PBN procedures are examined for KBOS Runway 33L departures. Next, a hypothetical procedure is designed to intentionally introduce lateral dispersion to KBOS Runway 33L departures. Finally, the tool is used to rapidly model noise impacts on due to both arrival and departure operations on all runways at KBOS. The model is shown to reduce computational expense by 1-2 order of magnitude relative to traditional methods. The results of these example analyses show that increased lateral dispersion causes a significant noise reduction at higher noise levels directly below the flight track at the cost of wider contours at lower noise levels. Because of this, any decision to add or remove flight track lateral dispersion has highly localized impacts that depend on the geometry of the route and the population of the surrounding area, and thus must be closely analyzed on an individual basis.

Thesis Supervisor: R. John Hansman
Title: T. Wilson Professor of Aeronautics and Astronautics

PAGE INTENTIONALLY LEFT BLANK

ACKNOWLEDGEMENTS

I am thankful for the feedback and insights provided by Joseph DiPardo and Christopher Dorbian at the Federal Aviation Administration (FAA) Office of Environment and Energy, who helped manage and guide my research.

I also greatly appreciate the help of Massport and HMMH and their advice, analysis, and access to some of the data used for this thesis.

DISCLAIMER

This work was sponsored by the FAA under ASCENT Center of Excellence Project 23, Cooperative Agreement 13-C-AJFE-MIT-008. Opinions, interpretations, conclusions, and recommendations are those of the authors and are not necessarily endorsed by the United States Government.

PAGE INTENTIONALLY LEFT BLANK

TABLE OF CONTENTS

LIST OF FIGURES

LIST OF TABLES

LIST OF EQUATIONS

PAGE INTENTIONALLY LEFT BLANK

CHAPTER 1 INTRODUCTION

1.1 MOTIVATION

This study seeks to model and interpret the effects of flight trajectory variability on airport noise. Flight tracks vary in many ways: altitude, speed, ground track, thrust, and configuration can all vary for flights nominally flying the same route. Each of these differences can affect how much noise the aircraft generates, and how that noise impacts communities surrounding the airport. **Figure 1** shows illustrations of flight trajectory variability in lateral position, speed, and altitude. For clarity, throughout this thesis "dispersion" is used to refer exclusively to lateral variability, while variability is used generally to refer to any form of trajectory variability.

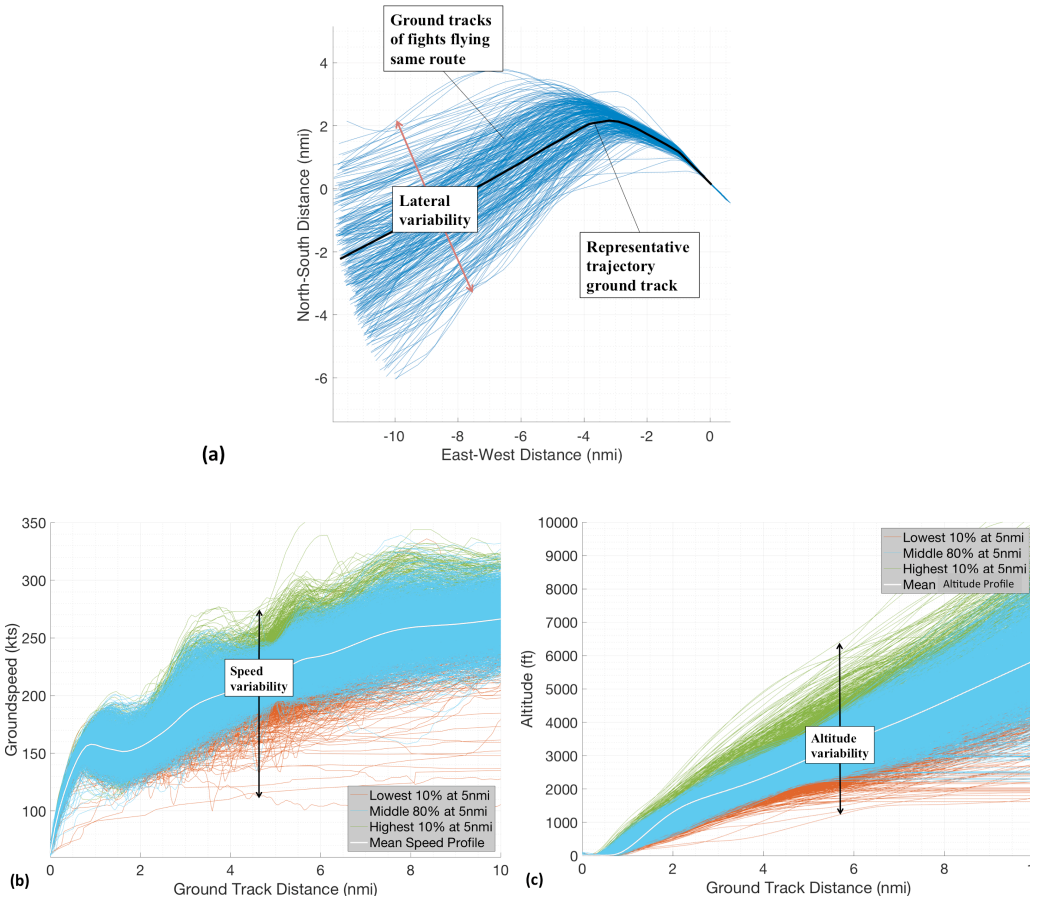

Figure 1. Illustration of variability. Lateral variability of flight tracks is shown in (a), variability in speed as a function of along-track distance is shown in (b), and variability in altitude as a function of along-track distance is shown in (c).

Variability of the lateral position of aircraft trajectories has become a highly pertinent issue due to the recent implementation of the Federal Aviation Administration's (FAA) of its NextGen program. NextGen seeks to modernize the National Airspace System (NAS) through updated infrastructure, air traffic control, and navigational techniques. The linchpin of this program is Performance Based Navigation (PBN). PBN is a general term for procedures that "use satellite-based precision to fly more direct routes, saving fuel and time, increasing traffic flow, and resulting in fewer carbon emissions". [1] One consequence of PBN, however, is a significant reduction of flight track lateral dispersion relative to legacy radar-based procedures. This decrease in lateral dispersion is called flight track concentration, and Area Navigation (RNAV) is one subtype of PBN that has flight track concentration effects. **Figure 2** shows this concentration for the case of Runway 33L departures at Boston's Logan International Airport (KBOS).

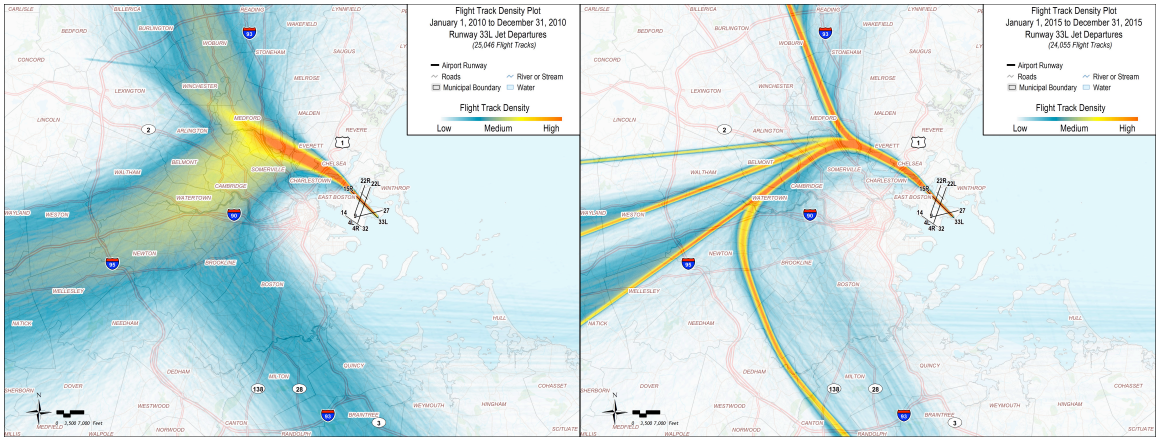

Figure 2. Boston Logan Runway 33L departures in 2010, before the implementation of RNAV (left), and in 2015, after implementation (right). [1]

Flight track concentration has had a significant impact on perceived noise exposure directly below RNAV tracks, as evidenced by a nationwide increase in noise complaints since the implementation of RNAV routes has become widespread. For example, at San Francisco International Airport, PBN flight tracks were implemented in 2014. After this implementation, noise complaints increased by an order of magnitude, from 14,726 in 2014 to 152,336 in 2015. Similarly, in Washington D.C. complaints

[1] Figure generated by Harris Miller Miller & Hanson (HMMH) from Massport Noise & Operations Monitoring System (NOMS) data. Used with permission from Massport and HMMH.

increased from 1,286 in 2014 (before PBN implementation) to 8,670 in 2015 (after implementation) [2].

This increase in complains leads to an obvious question: has concentration caused an increase in noise impacts? To answer this question, noise impact must be quantified. The FAA's primary metric for noise impact measurement is called Day Night Level (DNL or L_{DN}). This is the metric used in FAA's primary source of noise policy, a regulation called the Federal Aviation Regulation, Part 150 – Airport Noise Compatibility Planning. Part 150 defines "compatible use" – that is, what noise levels are compatible with various uses of land. **Table 1** shows the key result of this legislation: Part 150 deems residential areas to be compatible with noise levels below 65 dB DNL and incompatible with any higher noise levels.[1]

	Yearly day-night average sound level (L_{dn}) in decibels					
Land use	**Below 65**	**65-70**	**70-75**	**75-80**	**80-85**	**Over 85**
RESIDENTIAL						
Residential, other than mobile homes and transient lodgings	Y	N(1)	N(1)	N	N	N
Mobile home parks	Y	N	N	N	N	N
Transient lodgings	Y	N(1)	N(1)	N(1)	N	N

Table 1. Land use compatibility with various DNL values as dictated by FAR Part 150. Importantly, residential land is deemed compatible with noise levels below 65 DNL and incompatible with anything above that. [3]

Using this 65 dB DNL threshold, airport noise has been steadily decreasing for decades despite significant growth in air traffic, as shown in **Figure 3**. In fact, at the 65 dB level, RNAV routes have led to almost no change in noise exposure.

[1] Noise metrics will be covered in much more detail in Section 2.1.1, including the rationale for selecting 65 dB as compatible and a description of some alternative metrics.

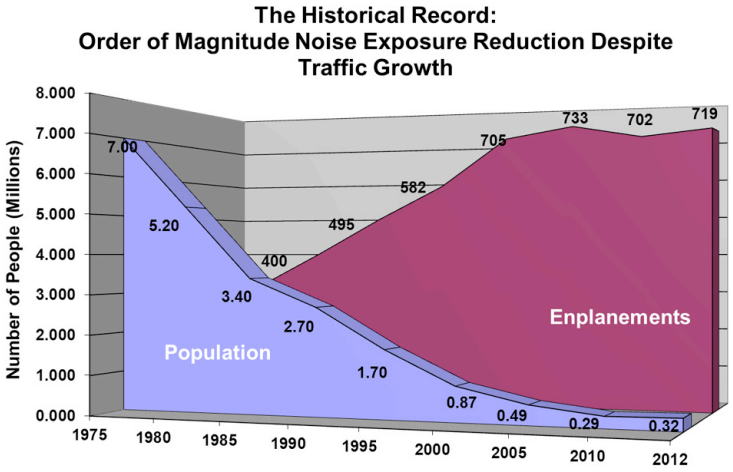

Figure 3. Noise exposure at the 65 dB DNL level has been steadily decreasing for decades despite a large increase in the number of enplanements. [4]

At the 65 dB level, noise has not increased due to the implementation of RNAV. Nonetheless, complaints have clearly increased significantly. This suggests that many people are bothered by noise concentration effects occurring at DNL levels lower than 65 dB. **Figure 4** is a clear example of this, showing that a large number of complaints occur directly below RNAV tracks but outside the 65 DNL contour.

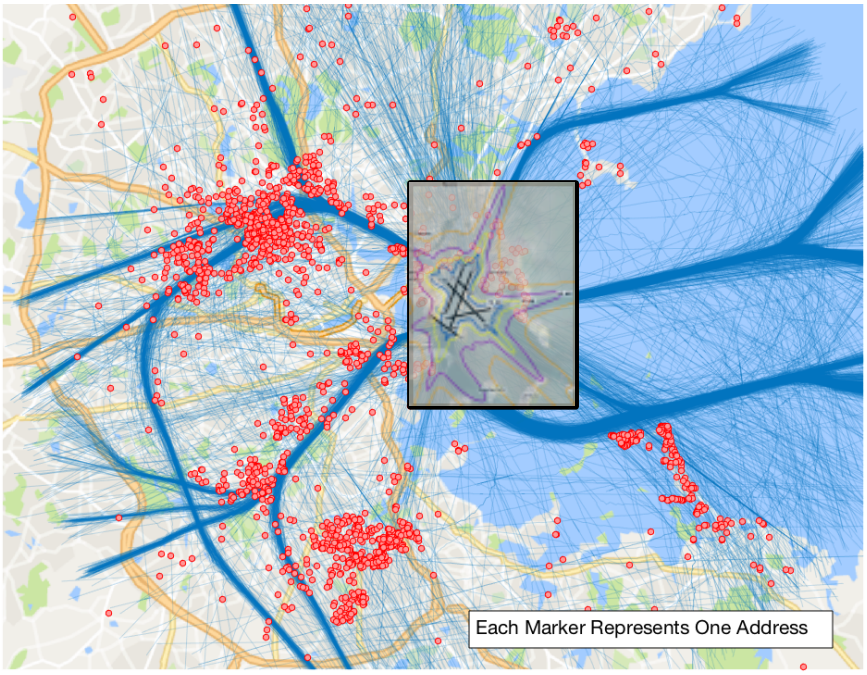

Figure 4. Noise complaints from 2015-2016 at Boston Logan Airport (KBOS) are shown as red dots, with each dot corresponding to 1 complaint. Departure flight tracks are shown in blue. Noise contours from the official 2015 Logan Airport Environmental Data report are overlaid, with the 65 DNL contour shown in purple. [5][6]

This pattern of complaints indicates a need to model the noise due to lateral dispersion and concentration effects at noise levels below 65 dB DNL. Unfortunately, this analysis is difficult and time consuming using existing noise modeling tools. Using current state-of-the-art noise modeling tools, such as the FAA's Aviation Environmental Design Tool (AEDT), modeling dispersion accurately requires modeling noise individually for each flight, which makes comparing dispersed and concentrated routes extremely work intensive. In order to make such a comparison, it would be necessary to determine a precise path for each flight traveling the route, to model noise for each flight, and then to sum the overall noise. For realistic cases, this would need to be done for thousands of flights, making this process very time consuming. Additionally, flights flying any procedure will exhibit some variability in other forms, such as speed and altitude. Current noise models also do not allow for these effects to be efficiently captured—once again, the current method for modeling these effects is to define a unique trajectory for each flight and model each one individually.

With the procedure design tools available as part of NextGen, it could be possible to intentionally add or remove trajectory variability to mitigate noise, but it remains unclear what the best strategies are to take advantage of these procedure design tools. Thus, a tool capable of efficiently and accurately modeling the noise impacts of flight track dispersion and other forms of variability would be very useful for decision-making and procedure design.

A tool capable of modeling the noise impacts of flight track variability would also be extremely useful in a rapid noise modeling application. Current methods for modeling the noise impacts of all operations across an entire airport require the calculation of noise contributions from each flight. This approach is extremely computationally expensive. Only modeling the noise due to a select few representative flights can drastically reduce this computational expense, but this savings comes at the cost of a significant decrease in fidelity since it cannot account for the variability of the real routes. If it were possible to quickly model the variability about these central routes, it would be possible calculate the noise impacts of all flight operations at an airport at a much lower cost in terms of money, manpower, and computation time.

1.2 OBJECTIVE

The primary objective of this thesis is to develop a tool capable of modeling the noise impacts of flight track variability, and to use that tool to explore some insights into how variability—and in particular flight track lateral dispersion—impacts aircraft noise. Existing noise tools such as the FAA's Aviation Environmental Design Tool (AEDT) or the NASA developed Aircraft NOise Prediction Program (ANOPP) are well validated, industry accepted tools; this thesis does not seek to replace them. In fact, the FAA is federally mandated to use AEDT for all of its environmental analyses and policy decisions [7]. With this in mind, this study seeks to create a tool that can utilize results from these noise models, lending the new tool the benefits of the credibility and validation of existing models. In particular, the ability to use AEDT results as an input greatly increases the usefulness of the tool for policy related analysis. Because of this, and because of AEDT's relatively low computational expense relative to physics-based models like ANOPP, the tool will be validated against results from AEDT. Since AEDT has been extensively validated against real-world measurements, this validation will also provide a reasonable degree of real-world validation.

Using results from existing noise models as an input, the tool must be capable of rapidly and accurately calculating the noise due to many distributed flights, eliminating the need to model each flight individually. **Figure 5** shows a simple architecture diagram that illustrates what inputs the model will receive in order to calculate the noise impacts of variability. The model will require inputs of a "variability profile" precisely defining how much trajectories vary as a function of along-track distance. It will also require gridded single fight noise results from a single "representative trajectory" flying the variable route. This representative trajectory will be defined by a flight ground track and a "flight profile" defining speed, altitude, and thrust. With these inputs, the model will be able to quickly calculate the noise impacts of many flights flying variable trajectories along the route.

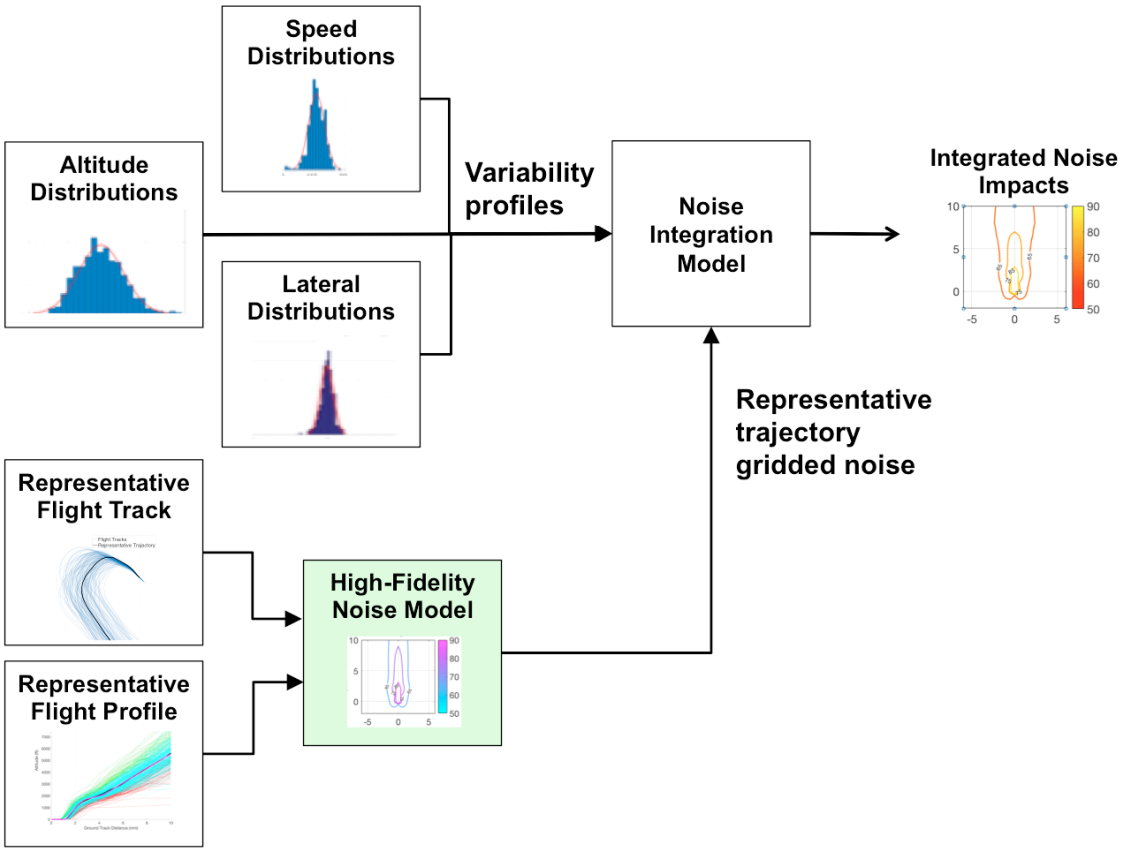

Figure 5. An architecture showing what the inputs and outputs of the variability model must be.

To accomplish this objective, first, some useful background information on noise and PBN will be presented in Chapter 2. Next, in Chapter 3, flight track variability will be quantified to determine how that variability affects noise impacts. Variability will be quantified in terms of speed, altitude, and lateral flight track dispersion. Using this information, Chapter 4 will discuss noise modeling techniques, beginning with an explanation of AEDT and going on to discuss how variability impacts noise modeling. Using this information, Chapter 5 will develop a tool capable of quickly and flexibly modeling the noise impacts of trajectory variability. Finally, Chapter 6 will present several examples of applications of the tool, including procedure design and rapid noise modeling of all flight procedures at an airport, and Chapter 7 will discuss some conclusions drawn from this work.

CHAPTER 2 BACKGROUND

2.1 UNDERSTANDING NOISE IMPACTS

Fundamentally, noise is a term for undesirable sound. Sound, in turn, is a term for fluctuating pressure waves, which can be observed by humans via the ears. These sound waves have both amplitude—perceived as volume or loudness—and frequency—perceived as pitch or tone. The human ear has evolved the ability to detect and interpret a vast range of both amplitudes and frequencies. In terms of volume, its audible range spans six orders of magnitude of pressure amplitude from the lower limit of audibility to the onset of pain from excessive volume. Audible frequencies span from about 20 Hertz (Hz) to about 20,000 Hz, or about three orders of magnitude. [8]

The volume of sound, as mentioned above, roughly corresponds to the amplitude of the pressure wave. Human sensitivity to loudness corresponds well to a logarithmic scale, however, rather than a linear one. Because of this, the standard unit for sound measurement is the decibel (dB), which is logarithmically related to sound pressure. More specifically, the relationship shown in Equation (1) relates Sound Pressure Level (SPL), measured in decibels, to P_0, the pressure amplitude of the sound wave, and P_{ref}, a reference value 20 μPa rms. [9]

$$SPL = 20\log_{10}\left(\frac{P_0}{P_{ref}}\right) \tag{1}$$

Because this measurement scale is logarithmic, a doubling of pressure only results in an increase of about 3 dB. But, as mentioned above, human perception corresponds much better to decibels than pressure, so for the purpose of understanding noise, it is much more useful to try to develop an understanding of the decibel scale. According to one study, for noise levels above 40 dB, the minimum audible change in noise is

approximately just below 3 dB. [10]. To help build an intuition for this scale, **Figure 6** presents various noisy events and their respective SPL values.

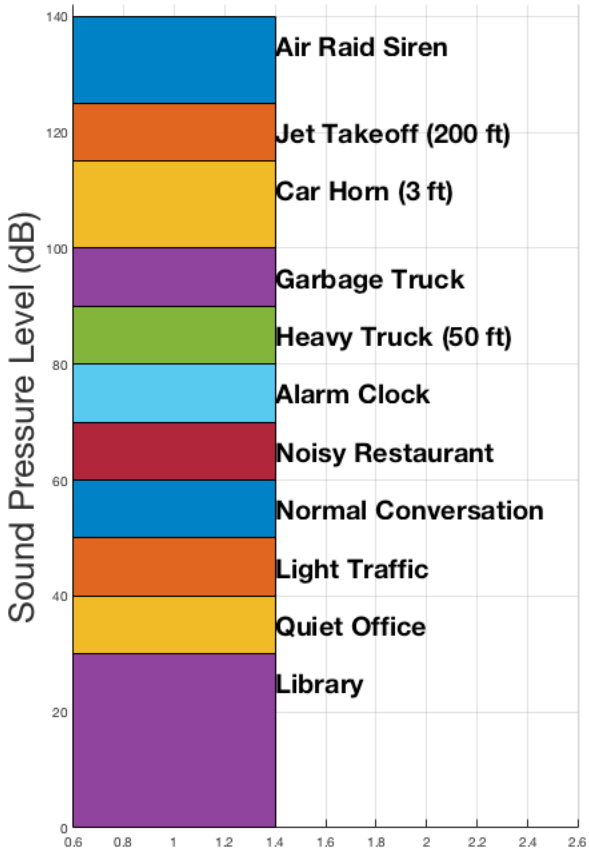

Figure 6. The sound pressure level (SPL) values of various noisy events. [11]

2.1.1 NOISE MEASUREMENT & METRICS

SPL allows for an instantaneous measurement of an event, but it is unable to capture impacts over some duration of time or to capture differences in frequency. Various other metrics have been created to capture the impacts of aircraft noise. Several factors besides volume influence how annoying aircraft noise is: first, the human ear is more sensitive to some frequencies of noise, and second, the total number of events, measured in terms of how frequently a flight is audible, can be a significant contributor to annoyance.

To model the increased annoyance that some frequencies cause, decibel values are weighted. To perform this weighting, frequencies are divided into ⅓-octave bands, and noise in each band is increased or reduced by a factor. Two different weighting systems are commonly used: A-weighted and C-weighted. A-weighted noise metrics heavily rate the mid-range frequencies (2,000-6,000 Hz) because these ranges are where most human speech resides, and is where the human ear is most sensitive. C-weighting more heavily weights low frequencies (100-2,000 Hz), and is intended to account for the sensitivity of the human ear to sound at high volume (above 90 dB SPL). A-weighting is used much more commonly for evaluating aircraft noise, and most metrics used in this thesis will be A-weighted metrics. C-weighting is used, however, for some analysis of aircraft noise, such as situations when noise behind takeoff roll is important. [12] These weighting factors are shown in **Figure 7**.

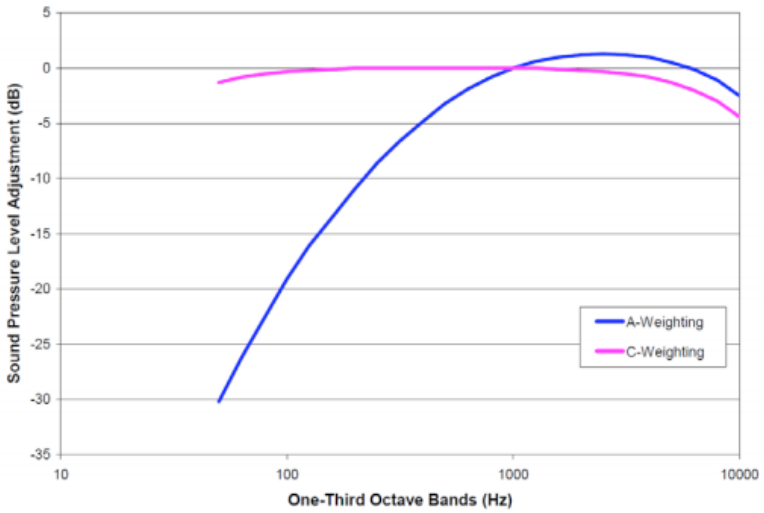

Figure 7. A-weighted and C-weighted adjustment curves. [12]

The second factor that noise metrics must quantify is the durative nature of aircraft noise. Some metrics, such as the A-weighted LAMAX, simply report the highest noise level observed for a given event. Others, such as Sound Exposure Level (SEL), another A-weighted metric, perform an integration of noise over a certain time period. SEL integration has several steps. First, the maximum noise value is recorded (this value is what would be reported by LAMAX). Then, the points in time with noise levels 10 dB

lower than the peak value are found (one point before and one after the peak), and noise is integrated in time between these points. SEL and LAMAX are illustrated in **Figure 8**.

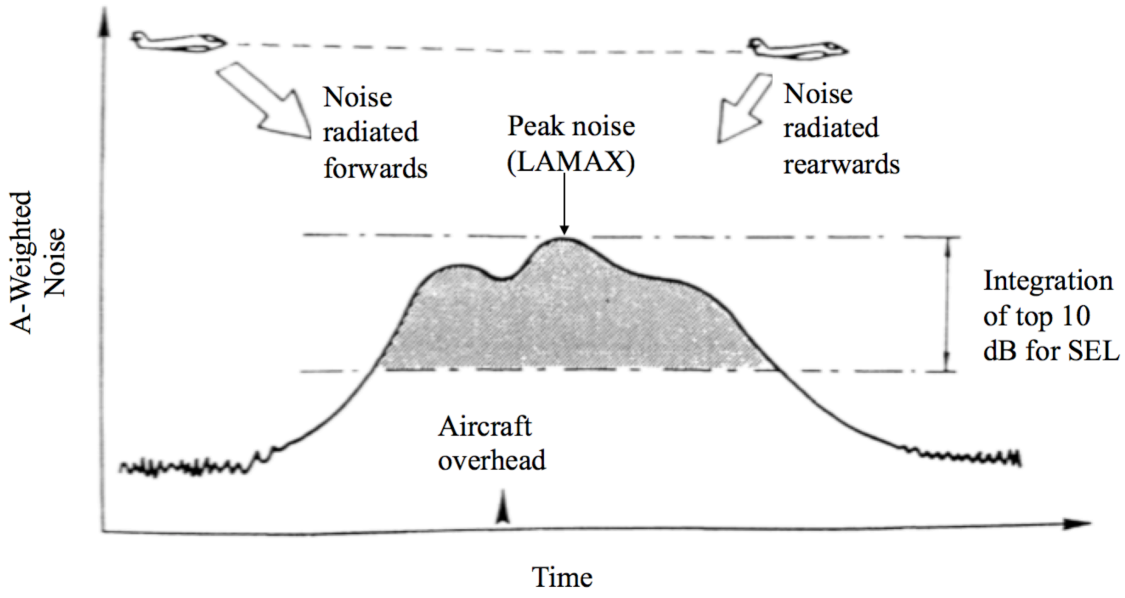

Figure 8. Illustration of LAMAX and SEL calculation. [8]

SEL and LAMAX are both single event metrics, meaning that they only measure the noise exposure due to one flight. To account for the effects of multiple flights, other metrics have been developed to sum contributions from many events. The most widely used multi-event metric is Day-Night Average Sound Level (DNL). DNL is calculated by summing the noise of different SEL events over some time period, T, and dividing by that time in seconds. Typically, one day (86,400 seconds) is used. A 10 dB penalty is applied to night events (10 pm to 7 am) to account for the increased annoyance these events cause. This calculation is illustrated in **Figure 9** and the equation for calculating DNL is shown in Equation (2).

$$DNL = 10\log_{10}\left(\frac{1}{T}\left[\sum_{i=1}^{n} 10^{\frac{SEL_{day,i}}{10}} + \sum_{i=n+1}^{m} 10^{\frac{SELnight_{,i}+10}{10}}\right]\right) \quad (2)$$

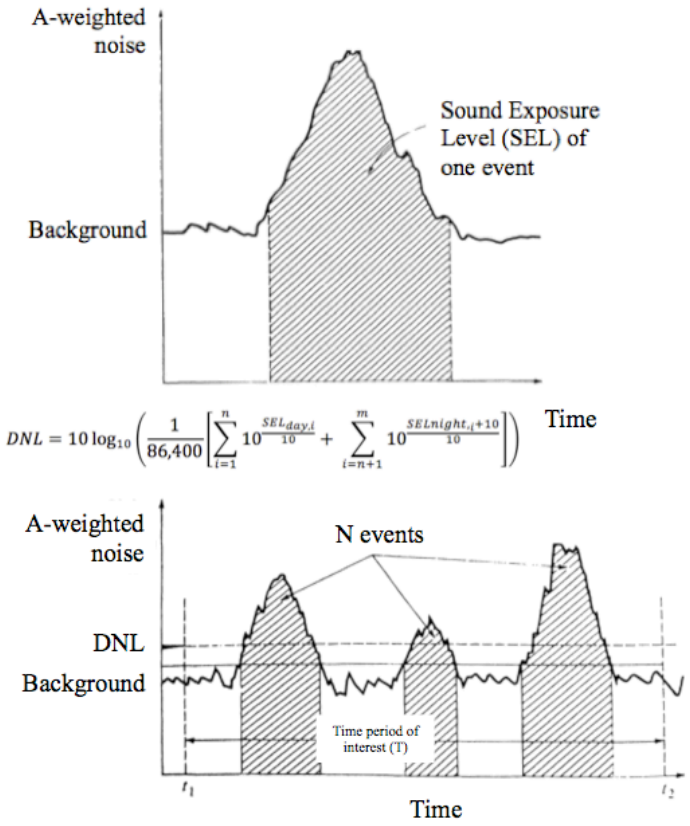

Figure 9. Calculation of DNL.[8]

Another multi-event metric that has gained popularity more recently is Number Above (N_{above}). Number above is a simple count of the number of flights producing an LAMAX value above a certain threshold, with 60 dB or 70 dB often chosen for the threshold value.

DNL has become the standard metric for noise exposure modeling largely due to its importance in policy. The land use compatibility requirements dictated by FAR Part 150 (shown in **Table 1** above) are all measured in DNL. This regulation is the basis of most airport environmental analyses, and thus procedure design is often driven by noise exposure measured in DNL. DNL was chosen as the metric for compatible land use requirements in a large part due to the work of Theodore Schultz. Schultz compiled many surveys on annoyance due to aircraft noise and created what is now known as the "Schultz Curve", with noise level in DNL on the X-axis percentage of the population annoyed on the Y-axis. The Schultz curve is shown in **Figure 10**.

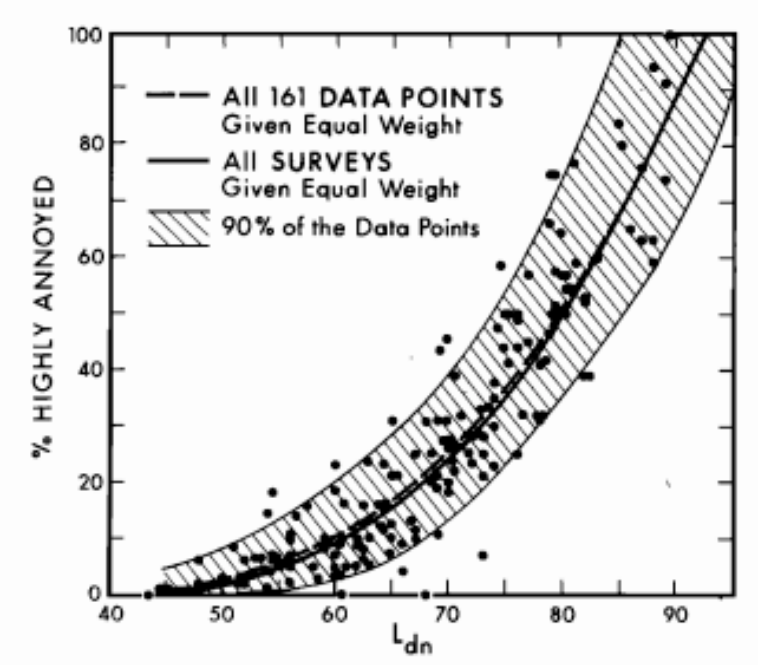

Figure 10. Schultz Curve, showing percentage of people who are "highly annoyed" by a certain DNL value. [13]

As discussed in Section 1.1 above, however, recent trends in complaints well outside the 65 DNL contour indicate that this threshold may not be a sufficient to model community annoyance. It is also important to note that DNL does not scale linearly as operations are added; instead, it increases sharply at first as new operations are added where there were few before, and increases very gradually if more operations are added where there were already a large number of flights. This trend is shown in **Figure 11**.

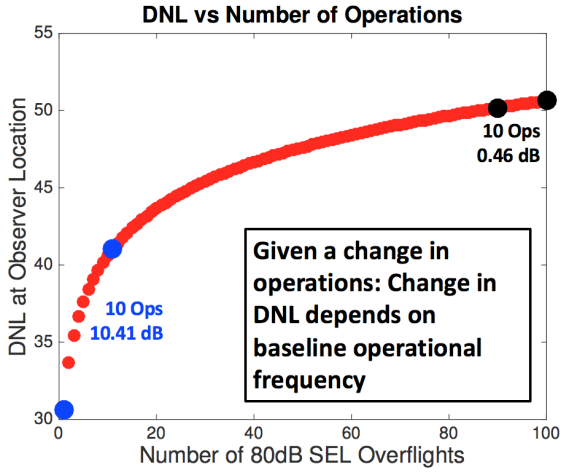

Figure 11. DNL scaling with changes in flight frequency.

This scaling can have some advantages. An observer who previously had no flights overhead will be much more likely to notice and be annoyed by aircraft noise, while someone who already has frequent exposure to aircraft noise may not notice or care if a few more flights are added each day. The implementation of PBN and resulting decrease in flight track lateral dispersion, however, has taken this concept to a new extreme. Reducing the flights over some areas to near zero creates significant DNL benefits, but increasing the frequency drastically over a select few individuals shows a less extreme increase in DNL, which could make concentration seem very appealing. This concern is a major reason that many community noise activists advocate for using N_{above} metrics, which scale linearly with frequency.

2.1.2 HEALTH IMPACTS OF NOISE

In addition to annoyance, there is some research suggesting that aircraft noise can have significant health impacts. While sleep disturbance and annoyance are the most common forms of noise impact, one recent study found that approximately 61,000 healthy life years are lost annually in Europe due to noise-related heart disease. A series of five other recent studies found that the risk of hypertension increases by about 10% for those living in regions exposed to DNL levels greater than 60 dB. [14] Another 2013 study tracked hospital admissions for strokes in the area surrounding London Heathrow International Airport and found that people living in regions with a daytime noise level greater than 63 dB or a night time DNL value greater than 55 dB were approximately 25% more likely to be admitted to a hospital for a stroke, controlling for ethnicity, income level, and likelihood of smoking. [15] Although simply preventing annoyance could be enough to motivate noise mitigation efforts, the body of work suggesting that aircraft noise could have serious health impacts makes an even more compelling case that noise mitigation efforts should be a priority.

2.3 PERFORMANCE BASED NAVIGATION

As mentioned in the introduction, the FAA's commitment to PBN as part of the NextGen initiative has had significant implications for flight track variability. There are

various different types of PBN procedures that have different constraints and impact variability and noise in different ways. Some different types of PBN procedures will be discussed to help build an understanding of the tools available for procedure design, and how these tools might impact trajectory variability and noise. An overview of the different types of flight procedures is shown in **Figure 12**, and in the following subsections each type of PBN procedure is explained in more detail.

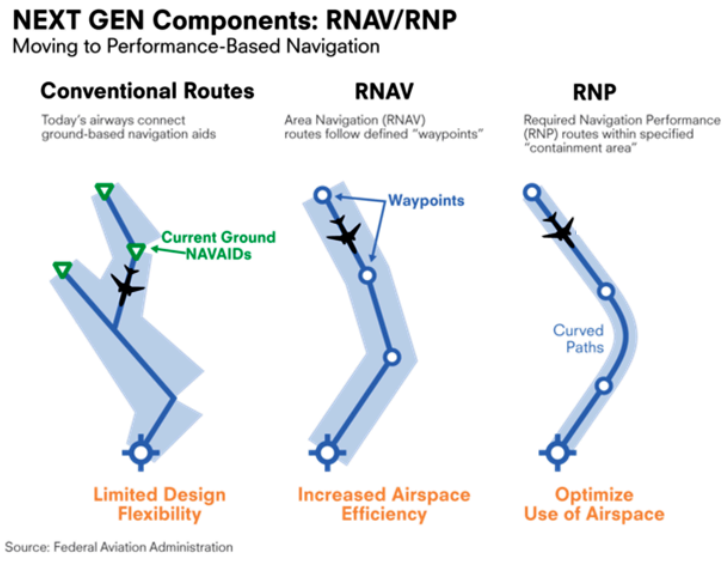

Figure 12. An overview of the differences between conventional routes, RNAV, and RNP procedures.

2.3.1 Different Types of Performance Based Navigation

Area Navigation (RNAV)

Area Navigation, or RNAV, is a type of instrument flight rule (IFR) procedure that has existed since the 1960's. Originally, rather than flying directly to ground-based navigational aids (NAVAIDS), RNAV procedures allowed pilots to follow a user-defined flight track so long as it passed within a certain range of waypoints along the route. In these early RNAV routes, pilots used NAVAIDS for navigational information but no longer had to travel directly from beacon to beacon, allowing for more efficient routes. [16]

With the advent of satellite navigation and the Global Positioning System (GPS), however, this class of procedures has changed significantly. Now, procedures are

designed using precise GPS waypoints, and aircraft typically fly within at most one nautical mile of each waypoint. [16] This GPS navigation often allows for very precise flight tracks with lateral deviation of less than 0.5 nautical miles for the vast majority of aircraft, as will be discussed in more detail in Section 3.2.1. In the past 3-5 years these routes have become widely used across the NAS, causing significant reduction in lateral flight track variability. Because RNAV only provides lateral guidance, not altitude or speed guidance, however, variability in its other forms has remained largely unchanged with the implementation of RNAV.

Required Navigation Performance (RNP)

While RNAV has existed for decades, RNP procedures are a much more recent form of PBN. RNP functions similarly to RNAV in many ways, but there are some important differences. First, RNP allows for the definition of precise three-dimensional trajectories, providing precise vertical guidance in addition to lateral guidance. Second, aircraft require special instrumentation to fly RNP routes, because in order to be authorized to fly RNP routes the aircraft must be able to produce cockpit notifications if the aircraft deviates from the specified lateral path. Each RNP route is classified as RNP X, where X is the allowable lateral deviation in nautical miles. Each RNP-equipped aircraft is able to achieve a certain level of lateral precision, and must be able to guarantee that level of precision to within 10^{-5} integrity. [17] RNP routes allow for more precise procedure design, and equipage rates are rapidly increasing, but usage rates remain quite low for RNP routes. This lack of usage is largely due to difficulties for pilots and air traffic controllers in determining which flights are eligible for RNP routes and how to merge RNP traffic with other air traffic. Thus, while RNP shows great potential for designing advanced operational procedures in the future, it does not currently have major noise impacts.

2.3.2 OPEN SID PROCEDURES

In 2015, the FAA approved the usage of a new type of procedure called an Open Standard Instrument Departure, or Open SID. An Open SID is a departure procedure that combines an RNAV route with embedded air traffic control vector segments. This allows aircraft to leave and/or join RNAV routes at different locations. [18] One potential

benefit of an Open SID procedure is that it allows air traffic controllers to send an aircraft directly to a waypoint on the RNAV route, decreasing path length and fuel burn. The primary reason Open SID procedures have been gaining interest across the NAS, however, is their ability to add flight track lateral dispersion to an RNAV route. The intentional re-introduction of dispersion is one method that could be used to combat the increase in complaints related to concentration effects. Open SID procedures allow for an increase in lateral dispersion without losing most of the benefits that RNAV brings, and thus could be an attractive option for procedures where dispersion is shown to have noise exposure benefits. A graphic demonstrating the principle of an Open SID is shown in **Figure 13**.

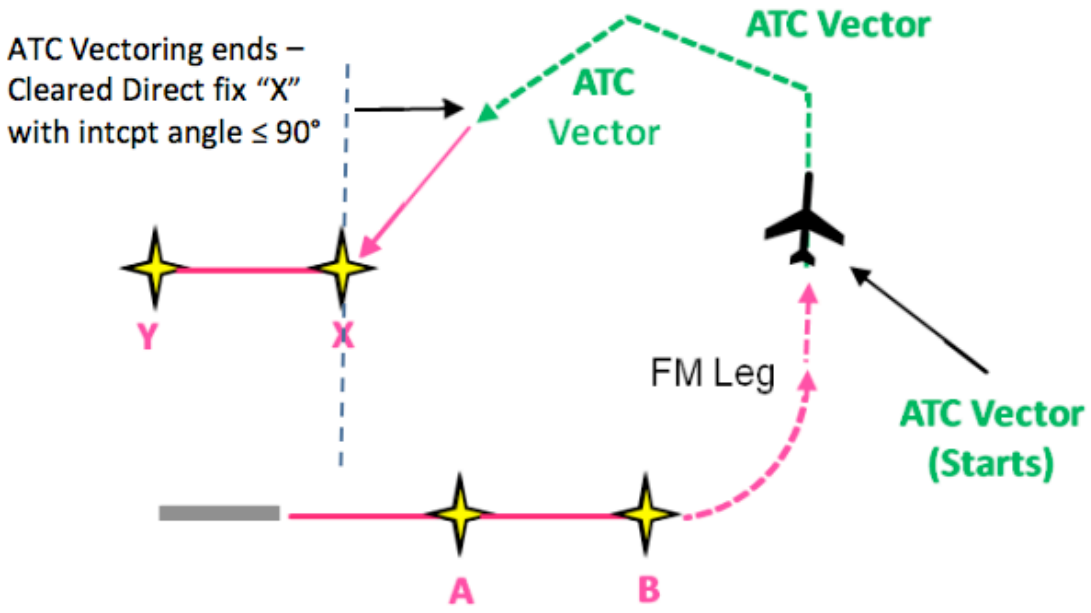

Figure 13. Open SID example with RNAV track shown in pink and vectored segments shown in green. A, B, X, and Y are RNAV waypoints. [19]

One example of existing Open SID procedures are departures at Charlotte Douglas International Airport (KCLT). Like in many other communities around the country, the residents of Charlotte, North Carolina and the surrounding area expressed serious concerns with the effects of flight track concentration after the implementation of RNAV routes. Due to this pressure, the FAA agreed to reintroduce flight track dispersion through a series of Open SID procedures called the "Metroplex Departures" [20]. The

KCLT departure flight tracks with RNAV and with the new Open SID are shown in **Figure 14**.

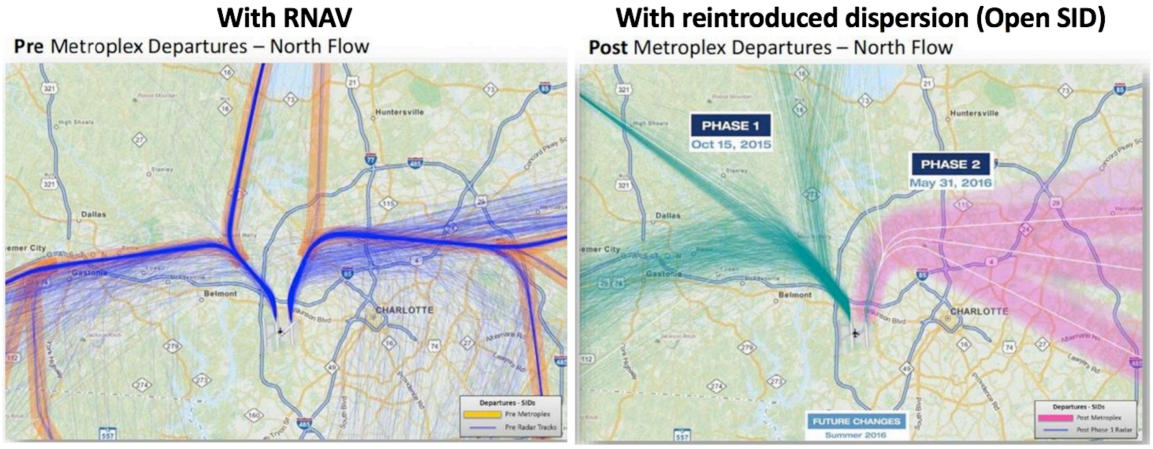

Figure 14. Open SID departure procedures currently being implemented at Charlotte Douglas International Airport (KCLT). [20]

These Metroplex Procedures have only recently begun to be implemented, so the full extent of their noise impacts are not yet known, but it is clear that these procedures have successfully reintroduced significant flight track dispersion. These procedures also serve as an existence proof, demonstrating that it is politically and logistically feasible to implement Open SID procedures. Given this feasibility, the tools presented in this thesis will allow for faster, more accurate modeling of the effects of trajectory variability inherent in Open SID procedures, which will in turn allow for more effective procedure design.

CHAPTER 3 QUANTIFYING FLIGHT TRACK VARIABILITY

In order to understand the impact that flight track variability has on community noise exposure, it is first necessary to understand how flight tracks vary. As mentioned in Section 1.1, flights flying the same route can exhibit variation in speed, altitude, lateral track, power setting, and configuration. Each of these differences will have some impact on noise. For the purposes of this analysis, however, only speed, altitude, and lateral offset effects are considered. Although thrust and configuration variability will have some impact on noise, data on thrust and configuration are not available in typical radar datasets, making them more difficult to analyze. Thus, it was decided that these forms of variability are out of scope of this thesis, although they could be interesting to model in future work. Therefore, it is assumed that the thrust and configuration of all flights on a route can be represented by the thrust and configuration of the mean flight. For configuration, this should be a reasonable assumption, because aircraft configuration variability is not expected to have a major impact on noise—in fact, AEDT does not model aircraft configuration differences at all. Although thrust variation does cause significant changes in noise, this assumption is aided by the fact that some flights will have higher thrust than the mean and some will have lower thrust, causing at least partial cancellation of thrust effects.

Given these assumptions, radar data was utilized to quantify the most noise-relevant forms of trajectory variability: speed, altitude, and lateral offset. This analysis was conducted using the method shown in **Figure 15**.

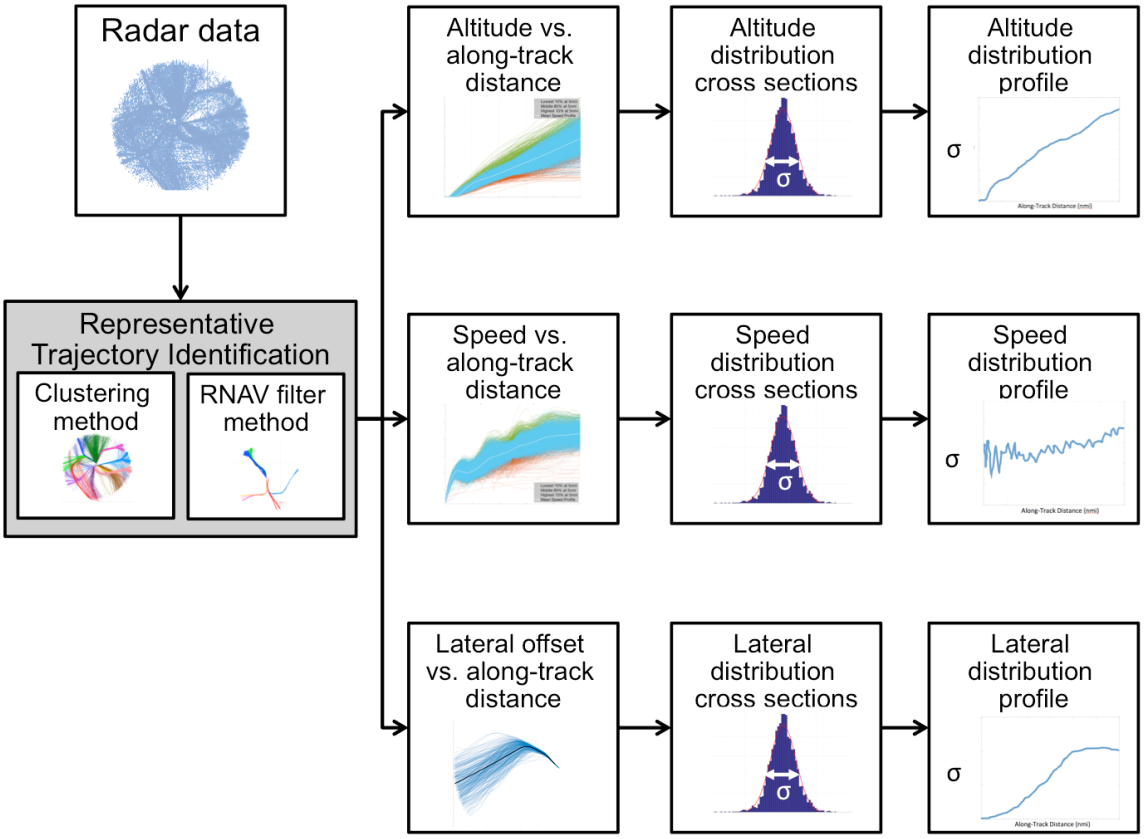

Figure 15. Architecture diagram showing variability quantification approach.

First, each radar trajectory was classified into a "route" of flights flying along a similar ground track. Next, altitude, speed, and thrust were calculated as a function of along-track distance for each flight in the route. These quantities can be plotted to give useful insight into how much the chosen quantity varies as a function of along-track distance. Next, cross sections were taken of speeds, altitudes, and lateral offsets at various along-track distances to determine what kind of distribution was present, and at each cross section, the width of the distribution, σ, was calculated. Finally, the widths of the distribution cross sections at each point were used to create a "distribution profile"—distribution width as a function of along-track distance at each point.

3.1 RADAR DATA ANALYSIS METHODOLOGY

3.1.1 RADAR DATA SOURCES

For this analysis, high spatial and temporal fidelity was required, because the most important noise effects occur in a relatively small region close to the airport. For this reason, two radar data sources were used: the FAA's Airport Surface Detection Equipment Model X (ASDE-X) and the Massachusetts Port Authority's (Massport's) Noise and Operations Monitoring System (NOMS). An example of ASDE-X radar data is shown in **Figure 16**. This figure shows 20 days of ASDE-X departure data at KBOS spread over 2015 and 2016.

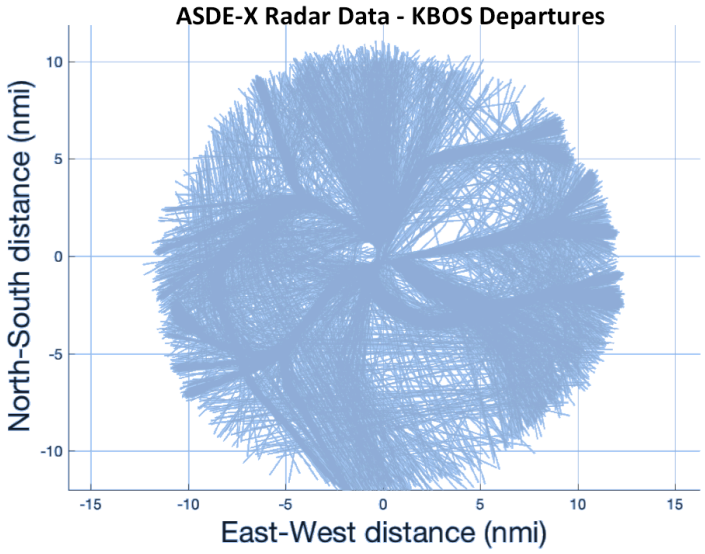

Figure 16. ASDE-X flight track radar data from 20 days of departures at KBOS.

ASDE-X data is a surveillance system that uses a combination of surface surveillance radar, multilateration sensors, airport surveillance radar, and ADS-B data. A filtering algorithm combines data from all of these sources to provide high fidelity, 1-second update position data. This system was built to give air traffic controllers a tool to track aircraft on the surface and near the airport; as a result, ASDE-X data is only available in the vicinity of the airport (within a 10 nautical mile radius). ASDE-X data includes trajectory information, aircraft type, and call sign. [21] Because most important

noise impacts occur within this region, and because ASDE-X provides the necessary spatial and temporal fidelity, it is a useful source for noise analysis.

NOMS data is a dataset complied and curated by Massport. The full NOMS dataset contains a variety of data, but the portion used for this analysis is a detailed record of all radar data for flights at KBOS. This dataset includes radar trajectories updated every five to ten seconds, aircraft type, and aircraft call sign, but also links each trajectory to a runway and contains origin and destination airport information. [22] For this analysis, ASDE-X data was used where available due to its higher update rate.

3.1.2 REPRESENTATIVE TRAJECTORY IDENTIFICATION

For some applications, it is necessary to compare variability only of flights flying the same route. To accomplish this, first, arrival and departure flows are identified, and in a process called "trajectory classification", each radar trajectory is classified to an arrival or departure flow, or is classified as an outlier (not conforming to any of the flows). Next, the trajectory closest to the mean of each flow is selected as the representative trajectory of that flow. This representative trajectory is used as a baseline for each flow, and variability in altitude, speed, and lateral offset is defined as a delta from the representative trajectory.

Two methods were developed to accomplish this identification. The first is a clustering-based method that leverages the density-based clustering algorithm Density-based spatial clustering of applications with noise (DBSCAN) [23] to find routes with no a priori knowledge. The second method uses a filter to detect which flights are flying known RNAV routes, and either assigns flights to an RNAV route or labels them as nonconforming. Both methods are discussed in more detail in Appendix A. An example of this process using the DBSCAN method is shown in **Figure 17**.

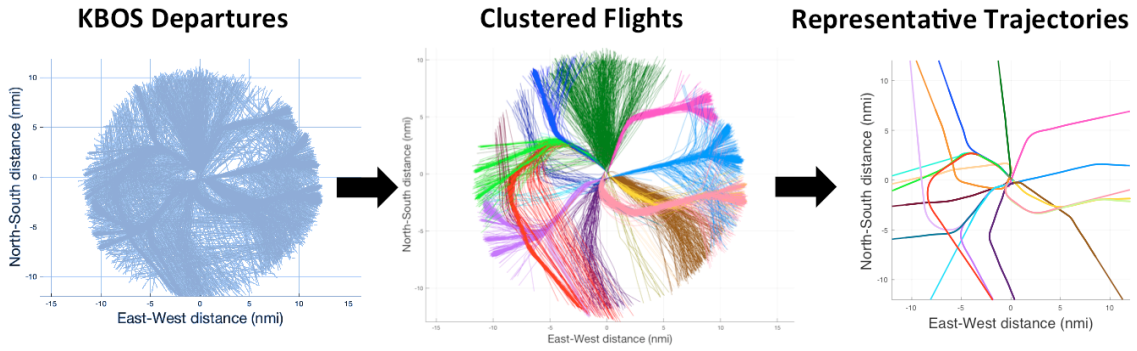

Figure 17. An example of Representative Trajectory Identification analysis performed using the clustering method on 20 days of departures at Boston Logan International Airport (KBOS).

In this figure, the left hand side shows the raw radar tracks. The middle shows the result of trajectory classification, with each departure flow represented by a different color. On the right hand side of the figure, the ground tracks of the representative trajectory for each flow are shown.

3.2 VARIABILITY QUANTIFICATION RESULTS

The results in this section show the variability quantification methodology shown in **Figure 15** applied to several example routes at KBOS. These examples demonstrate the method and give useful insights into how much variability exists on typical routes. All analysis labeled "2015" uses 20 representative days of ASDE-X data at KBOS spread between the end of 2015 and beginning of 2016, while all analysis labeled "2010" uses the same 20 dates in 2010 using NOMS data at KBOS. Because the implementation of RNAV caused significant changes to flight track lateral dispersion between 2010 and 2015, variability was quantified for both 2010 and 2015. RNAV, however, does not provide altitude or speed guidance, so variability in altitude and speed have not experienced notable changes in this timeframe, and therefore only 2015 results are presented for altitude and speed variability.

3.2.1 LATERAL VARIABILITY

Because lateral flight track dispersion at KBOS has seen such significant change due to the implementation of RNAV, lateral variability was analyzed for both 2010 and 2015-2016 so that the results could be compared. In 2010, a good deal of natural dispersion was present due to the relative imprecision of heading-based flight procedures,

while in 2015-2016, very little dispersion is expected due to the high lateral precision present in GPS-based procedures.

To begin the analysis, representative trajectory identification was performed on radar data using the clustering methodology described in Appendix A for both the 2010 NOMS dataset and the 2015 ASDE-X dataset. From the widths of these arrival and departure flows, shown in **Figure 18**, the concentration effects of RNAV are clear, particularly for the departures.

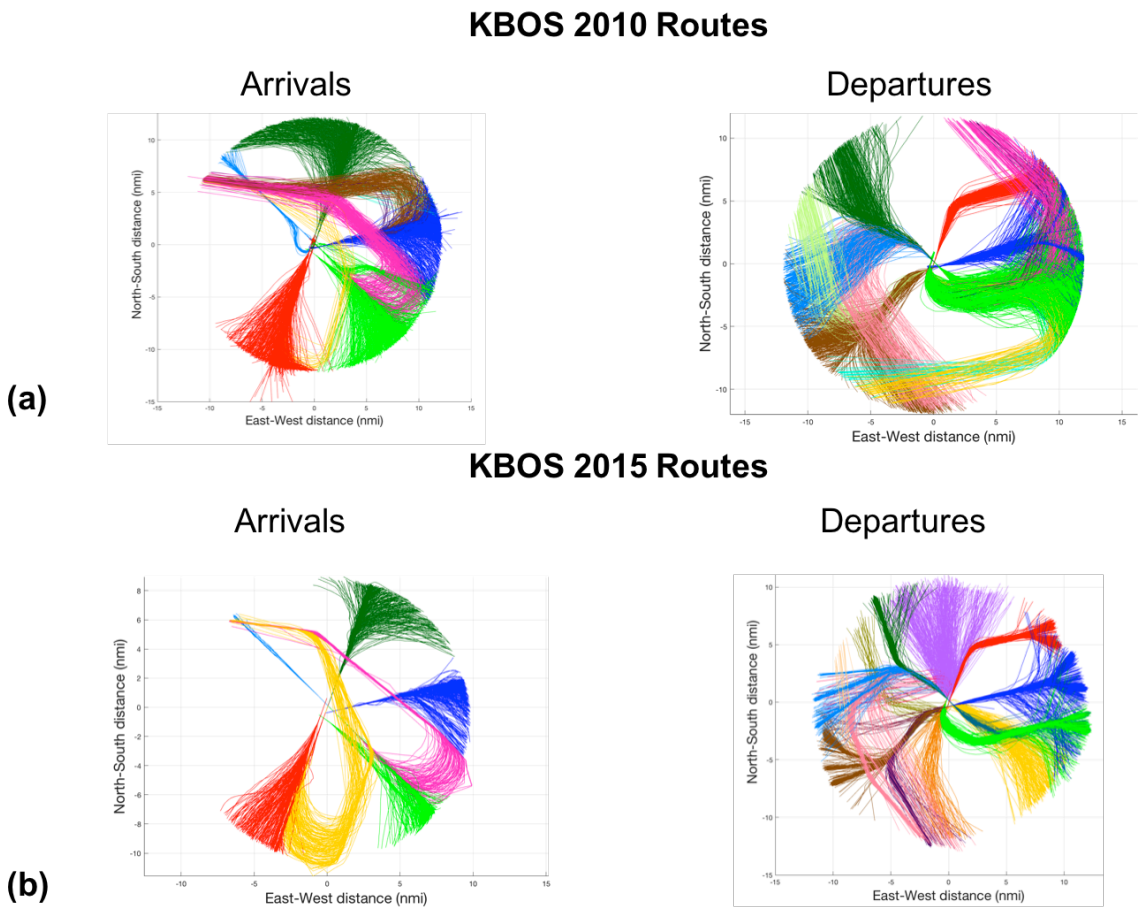

Figure 18. Arrival and departure flows at KBOS. Representative trajectory identification was performed using the clustering method described in Appendix A.

For each flow, the above analysis allows for the calculation of lateral dispersion as a function of along-track distance. Dispersion is defined as lateral offset from representative trajectory ground track, and the distribution of these lateral offsets was examined at various along-track distance cross sections. Each route's dispersion

distribution was analyzed individually, but all aircraft types were considered when calculating dispersion profiles, because for typical procedures different aircraft types are able to fly the same ground track. As an example, Runway 27 arrivals were analyzed, and cross sections of the distribution were analyzed at 4, 6, and 8 nautical miles. The ground tracks for this analysis in both 2010 and 2015 are shown in **Figure 19**.

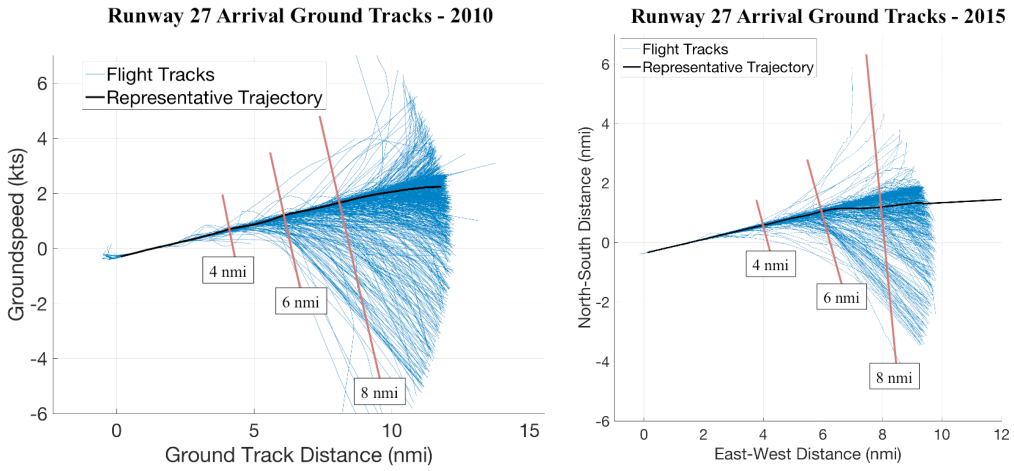

Figure 19. Runway 27 arrival tracks in 2010 and 2015. Cross sections where distributions were examined are shown in red.

The distribution of lateral offset at each of these three cross sections are shown in **Figure 20** for both the 2010 and 2015 datasets. Note that the standard deviations shown in the figure are that of the fitted Gaussian function, so the value shown may not accurately represent non-normal distributions.

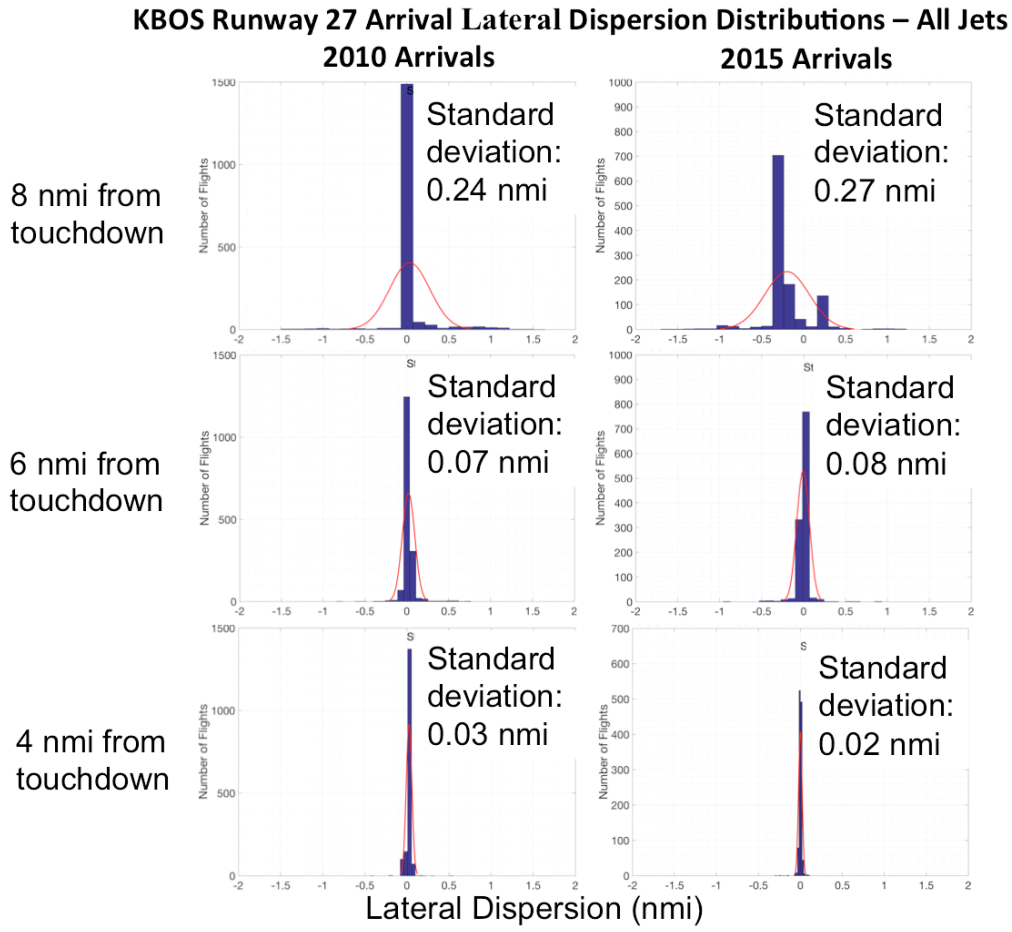

Figure 20. Lateral dispersion distributions for Runway 27 arrivals at KBOS. On the left, 2010 distributions at 4, 6, and 8 nmi from touchdown are shown. On the right, the same distributions for 2015 are shown.

This analysis shows that lateral dispersion is mostly accurately modeled by a normal distribution, particularly close to the airport. The normal distribution fits well at 4 and 6 nautical miles. When the flights are 8 nautical miles from touchdown in both 2010 and 2015, however, the normal distribution does not fit as well. Instead, there is a sharply peaked normal distribution in the center of the distribution with some outliers distributed to either side. This is likely due largely to difficulties with matching flights to representative trajectories. Based on how clustering parameters are tuned, the clustering algorithm may match some flights that follow the representative track closely near touchdown but diverge farther from the airport. This could lead to the appearance of some outliers, like those at 8 nautical miles from the 2010 data, or could lead to the inclusion of flights from two arrival flows that merge several miles away from

touchdown, which appears to be the case at 8 nautical miles in the 2015 case. Tuning clustering parameters to eliminate these issues completely is very difficult, if not impossible. Thus, due to the difficulty of trajectory classification, arrival lateral dispersion is modeled accurately by a normal distribution near the airport, but the presence of outliers or merging flows makes the fitting of a single normal distribution less accurate farther from the airport.

Next, the lateral dispersion distribution profile—that is, distribution width as a function of path length—was calculated. To represent distribution width, a normal distribution was assumed, and standard deviation of the distributions was used as to quantify width. Given the results described above, these results must be examined with caution, as this method could lead to an apparent increase in width farther from the airport due to the presence of outliers or merging flows. The lateral dispersion profiles are shown in **Figure 21**.

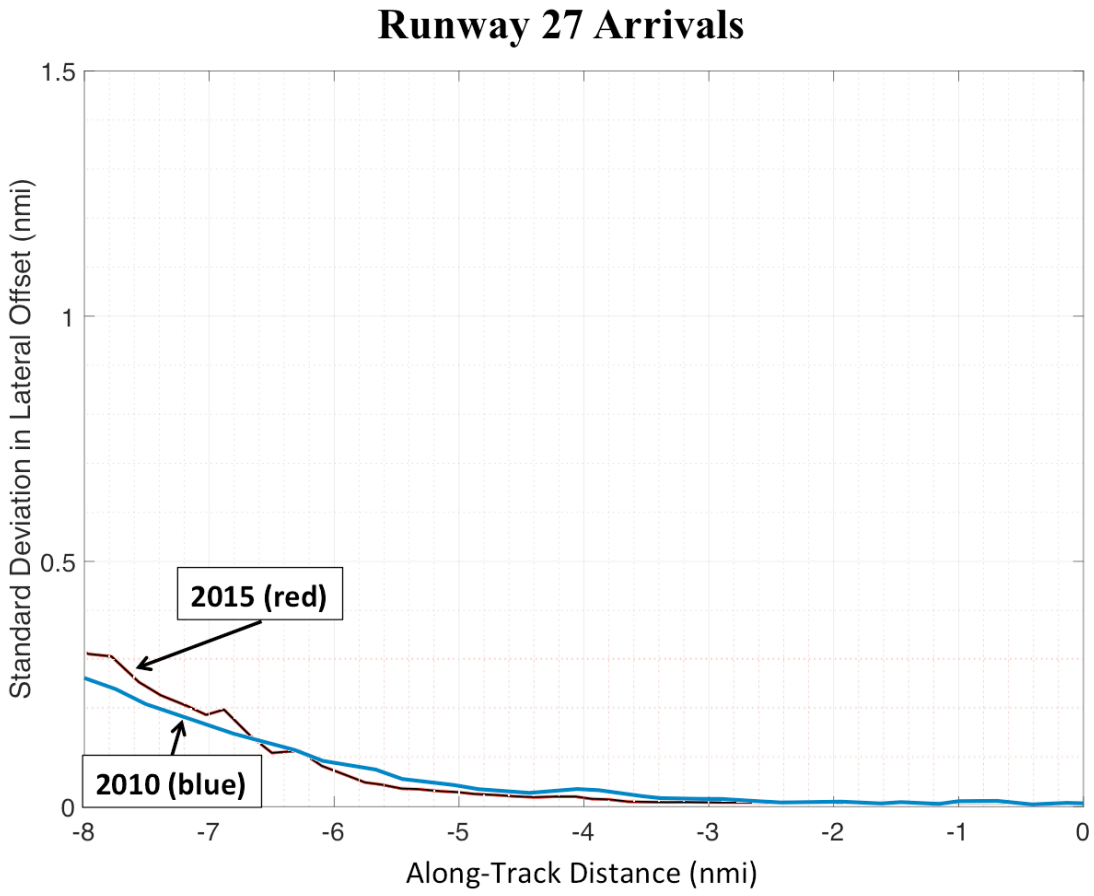

Figure 21. Lateral dispersion profiles for KBOS Runway 27 arrivals in 2010 and 2015.

While dispersion does increase farther from the airport, some of this increase is due to the trajectory classification issues described above. It is interesting to note, however, that there is very little flight track dispersion for most arrivals close to the airport in both 2010 and 2015. This is expected, most aircraft use precision approach procedures such as instrument landing system (ILS) or RNAV. These procedures allow for close precision in lateral track. Because precision approach procedures have been available for many years—much before RNAV procedures were present—in the vicinity of the airport, lateral dispersion does not exhibit major changes from 2010 to 2015.

For departures, however, no such precision procedures existed in 2010. Because of this, it was expected that departures in 2010 would have much more lateral dispersion than departures in 2015. This expectation was confirmed by the analysis, and an example of this analysis is shown for KBOS Runway 33L departures. The ground tracks for these departures are shown in **Figure 22**.

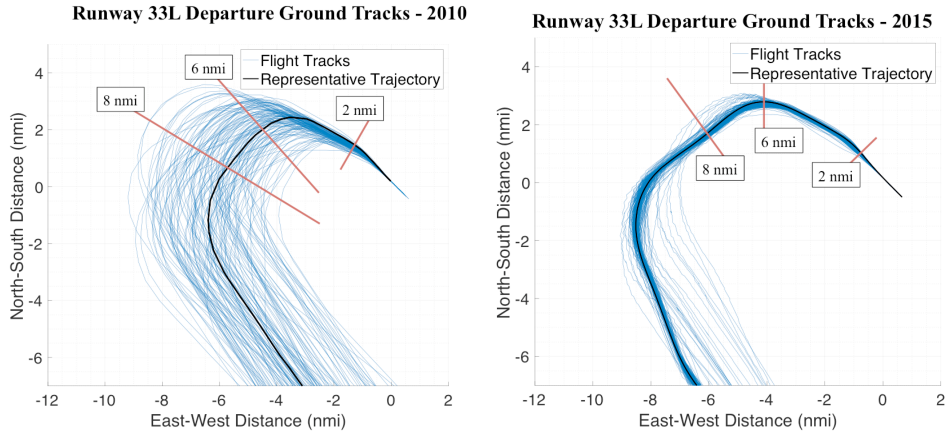

Figure 22. Runway 33L departure tracks in 2010 and 2015. Cross sections where distributions were examined are shown in red.

As shown in the figure above, cross sections of these ground tracks were taken at 2, 6, and 8 nautical miles in order to examine the distribution of lateral offset values. The results of this analysis are shown in **Figure 23**.

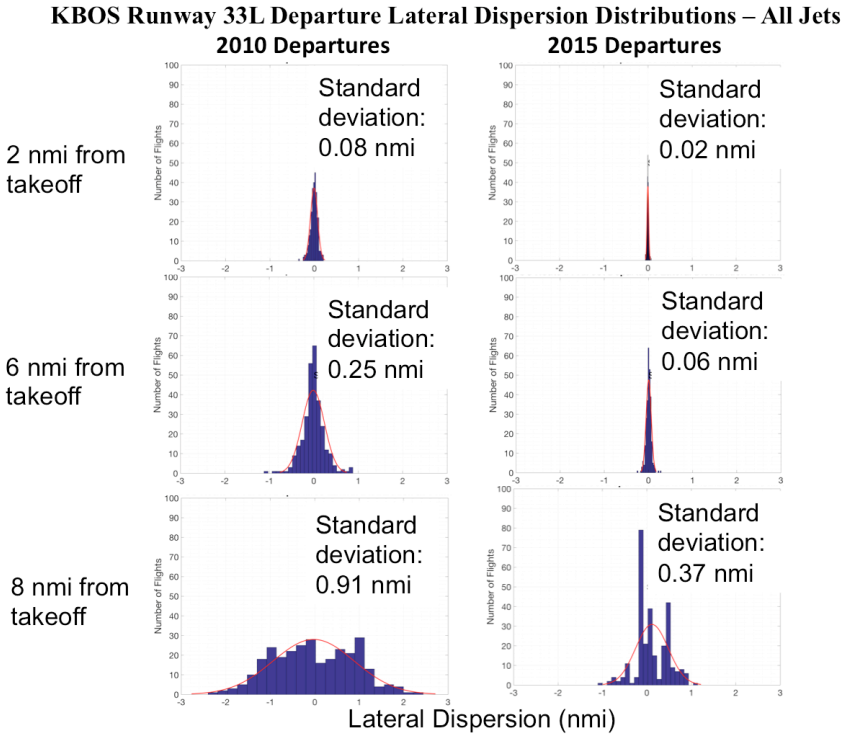

Figure 23. Lateral dispersion distributions for Runway 33L departures at KBOS. On the left, 2010 distributions at 2, 6, and 8 nmi from takeoff are shown. On the right, the same distributions for 2015 are shown.

As expected, dispersion was found to have a much wider distribution in 2010. At each station, the standard deviation of the fitted Gaussian curve is 2-4 times larger in 2010. It also appears that a Gaussian curve fits the distributions quite well closer to the airport, at the 2 and 6 nautical mile stations, but once again is less accurate as the aircraft get farther away at the 8 nautical mile station. Similarly to arrivals, this is likely because aircraft that follow the same initial departure procedure later split into several different flows based on their final destination, meaning that the distribution would be better modeled at these stations by multiple different Gaussian distributions. In general, then, it seems that a single normal distribution can be used to model lateral distribution near the airport, but due to the trajectory classification methods used, a single normal distribution may not be sufficient farther from the airport.

Using this analysis, lateral dispersion distribution profiles were also calculated for departures, and these profiles are shown in **Figure 24**.

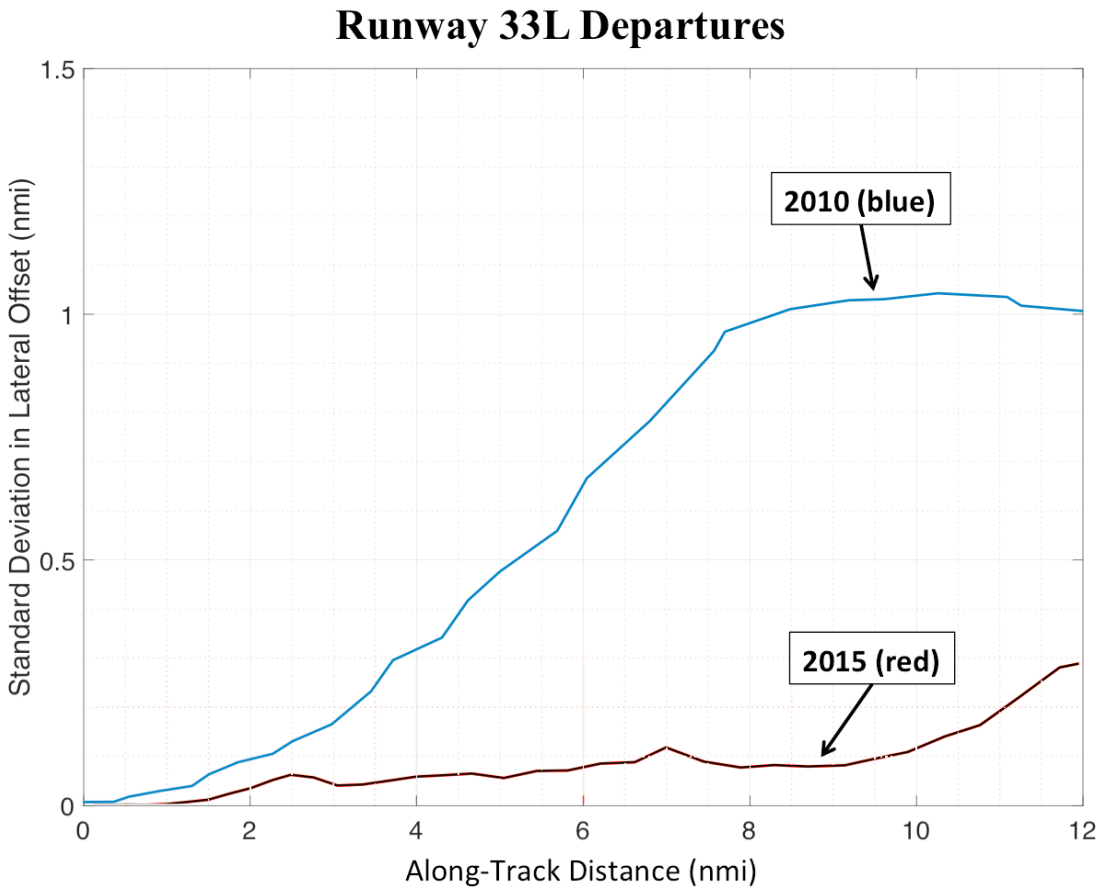

Figure 24. Lateral dispersion profiles for KBOS Runway 33L departures in 2010 and 2015

As expected, these profiles show a sharp concentration effect between 2010 and 2015 due to the implementation of RNAV.

3.2.2 ALTITUDE VARIABILITY

As mentioned above, altitude variability has not changed significantly from 2010 to 2015. Because of this, only 2015 results are shown in this analysis. **Figure 25** shows analysis of 20 day 2015 ASDE-X dataset at KBOS.

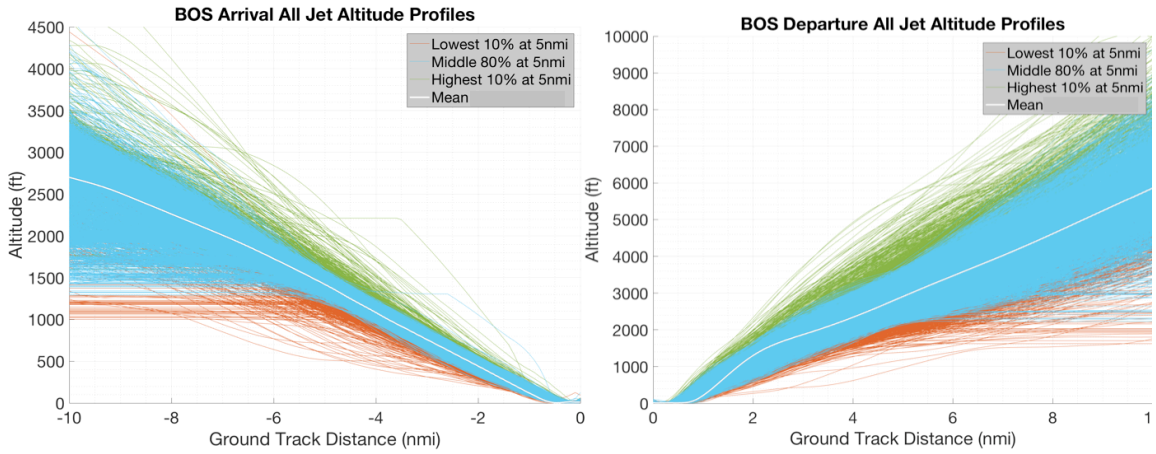

Figure 25. Variability in altitude for 20 days of jet departures at Boston Logan Airport (KBOS).

This figure shows all jet aircraft types, and thus a good deal of variability is present, particularly for departures. Some of this variability is because these figures show all procedures, and altitude profiles may be different for different procedures based on procedure definition or aircraft performance when turning. Further variability is present because different aircraft types have significantly different climb performance attributes. Because of this, and because noise must be modeled separately for each different aircraft type and representative ground track, the following altitude variability analysis was conducted independently for each aircraft type and arrival or departure flow.

For each aircraft type and each route, cross sections were taken at various along-track distances for both arrivals and departures, and each was fitted with a normal distribution. An example of this analysis is shown for Airbus A320 family arrivals on KBOS Runway 4R and KBOS Runway 9 departures. The altitude profiles (altitude as a function of along-track distance) are shown in **Figure 26**.

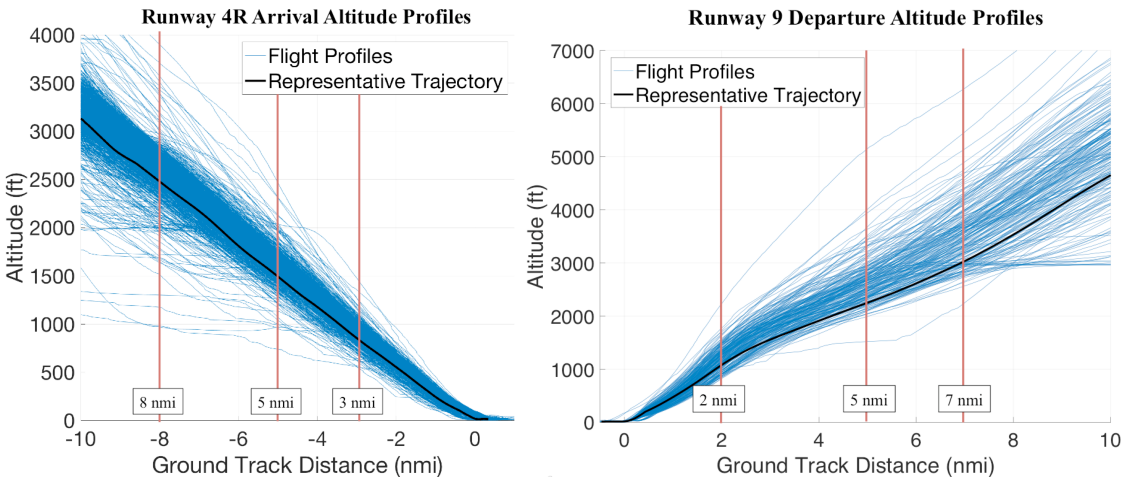

Figure 26. Altitude flight profiles for A320 KBOS Runway 4R arrivals and Runway 9 departures. Cross sections where distributions were examined are shown in red.

Cross sections of these profiles were taken at 3, 5, and 8 nautical miles for the arrivals and 2, 5, and 7 nautical miles for the departures, as shown in the figure above. The distributions at these cross sections are shown in **Figure 27**.

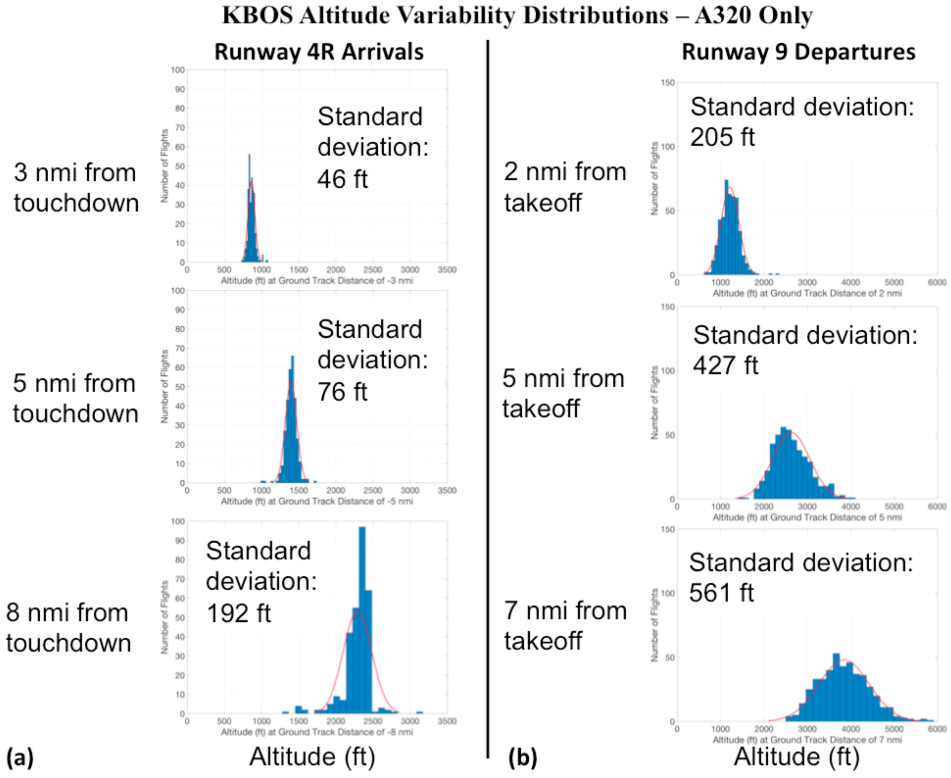

Figure 27. Altitude distributions at KBOS at various along-track distances. On the left, (a) shows A320 Runway 4R arrivals at 3, 5, and 8 nmi from touchdown. On the right, (b) shows A320 Runway 9 departures at 2, 5, and 7 nmi from takeoff. Fitted Gaussian curves are shown in red for each distribution.

It is clear from **Figure 27** that a normal distribution is a fairly close representation of altitude variability in most cases. The worst fit is the arrival case 8 nautical miles from touchdown, likely due to the fact that some outliers level off at unusual altitude due to cloud cover or ATC recommendations before entering the ILS glide slope. Even in this case, however, the Gaussian fit is a reasonably good approximation. Therefore, it does seem to be valid to assume that altitude variability can be modeled by a normal distribution. Using this assumption, altitude distribution profiles were calculated. These profiles are shown in **Figure 28**.

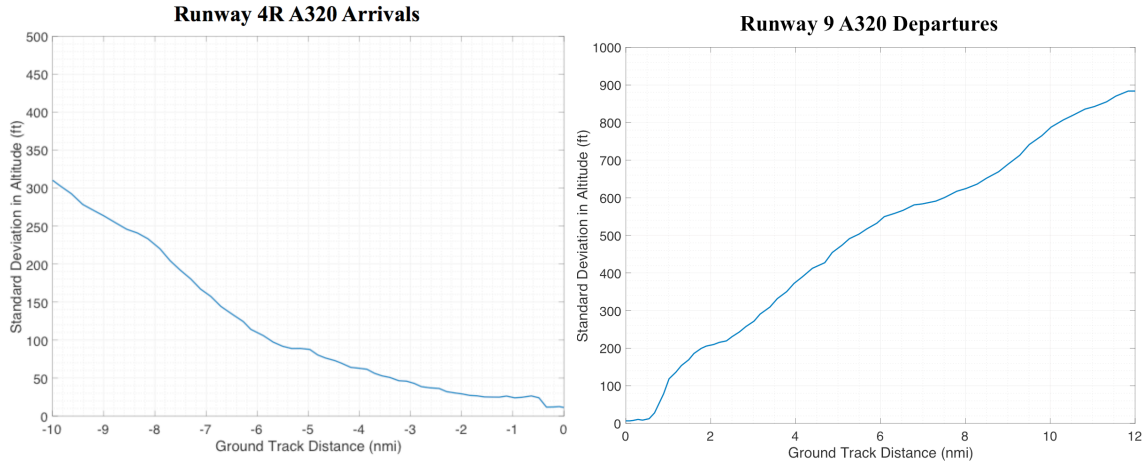

Figure 28. Altitude distribution profiles for A320 KBOS Runway 4R arrivals and A320 Runway 9 departures in 2015.

From this figure, it can be seen that departures exhibit significantly more altitude variability than arrivals, and in both cases variability increases farther from the airport. Arrivals have relatively little variability because they typically use precision approaches such as an ILS, which give pilots the ability to closely track a 3-degree glide slope for their final approach. These precision approaches provide close vertical guidance, which significantly reduces altitude variability for approach procedures.

3.2.3 SPEED VARIABILITY

Because the radar data used for this analysis supplies data on groundspeed, not airspeed, groundspeed data was used to analyze speed variability. Using the same radar data as the previous two sections, speed as a function of along-track distance was plotted for all jets over the 20 days in 2015 and 2016 at KBOS and is displayed in **Figure 29**.

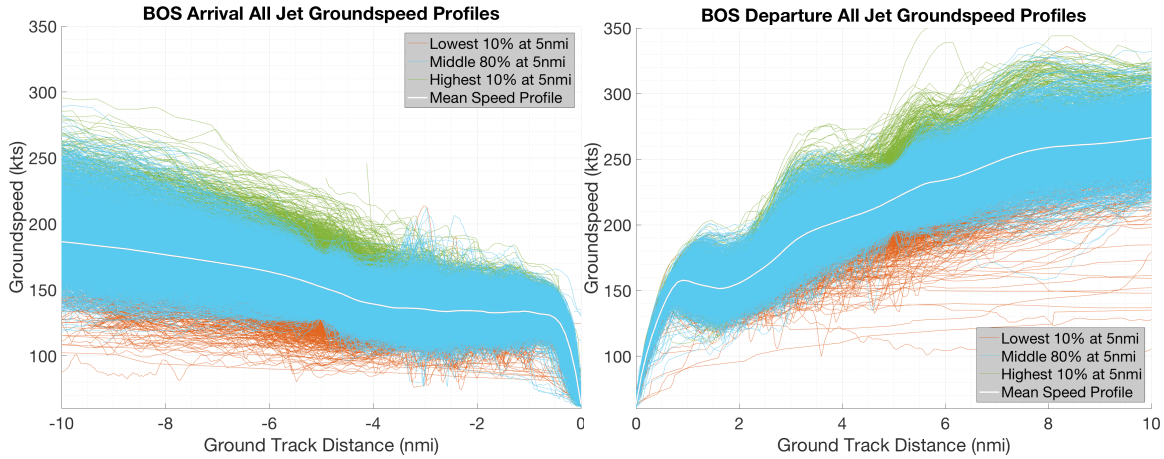

Figure 29. Variability in speed for 20 days of jet departures at KBOS.

Next, as for altitude, speed was analyzed independently for each aircraft type and route. First, distributions of speeds at several discrete along-track distances were analyzed for both arrivals and departures. An example set of speed profiles are shown in **Figure 30** for aircraft in the Airbus A320 family. Once again, this example shows KBOS Runway 4R arrivals and Runway 9 departures.

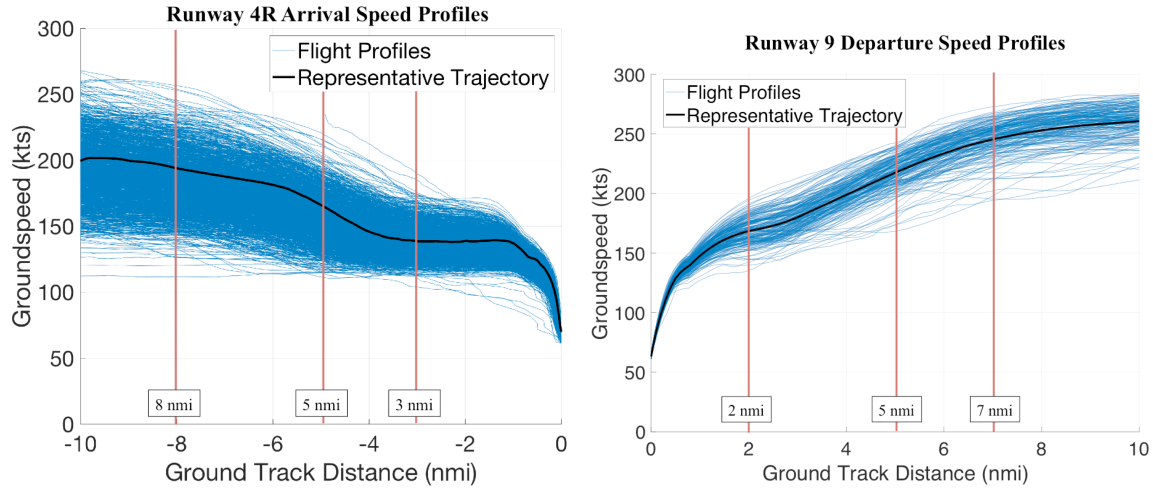

Figure 30. Speed flight profiles for A320 KBOS Runway 4R arrivals and Runway 9 departures. Cross sections where distributions were examined are shown in red.

The distributions taken at the cross sections shown in the above figure are shown in **Figure 31**.

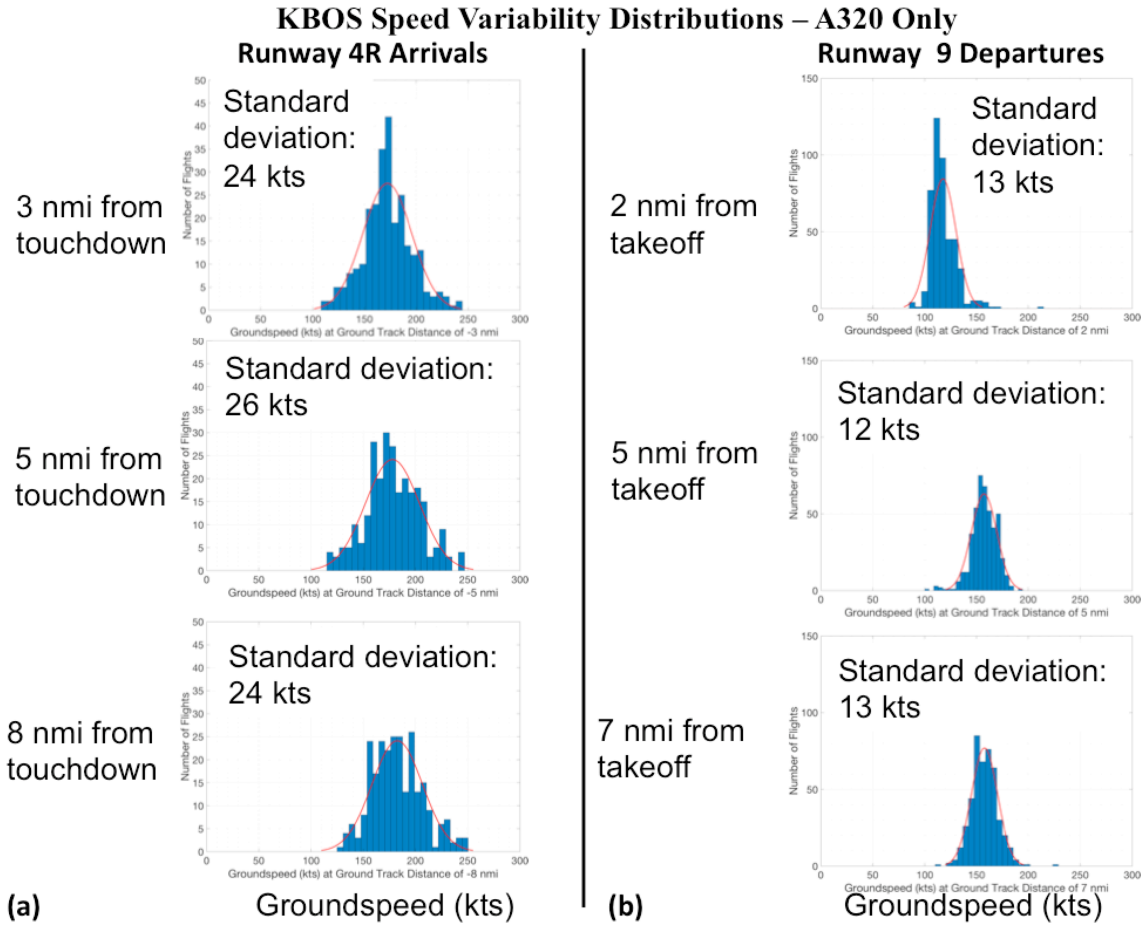

Figure 31. Speed distributions at KBOS at various along-track distances. On the left, (a) shows A320 Runway 4R arrivals at 3, 5, and 8 nmi from touchdown. On the right, (b) shows A320 Runway 9 departures at 2, 5, and 7 nmi from takeoff. Fitted Gaussian curves are shown in red for each distribution.

The Gaussian curves used to fit these distributions represent the distribution quite accurately, although there is some noisiness in the fit for arrivals, likely due to arrival aircraft carefully holding discrete speeds in some cases, making those values spike in the distribution. Nonetheless, it does appear from this analysis that speed variability can be fairly accurately modeled as a normal distribution. Using this assumption, speed distribution profiles were calculated and are shown in **Figure 32**.

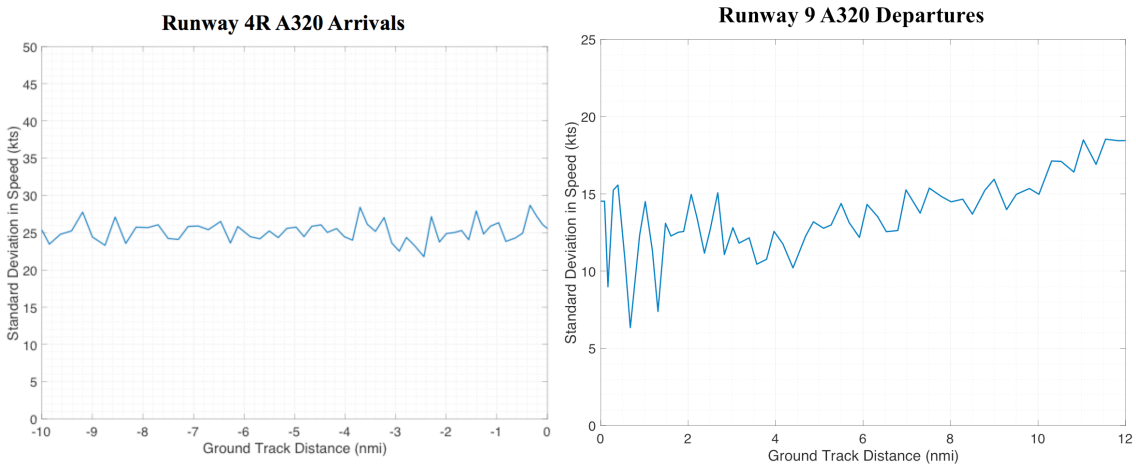

Figure 32. Speed distribution profiles for A320 KBOS Runway 4R arrivals and A320 Runway 9 departures in 2015.

Interestingly, speed variability shows little correlation with distance from the airport. This is likely because most variability in speed within aircraft of the same type on the same route is due to differences in aircraft weight or wind speeds, which do not vary significantly on this scale with distance from the airport.

3.2.4 VARIABILITY CORRELATION

So far, each type of variability has been considered independently. To fully capture the effects of flight track variability on noise, however, it is important to understand any correlations between flight track lateral dispersion and speed or altitude. Although speed and altitude are well modeled by a normal distribution, it is possible that these distributions have some correlation with lateral dispersion. For example, if flights with a higher lateral offset from the route's representative trajectory tend to be at a higher altitude or a faster speed, this effect could be important to model.

To detect these correlations, the 2015 KBOS radar dataset was analyzed to find both altitude and speed as a function of lateral offset at each flight segment. First, data was examined manually to look for immediately apparent correlations, but there was no clear correlation for either speed or altitude and lateral offset. Next a more rigorous analysis was performed: at each segment, a linear best fit was applied and its r-squared value was checked. None of these fit lines had an r-squared value greater than 0.2. **Figure 33** shows speed and altitude plotted against lateral offset for an example departure route.

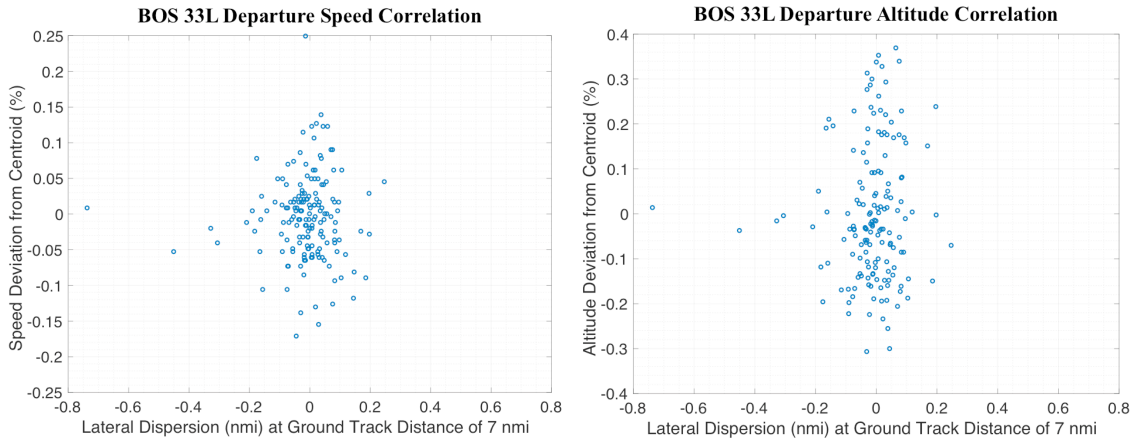

Figure 33. Examples of correlation analysis performed on 2015/2016 radar data at KBOS. There does not appear to be a correlation between either speed or altitude and lateral offset.

This shows that there is no significant correlation between the different forms of variability, and thus that each can be modeled independently.

CHAPTER 4 NOISE MODELING

This chapter will first describe the current state of noise modeling, which helps elucidate the need for fast, accurate variability modeling. Next, the results of Chapter 3 will be examined to determine which forms of variability are most important for noise modeling.

4.1 CURRENT STATE OF NOISE MODELING

The current tool used for all official FAA for noise modeling is the Aviation Environmental Design Tool (AEDT). AEDT is an integrated tool capable of modeling a wide range of environmental impacts. Its noise model uses the same method as the FAA's former standard noise modeling tool, the Integrated Noise Model (INM). This noise model is a faithful implementation of Society of Automotive Engineers (SAE) Aerospace Information Report (AIR) 1845, titled "Procedure for the Calculation of Airplane Noise in the Vicinity of Airports". This report is recognized by the FAA as the official methodology for the calculation of aircraft noise, and both the European Civil Aviation Conference (ECAC) and the International Civil Aviation Organization (ICAO) have accepted nearly identical methods. [24]

SAE AIR 1845 employs a Noise-Power-Distance (NPD) approach to modeling noise. Each aircraft type has a database of noise vs. distance curves for a range of thrust settings and for both approach and departure. These curves are constructed from measured noise certification data. From this database of NPD curves, noise can be interpolated at any observer location based on the position and thrust setting of the aircraft. Because noise certification data is measured for strictly defined flight profiles with constant configuration—full flaps and gear for arrivals, takeoff flaps for departures—noise effects due to different aircraft configurations cannot be captured by NPD methods. This approximation is reasonable near the airport when aircraft are usually close to the configuration used for the certification testing, but could break down for cleaner configurations farther from the airport. Some example NPD curves used by AEDT are shown in **Figure 34**. In addition to the raw NPD values, frequency information

at each 1/3-octave band is measured and captured through spectral adjustments based on representative classes of aircraft.

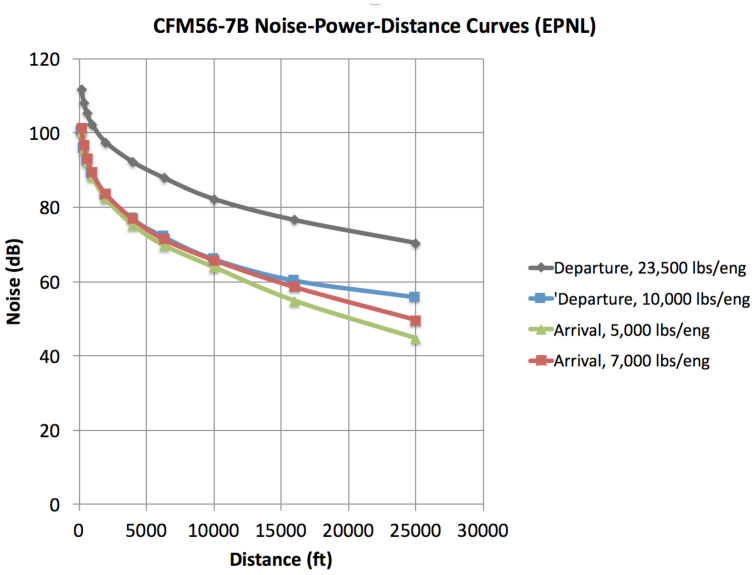

Figure 34. Noise-Power-Distance curves for the CFM56-7B, an engine commonly used in the Boeing 737-800. Two arrival and two departure curves are shown. Typically five thrust settings for arrivals and five for departures are used for a full set of NPD curves.

In order to apply this methodology, flight profiles are modeled as a series of segments with thrust, speed, and altitude modeled for each segment. This flight profile is then matched to the specified ground track. A series of observer locations are defined to create a grid of points where noise is calculated. This process is illustrated in **Figure 35**.

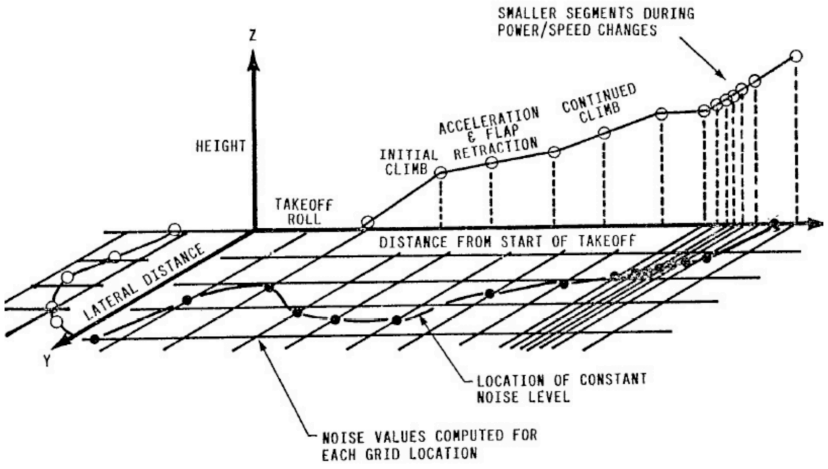

Figure 35. Illustration of flight profile segments, ground track, and observer grid definitions for AEDT. [25]

In addition to the NPD calculation, AEDT has empirically derived corrections to adjust for atmospheric attenuation of noise, engine shielding effects, changes in exposure duration due to speed, and ground absorption effects. Atmospheric attenuation can be modeled according to several standards. SAE AIR 866A defines a simple set of atmospheric attenuation assumptions based on ½ octave band attenuation. It assumes a "reference day" of 25 degrees C and 70% relative humidity and a standard atmosphere. SAE 5534, published in 2013, provides a more detailed atmospheric attenuation model, accounting for changes in density and temperature of the air at different altitudes. [12]

One advantage of using a model that implements SAE AIR 1845 is that the method has been extensively validated. When the report was published in 1986, DNL values at 7 representative airports were both modeled using SAE AIR 1845 and were measured. On average, the modeled DNL values were within 0.3 dB, and for all airports the model agreed with the measured values to within 2 dB. [25] AEDT and its predecessor INM have also been the subject of numerous other validation efforts, such as a joint NASA-Boeing-FAA study in 2003 and continuous validation of AEDT's NPD curves and aircraft performance data through partnerships with aircraft manufacturers. [24]

One potential shortcoming of the NPD approach is its inability to model changes in aircraft noise due to changes in airspeed or configuration (changes in flap and gear settings). As mentioned earlier, using noise certification data to construct these curves assumes a constant aircraft configuration. Additionally, however, certification flight profiles specify fairly low speeds, and thus noise effects due to higher speed profiles also cannot be captured by NPD methods. Since noise generated by the airframe is highly speed dependent, this means that the assumptions used in NPD methods can cause substantial error in regimes where airframe noise dominates. [26] Airframe noise typically becomes dominant in higher speed, lower thrust flight segments, such as departure profiles after thrust cutback. This is a potential concern, because SAE AIR 1845 was created primarily with the intention to model the 65 DNL level accurately due to the land use compatibility requirements dictated by FAR Part 150. For modern airports, the 65 DNL level is quite close to the airport, where high thrusts causes engine noise to dominate airframe noise. This could mean that AEDT is able to accurately model

the 65 DNL noise contour, but loses fidelity for modeling farther from the airport, where complaints have spiked since the implementation of PBN procedures. Other higher-fidelity noise models, such as NASA's Aircraft Noise Prediction Program (ANOPP), are able to account for speed effects at the cost of significantly more computational expense.

4.2 EXISTING LATERAL DISPERSION MODELING METHODS

AEDT has limited capabilities for modeling flight track variability. The NPD approach makes it difficult to model any speed effects with much fidelity, so AEDT is essentially unable to model variability in speed. Also, no particular technique currently exists in AEDT to model variability in altitude (other than to define and model many flight profiles with a range of altitudes and model each flight individually). There is a built-in functionality to model flight track lateral dispersion, but the method provided is not physically realistic and not very accurate.

The current industry-standard practice for modeling lateral variability is to model each flight individually. Radar data is used to find a unique flight track for each flight and a standard flight profile is assigned based on the aircraft type of the given flight. Then individual noise impacts can be calculated for each flight—typically using AEDT—and these individual contributions are summed to yield overall noise impacts for the airport. Although this process yields accurate results, this process is extremely computationally expensive.

AEDT's built-in functionality for modeling lateral dispersion works by simply adding parallel flight tracks. The user can also specify a number of tracks from 3 to 9, and specify the width of the dispersion and the percentage of flights on each track. This approach could give accurate results farther from the airport, but is clearly inaccurate near the airport, where flights are modeled as taking off several miles laterally offset from the runway. AEDT's approach to dispersion modeling is pictured in **Figure 36**.

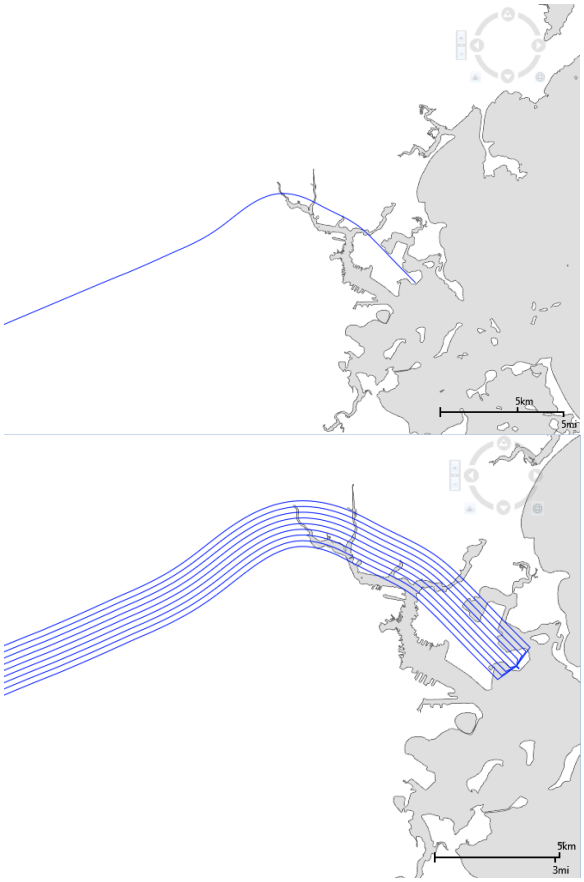

Figure 36. An example of AEDT's lateral dispersion modeling functionality. On the left, a single departure track on Runway 33L at Boston Logan Airport (KBOS) is shown. On the right, the same track is modeled with AEDT's dispersion modeling tool. This approach is not physically realistic near the runway.

This is a simple way to capture some effects due to flight track dispersion, but it does have limitations. First, with this method, dispersion cannot change over the course of the flight track—all tracks run parallel, so dispersion is present on the runway and stays constant throughout the flight. This introduces some error, because for real flights, dispersion typically increases as flights get farther from the airport, and, of course, there is no dispersion on the runway. Further, in selecting a limited number of flight tracks, some amount of discretization error will be introduced. Particularly for highly dispersed routes, a limited number of tracks could produce visibly discretized noise contours, with peaks in noise under each track that is not present in real operations.

Thus, existing methods for modeling the noise due to lateral dispersion are either extremely computationally expensive or are inflexible and inaccurate. This creates a need for an accurate, efficient tool capable of modeling flight track dispersion.

4.3 RAPID NOISE MODELING METHODOLOGY

Assessment of system-level aircraft environmental impact is a crucial component of decision making for analysts, regulators, and industry stakeholders. Changes in fleet mix, frequency, gauge, or operational procedures all drive change in noise. The FAA mandates the submission of a costly and time-intensive environmental analysis for any procedural or infrastructure modification that changes noise impacts by 1.5 dB within the 65 dB contour in terms of Day-Night Level (DNL) [3].

While NPD methods are efficient for the computation of a single flight, modeling the noise impacts of all flight operations for an entire airport is still a costly, time consuming process because each flight must be modeled individually in AEDT. This makes the exploration of multiple potential scenarios difficult. With the ability to rapidly model the noise impacts of all operations at an airport, stakeholders could quickly compare a much broader set of possibilities. This rapid assessment could then be supplemented by higher fidelity modeling using tools such as AEDT.

With this in mind, an approach for rapidly modeling noise was developed. [27] The central concept this rapid noise modeling method is to represent each route with a single representative trajectory. This allows for modeling noise from the entire airport using only tens of unique flight trajectories instead of the thousands that would be required for a direct calculation of each flight individually. One significant downside of this approach, however, is its inability to account for lateral flight track dispersion. The method uses radar data to find these representative trajectories and calculate flight profiles for each aircraft type modeled. These trajectories and profiles are then used to model single event noise for each representative trajectory using an existing noise tool (AEDT or ANOPP). At this point, the dispersion model can be implemented to allow each route to account for its unique lateral dispersion profile, and these results are saved in a gridded, single flight equivalent form. Next, the gridded single-event noise results for each are stored in a database, which can be queried to rapidly sum noise for various scenarios. One benefit of this approach is that once the single-event noise results are calculated, system-level noise results for different scenarios and schedules can be very

rapidly calculated. An architecture diagram for this approach is shown in **Figure 37**, and each component of this architecture is discussed in more detail below.

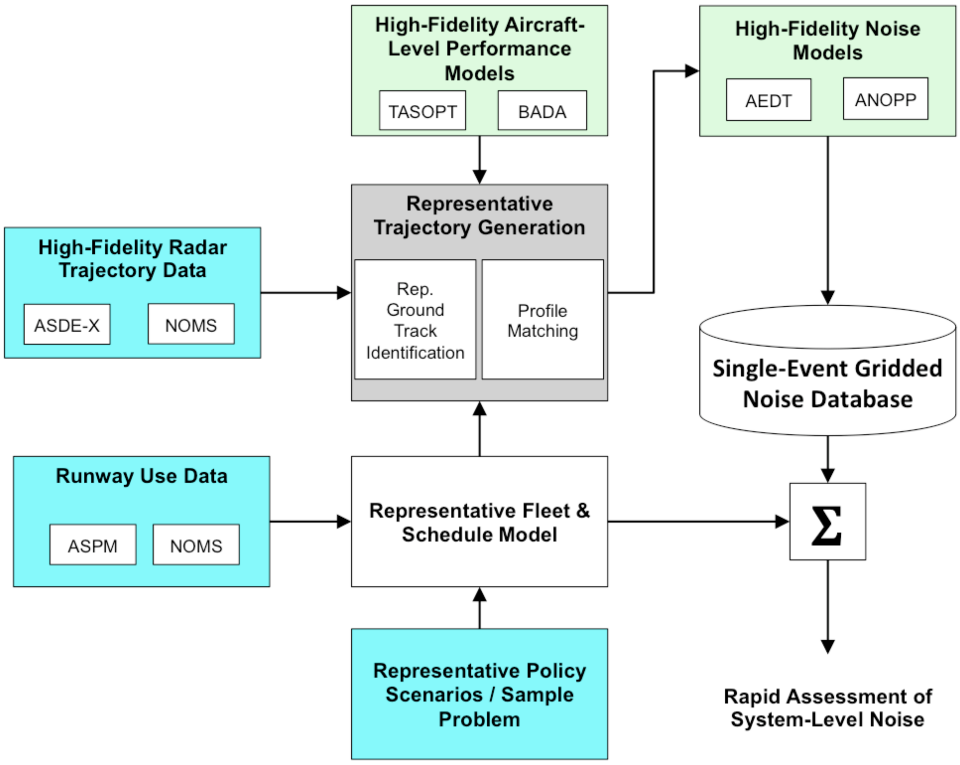

Figure 37. Rapid noise modeling method architecture without accounting for lateral dispersion.

4.3.1 Representative Trajectory Generation

A trajectory consists of two components: a ground track and a flight profile defining altitude, speed, and thrust as a function of along-track distance. Representative ground tracks were selected based on the radar data representative trajectory identification methods described in Section 3.1.2. Given these tracks, standardized flight profiles were calculated for each aircraft type used. In order to obtain the speed, thrust, altitude, and configuration parameters necessary to model each profile, a flight profile generator was created[1] to compute the thrust profile from existing radar track data or a user-defined procedure definition. The thrust calculation uses a kinematics approach based on flight path angle, aircraft weight, aerodynamic data, and thrust. The user specifies a subset of thrust, configuration, velocity, acceleration rates, position, and/or

[1] The flight profile generator was created by Jacqueline Thomas as part of her Master's thesis. [31]

flight path angle. Given enough defined requirements, the profile generator computes the remaining parameters to provide a fully defined arrival or departure profile in terms of position and thrust.

All arrivals were assumed to be at 75% of Maximum Takeoff Weight (MTOW) and to fly an ICAO standard 3-degree glide slope approach. This procedure was observed to match radar data quite well, as shown in **Figure 38** (a). Departures were assumed to be at 90% of MTOW and to fly an ICAO standard departure, but with several modifications to better match radar data. ICAO standard departures consist of an initial high-thrust climb segment, a thrust cutback between 800 and 1500 feet, an acceleration to 250 knots indicated airspeed (IAS), and finally a climb at 250 knots IAS to 10,000 feet. [28] The flight profile for each aircraft type was matched to the mean radar altitude profile for departures of the same aircraft type at the same airport. To do this matching, first, takeoff roll length was matched. Next, takeoff thrust was de-rated to match the initial angle of climb of the mean profile. With this de-rate applied, the thrust cutback altitude was allowed to vary to minimize root-mean-square (RMS) distance from the mean altitude profile. Finally, climb thrust was de-rated, once again to minimize RMS distance from the mean altitude profile.[1] An example of this matching for Boeing 737-800 departures at KBOS is shown in **Figure 38** (b).

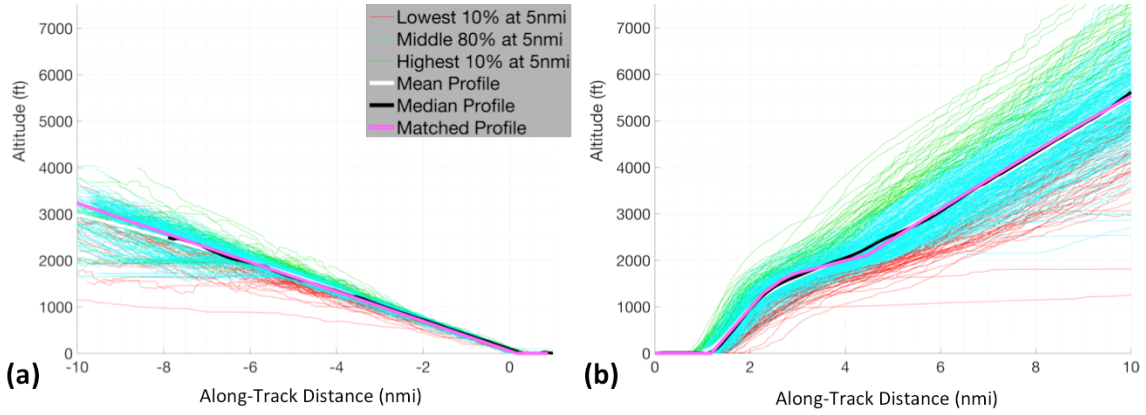

Figure 38. On the left, (a) shows radar matching of Boeing 737-800 arrival flight profiles at KBOS. On the right, (b) radar matching of Boeing 737-800 departure flight profiles at KBOS.

[1] This profile matching methodology was developed in collaboration with Morrisa Brenner.

An example of these matched flight profiles showing speed, altitude, and thrust as a function of along-track distance is shown for the Boeing 737-800 (B738) in **Figure 39**. The B738 is used as an example for many results in this thesis; unless otherwise specified, these matched flight profiles are used for all noise modeling.

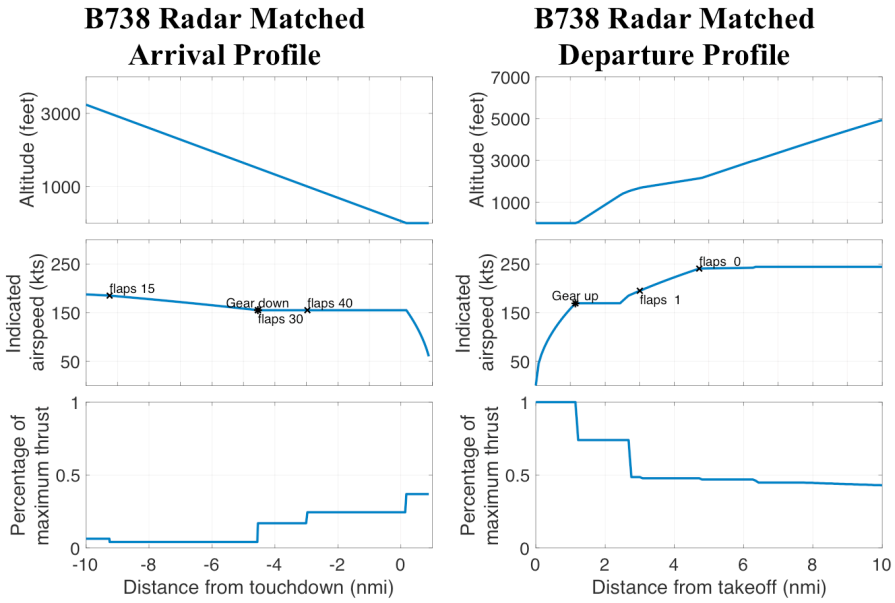

Figure 39. Example radar matched flight profiles for the Boeing 737-800.

4.3.2 REPRESENTATIVE FLEET & SCHEDULE

In order to calculate airport-scale noise, a fleet of representative aircraft types and a schedule of flights were defined. This information was derived from single-flight runway use records, which can be found in sources such as the Aviation System Performance Metrics (ASPM) database or airport-specific datasets like NOMS. The final output of this analysis had two components: the representative fleet and the representative schedule. The representative fleet is an assignment of each aircraft type present in the radar data to a representative type of a similar size and with similar noise impacts. Modeling the noise for each type individually would require defining a unique flight profile for aircraft type, so this approach produces significant computational savings.

Seven representative aircraft types were used, and each aircraft type was assigned to one of the representative types based on the categories shown in **Table 2**.[1]

Table 2. Table of aircraft categories and each category's representative aircraft type.

Aircraft Category	A320 Family	B737 Family	Older aircraft	Large regional jet	Small regional jet/ Business jet	B757 family	Large, twin-aisle jet
Representative Aircraft Type	A320	B738	MD88	E170	E145	B753	B773

The representative schedule is a full assignment of number of flights to representative ground tracks over a representative day—for example, a certain departure ground track could be assigned 50 Boeing 737-800 departures and 60 Airbus A320 departures on a representative day.

4.3.3 NOISE COMPUTATION

Given a set of representative trajectories and a fully defined schedule, noise computation had several steps. First, single-event noise contours were calculated using an existing noise model (e.g. AEDT) for each representative trajectory for each aircraft type in the representative fleet. This noise result is then saved to the single-event gridded noise database. Once saved, these results were summed according to the schedule to produce airport-wide contours for multi-event metrics such as DNL and N_{above}.

4.3.4 ACCOUNTING FOR VARIABILITY

While the method presented in this section is highly efficient, it does not account for any flight track lateral dispersion along arrival or departure routes. This could cause significant error, particularly for routes with significant lateral dispersion. This could be

[1] This aircraft type categorization was defined by Morrisa Brenner as part of her thesis. [30]

corrected, however, using a dispersion model capable of quickly and accurately calculating the noise impacts of dispersion. An updated architecture including lateral dispersion modeling is shown in **Figure 40**.

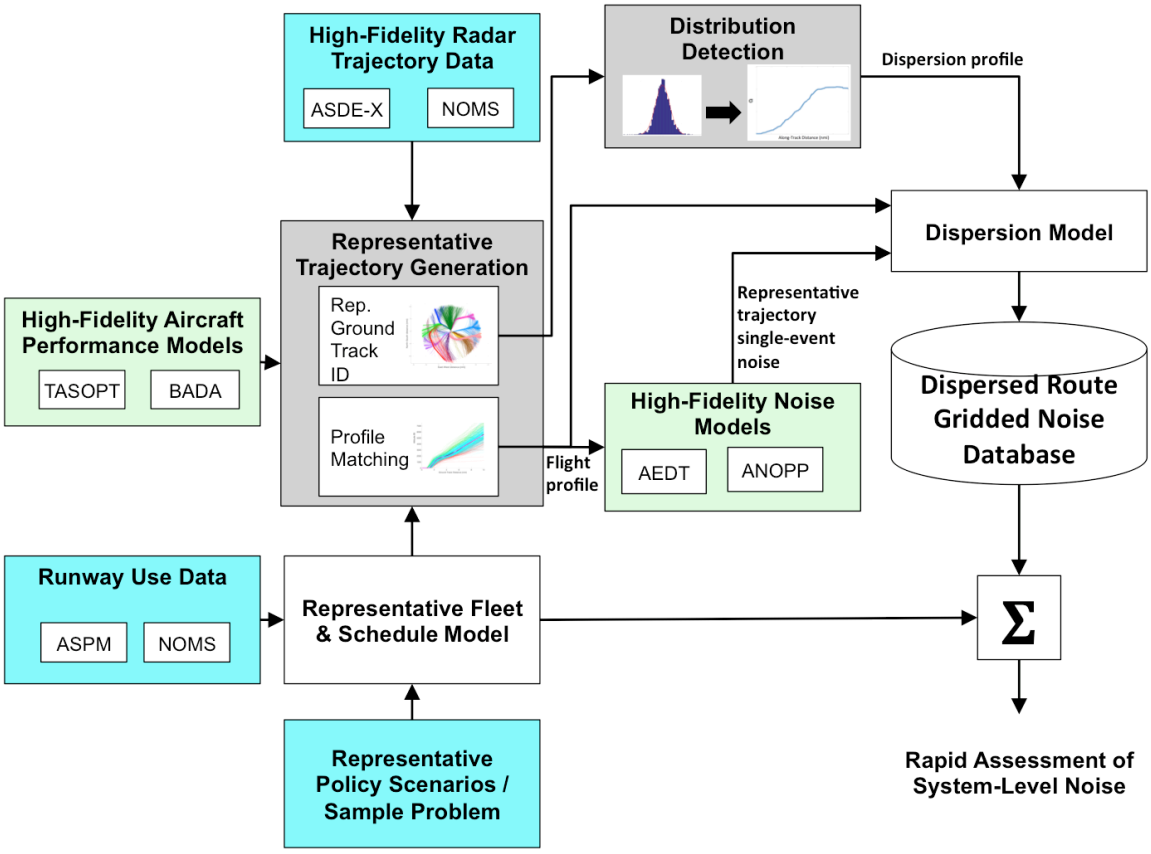

Figure 40. Rapid noise modeling architecture with lateral dispersion modeling.

Using this method, it would be possible to rapidly and accurate model noise on the scale of an entire airport. To date, however, no such dispersion model exists. In the following chapter, a dispersion model will be introduced capable of filling this role.

4.4 Noise Modeling Implications of Variability

In order to determine which effects must be modeled to create a tool capable of accounting for the noise impacts of flight track variability, this section will examine the noise impacts of the different forms of variability discussed in Chapter 3.

4.4.1 Altitude Variability Noise Modeling

Differences in altitude, of course, lead to differences in aircraft noise as the distance between the aircraft and the observer changes. Thus, once variability in altitude was quantified, the implications of this variability for noise modeling were considered. To do this, it was first necessary to define a relationship relating aircraft altitude to noise level. Without accounting for differences in atmospheric absorption or wind, the relationship between altitude and noise is dictated by the inverse square law, illustrated in **Figure 41**.

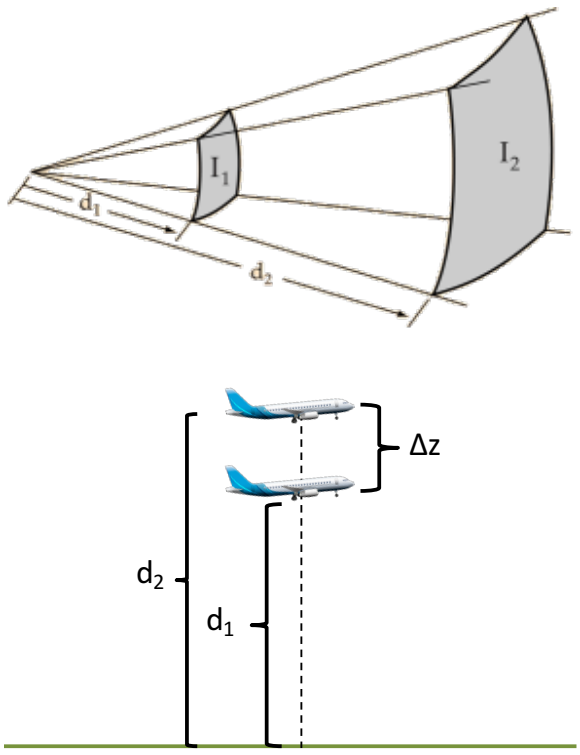

Figure 41. On the left, an illustration of the inverse square law, where d_1 and d_2 are two different observer differences and I_1 and I_2 are the sound intensities at each distance. On the right, d_1 and d_2 are illustrated in the context of airplane altitude differences.

Using this relationship, an expression for noise differences due to differences in altitude was derived, and is shown in Equation (3).

$$\Delta SPL = 10log10\left(\left[\frac{d_1}{d_2}\right]^2\right) \quad (3)$$

This equation can be used to build an intuition for how much altitude differences impact noise. Using the values determined from the analysis in Chapter 3, at an along-track distance of 8 nautical miles a typical altitude would be 4,500 feet and KBOS Runway 9 departures had an altitude standard deviation of about 6,00 feet. For a flight 1 standard deviation from the mean altitude, then, these values correspond to a noise difference of 1.1 dB, which is significantly less than the minimum audible difference of 3 dB (assuming that the mean noise is at least 40 dB).

While this simple analysis helps build intuition, a more important question from a modeling standpoint is how the full distribution of altitudes will impact noise. More specifically, a great deal of computational expense can be saved if each flight is modeled at the altitude of the mean of the distribution rather than on an individual basis. This approximation will introduce some error, however, due to the nonlinearity of Equation (3). To quantify how good or bad an approximation this is, an expression was derived to calculate the mean error in noise levels due to modeling aircraft normally distributed in altitude using only the mean altitude. This expression, shown in Equation (4), represents the mean noise difference, relative to the mean altitude, of all flights in the distribution. It was obtained by integrating the product of a Gaussian probability density and the expression for noise difference due to altitude difference (Equation (3)).

$$\Delta SPL_{mean} = \frac{1}{z_2 - z_1}\int_{z_1}^{z_2} \frac{20}{\sqrt{2\pi\sigma^2}} e^{-\frac{(z-z_{mean})^2}{2\sigma^2}} \log_{10}\left(\frac{z_{mean}}{z}\right) dz \qquad (4)$$

In this expression, z_1 and z_2 are the region over which the mean is taken, σ is the standard deviation of the Gaussian distribution, z is the altitude of a particular flight, and z_{mean} is the altitude of the mean of the Gaussian distribution. This integral has no indefinite result, but it can be evaluated numerically by choosing representative values for each variable. Again, using the values from Chapter 3, $z_1 = 0\ ft$, $z_2 = 10{,}000\ ft$, $\sigma = 600\ ft$, and $z_{mean} = 4{,}500\ ft$ yields the result $\Delta SPL_{mean} = 7.9 * 10^{-6}\ dB$. This miniscule noise difference occurs because in a normal distribution, the highest probability values are quite close to the mean, and for every flight above the mean that creates less

noise, another flight exists equally far below the mean that creates more noise and these effects largely cancel out. This analysis demonstrates that modeling flights normally distributed in altitude using only the mean altitude of the distribution is a very good assumption.

4.4.2 Speed Variability Noise Modeling

Given the assumption that speed variability is normally distributed, an analysis was conducted to model the extent to which speed variability impacts noise. To model this, it was first necessary to determine the relationship between aircraft speed and noise. Speed can impact aircraft noise in two ways: speed-dependent engine noise effects and speed-dependent airframe noise effects. Although both effects exist, airframe noise has a much larger dependence on speed than engine noise. [26] Because of this, it is reasonable to approximate speed-dependent differences in noise as the difference in airframe noise at different speeds. The relationship between airspeed and airframe noise is shown in Equation (5). [29]

$$< P_0^2 >= \frac{\Pi^*}{4\pi r_s^{*2}} * \frac{D(\theta,\phi)F(S)}{(1 - M_\infty cos\theta)^4} \quad (5)$$

In this equation, $< P_0^2 >$ is the mean-squared sound pressure, r_s^* is a dimensionless expression for observer distance, θ is polar angle, ϕ is azimuthal angle, $D(\theta,\phi)$ is a directivity function, $F(S)$ is a function modeling spectral effects, M_∞ is free stream Mach number, and Π^* is an expression for acoustic power that is uniquely defined for each airframe component. For many components such as wing trailing edge, horizontal tail, and vertical tail, however, this Π^* expression is equal to a constant times M_∞^5. Directly below the aircraft, $\theta = \frac{\pi}{2}$ and therefore $cos\theta = 0$. Thus, holding all variables except for speed constant, $< P_0^2 >$ depends on a constant times speed to the fifth power. Given these simplifications, an expression for the difference in noise directly below the aircraft for two flights with different speeds was derived and is shown in Equation (6).

$$\Delta SPL = 10log10\left(\left[\frac{v_1}{v_2}\right]^5\right) \quad (6)$$

This equation was first used for a simple test to determine how much speed changes impact noise. In Chapter 3 it was shown that at a flight track distance of 8 nautical miles, mean speed is about 250 knots and standard deviation is about 15 knots. Thus, a flight one standard deviation from the mean has an impact 2.1 dB different from the mean. Because this is below the minimum audible threshold, this suggests that speed variability effects may not be important to model.

Next, it was noted that Equation (6) is analogous to Equation (3), but models speed differences instead of altitude differences. Extending this analogy, an expression modeling the mean error in noise due to a normal distribution of speeds was derived, analogous to Equation (4). This expression is shown in Equation (7).

$$\Delta SPL_{mean} = \frac{1}{v_2 - v_1}\int_{v_1}^{v_2} \frac{50}{\sqrt{2\pi\sigma^2}} e^{-\frac{(v-v_{mean})^2}{2\sigma^2}} \log_{10}\left(\frac{v_{mean}}{v}\right) dv \quad (7)$$

Now, instead of altitudes, v_1 and v_2 the speeds over which the distribution is integrated, σ is the standard deviation of the Gaussian distribution modeling speed variability, v is the airspeed of a particular flight, and v_{mean} is the mean of the Gaussian distribution. Once again, this integral can only be evaluated numerically. Example values were chosen based on the Chapter 3 analysis for KBOS Runway 9 departures at an along-track distance of 8 nautical miles, which shows a mean speed of about 250 knots and a standard deviation of about 15 knots. This corresponds to $v_1 = 0\ kts$, $v_2 = 500\ kts$, $\sigma = 15\ kts$, and $v_{mean} = 250\ kts$. These values yielded the result $\Delta SPL_{mean} = 7.9 * 10^{-5}\ dB$, once again demonstrating that modeling each flight with the mean speed will not cause significant error. This allows for significant computational savings, since the speed of each individual flight does not need to be accounted for to yield accurate results.

4.4.3 Flight Track Lateral Variability Noise Modeling

Modeling each flight using the mean ground track will not accurately capture the noise impacts of flight track lateral dispersion. Noise peaks sharply directly under a flight track, and thus any track offset from the mean will produce a significant spike in noise underneath its offset. Because dispersion has decreased significantly with the implementation of RNAV, however, it is possible that this approximation could yield useful results for modeling the noise of RNAV routes, particularly for results closer to the airport where dispersion is at its least. To model any route with a significant amount of dispersion, however, using a representative ground track is insufficient.

The importance of accounting for flight track lateral dispersion can be shown using the inverse square law presented in Equation (3) and the results from Chapter 3. At a flight track distance of 8 nautical miles, the lateral dispersion on the 2010 Runway 33L departure flow has a standard deviation of approximately 1.0 nautical mile, and a typical is approximately 4,500 feet. For an observer offset 1 nautical mile from the representative flight track of the flow, a flight with a lateral offset 1 standard deviation from the mean would result in a 4.5 dB increase in noise relative to the flight flying the mean track. At 8 nautical miles, the corresponding noise differences in speed and altitude one standard deviation from the mean are respectively 2.1 dB and 1.1 dB, both less than the minimum audible threshold of 3 dB. 4.5 dB is a clearly noticeable difference; thus, even if the mean error would be relatively small when integrating over the entire distribution, lateral dispersion is clearly an important difference to model, because the differences for individual flights would be very noticeable.

CHAPTER 5 DISPERSION MODELING METHODOLOGY

One of the main objectives of this thesis is to create a tool capable of modeling the noise impacts of trajectory variability. The analysis in Chapter 4 shows that speed and altitude can be effectively modeled using only the mean values of the distribution, but lateral dispersion cannot, and thus, the tool created must model lateral dispersion.

Lateral dispersion can be modeled for a distribution of many flight tracks flying the same procedure based on known noise contours for a single, central representative trajectory. This concept is illustrated for the simple case of a straight, level overflight in **Figure 42**.

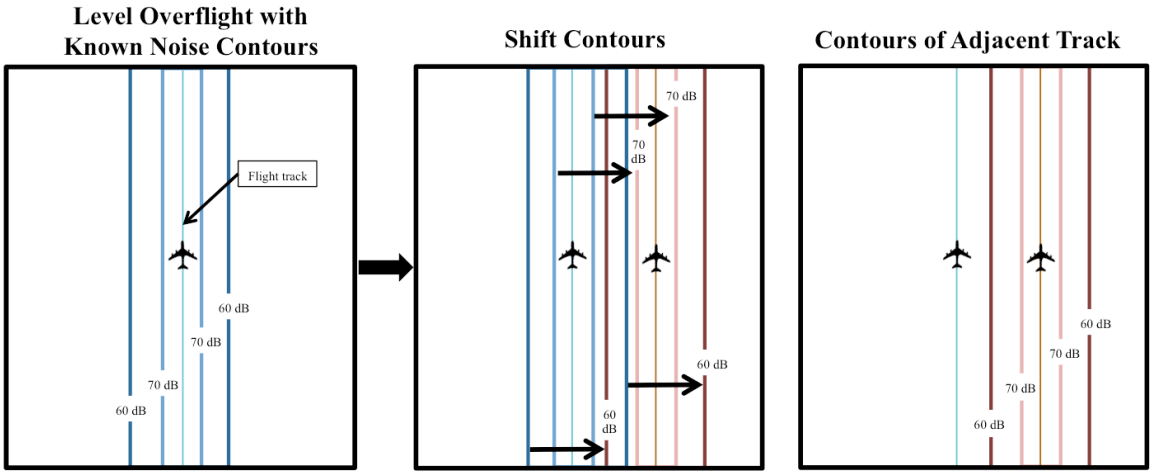

Figure 42. An illustration of using representative trajectory noise contours to calculate noise of laterally offset tracks.

Using this method, it is possible to calculate the noise impacts of any laterally offset tracks, and for a distribution of lateral tracks, a similar method can be employed to calculate and sum noise across the entire distribution. This method would require three inputs: a definition of a lateral dispersion profile, a ground track of the representative trajectory, and noise contours due to that representative trajectory. An architecture diagram demonstrating this approach is shown in **Figure 43**.

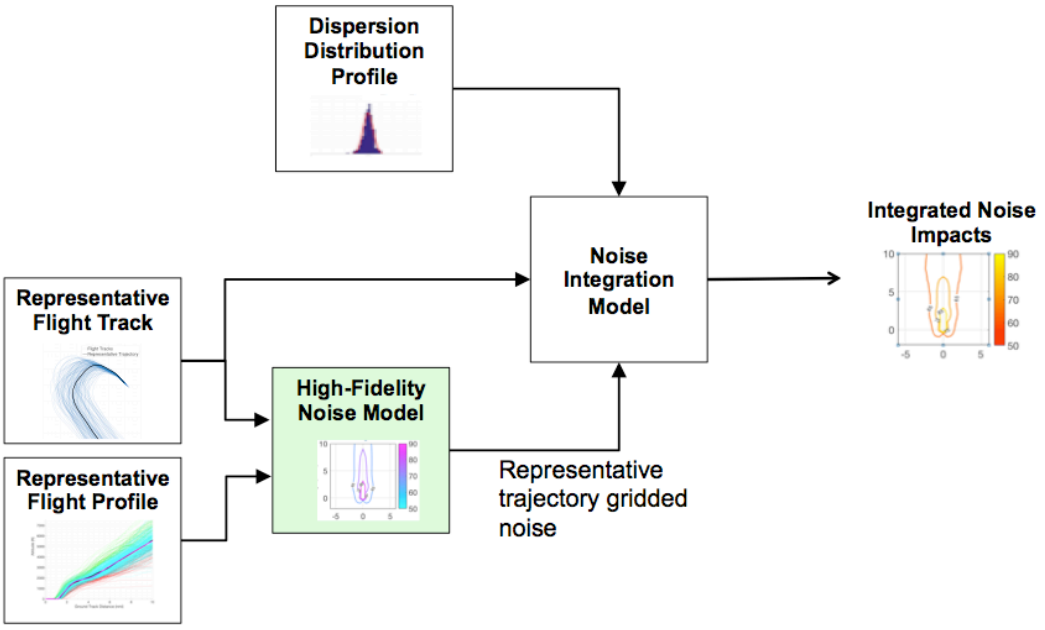

Figure 43. Lateral dispersion model architecture diagram

Similarly to other noise models such as AEDT and ANOPP, this model was designed to use a segment-based approach, dividing the trajectory into a series of segments and summing the noise impact from each segment. The lateral dispersion modeling approach will first be explained for the simplest case: a single, straight trajectory segment. Once this approach is demonstrated, the method will be expanded to allow for the summation of multiple segments, and finally the methods needed to account for turning tracks will be introduced.

As part of the noise integration model, a noise metric called "equivalent SEL" (SEL_{eq}) was created. SEL_{eq} is the single-flight equivalent noise level for a dispersed set of flight tracks. This metric can be obtained by summing many SEL contours into a DNL contour, then reversing the process mathematically to find a "single-flight equivalent" for that DNL contour. This equivalent SEL contour can then be compared directly to an SEL contour. Essentially, this metric represents the noise level if fractional flights corresponding to a probability distribution *P(x)* were flown at each lateral offset. This is a useful metric for modeling the noise of a dispersed route, because without it, the noise of the route would need to be represented using DNL or some other multi-flight metric tied to a specific number of flights. This metric instead allows for the representation of

impacts in a generic way, such that it can be summed into DNL with a certain number of flights. The DNL contour generated would produce the same result as individually calculating the SEL noise due to each flight and summing them into a DNL contour.

5.1 SINGLE STRAIGHT SEGMENT DISPERSION MODELING APPROACH

5.1.1 CONTINUOUS APPROACH

For a segment with many flights on it, each with some lateral offset, a continuous function can be used to model that distribution of lateral offset values. This function can be generated by fitting radar data or it can be selected by the user. This distribution function, *N(x)*, can be normalized into a probability distribution, *P(x,y)*. Dispersed noise for the segment can be calculated by shifting the representative trajectory noise function, $L_0(x,y)$, to each lateral offset, weighting it by the probability value associated with that offset, and summing across all offsets. This approach is presented pictorially in **Figure 44** for the 1 dimensional case where SEL is the noise metric used. In this figure, $L_0(x,y)$ is replaced with $SEL_0(x)$.

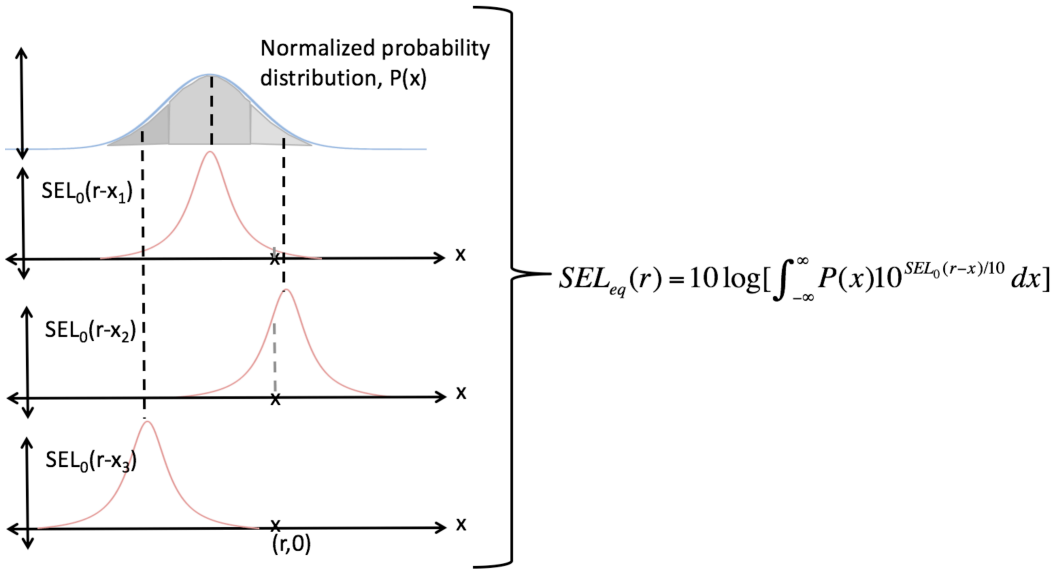

Figure 44. Illustration of summation of shifted noise. The blue curve on top shows the lateral distribution of flights on the flight track. The red curves show the noise curve of the center flight, SEL_0, and the dotted lines point to the weighting of each shifted noise curve due to the probability of flights at that shift.

Figure 44 demonstrates the basic principle of laterally shifting the noise function for the central track to recover an equivalent noise level for the entire dispersed route. This principle can be applied in two dimensions, and across multiple metrics. This lateral dispersion summation approach for SEL is shown in Equation (8). In this equation, $\boldsymbol{N_{tot}}$ is the total number of flights on the route, while r_x and r_y are the x and y shifts in the global frame representing the lateral offset from the representative trajectory track. This equation is derived from the summation method used for DNL calculation (Equation (2)).

$$SEL_{eq}(r_x, r_y) = 10\log_{10}\left(\frac{1}{N_{tot}}\iint_{\infty}^{\infty} N(x,y) * 10^{\frac{SEL_0(r_x - x, r_y - y)}{10}} dxdy\right) \quad (8)$$

This approach is also applicable to other metrics, such as the single-event LAMAX and its multi-event form N_{above}. In this thesis, N_{60} will be used because it has been shown to correspond closely to the location of noise complaints, [30] although other threshold values could easily be substituted. For this set of metrics, the dispersed route will be modeled in N_{60} using normalized fractional flights, which can be multiplied by the number of flights flying along the route to recover the aggregate N_{60} value for the route. The equation for the dispersion summation method for this family of metrics is presented in Equation (9).

$$N_{60}(r_x, r_y) = \frac{1}{N_{tot}}\iint_{\infty}^{\infty} N(x,y) * (LAMAX_0(r_X - x, r_Y - y) > 60)dxdy \quad (9)$$

In this expression, $LAMAX_0(x,y)$ is the noise in terms of LAMAX of the central flight, and the term $(LAMAX_0(r_X - x, r_Y - y) > 60)$ returns either 1 or 0 depending on the result of the inequality.

The continuous method's major shortcoming is its computational expense. This method was implemented for this thesis as a demonstration, but it was much more computationally expensive than the current method of calculating noise impacts individually for each flight and summing each individual impact. This computational intractability comes from the fact that, for each point at which noise is to be calculated, a

two-dimensional integration must be performed across the entire region to be examined for each segment. An example of this approach for a single segment near takeoff with limited dispersion is shown in **Figure 45. Single-segment, 1-dimensional noise, calculated using the continuous approach.**

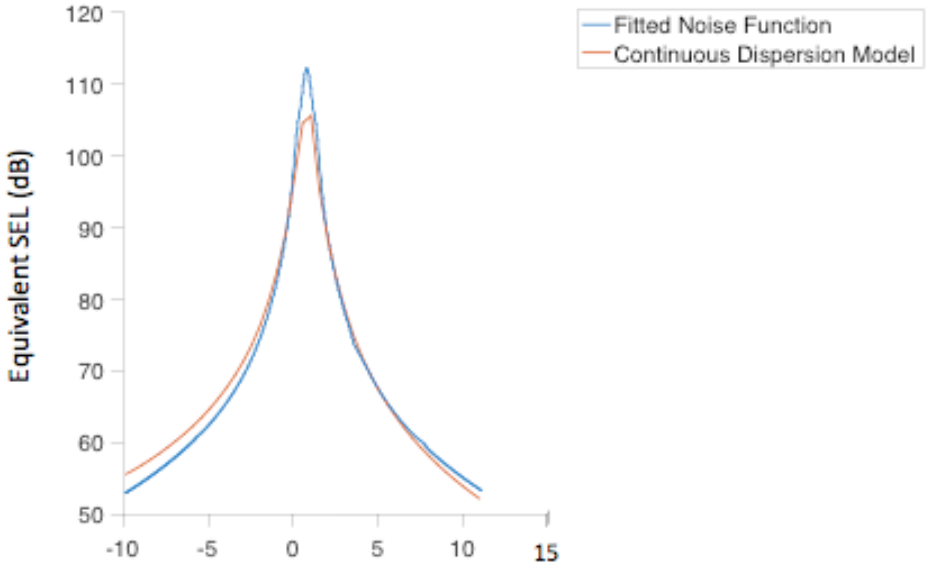

Figure 45. Single-segment, 1-dimensional noise, calculated using the continuous approach.

Because this segment is very close to takeoff, the contour calculated by the model should match the fitted noise function very closely, since almost no lateral dispersion is present. Although these results are accurate to within a few decibels, calculating even this simple, 1-dimensional cross section of noise took minutes. Most of this computational expense comes from having to perform a 2-dimensional integral at each grid point. For this work, 60 square nautical mile grids were typically used, with points sampled at densities ranging from every half nautical mile to every tenth of a nautical mile. Additionally, flight profiles were typically divided into between 50 and 100 segments. Thus, for a dense grid and a flight profile with 100 segments, $3.6 * 10^7$ 2-dimensional integrals must be performed over the entire grid area, which makes the continuous algorithm intractable for most analyses. To help limit computational expense, a discrete approach was implemented using similar principles to the continuous approach.

5.1.2 Discrete Approach

The discrete approach begins with the same concept as the continuous approach, but each integral with a discrete summation. To perform this discretization, a discrete lateral offset distribution must be generated, with probabilities at each discrete point. One method to generate this distribution is to assume that the lateral dispersion distribution will have the form of a particular function. This can be a particularly useful approach for procedure design scenarios when radar data may not be available. To generate the discretized distribution using this function, bin edges for a lateral offset histogram are defined, and the distribution function is integrated across each bin to determine an operation count for each bin. An example of a probability distribution function overlaid on a histogram generated using this approach is shown in **Figure 46**.

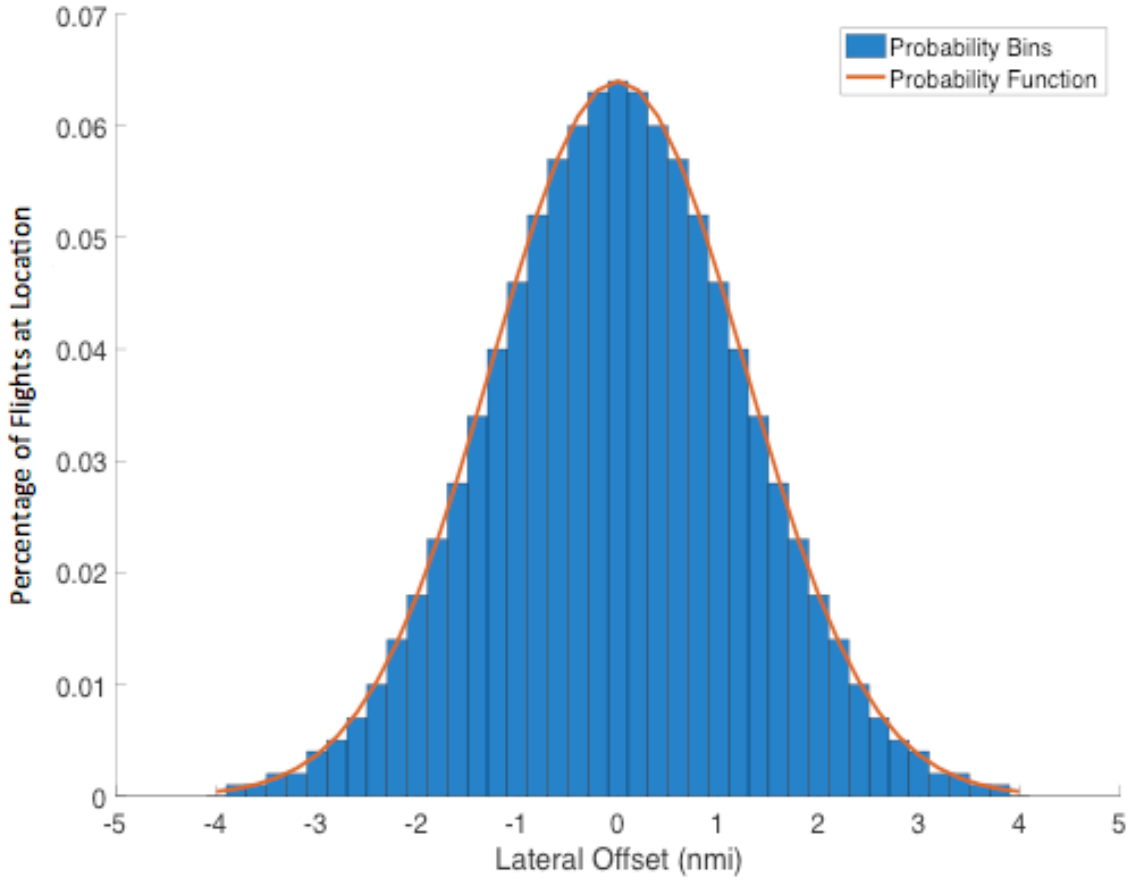

Figure 46. An example continuous probability distribution and its associated histogram generated. The probability distribution is a normal distribution shown in red. The blue bars represent the probability of a flight occurring at each discrete lateral offset.

A second method for generating the discrete distribution is to determine it directly from radar tracks. Using this method, for each flight segment, the lateral offset from the centroid is calculated for each radar track. Then, once again discrete bins are defined and populated based on the number of tracks within that offset range. An example of this method is shown in **Figure 47**.

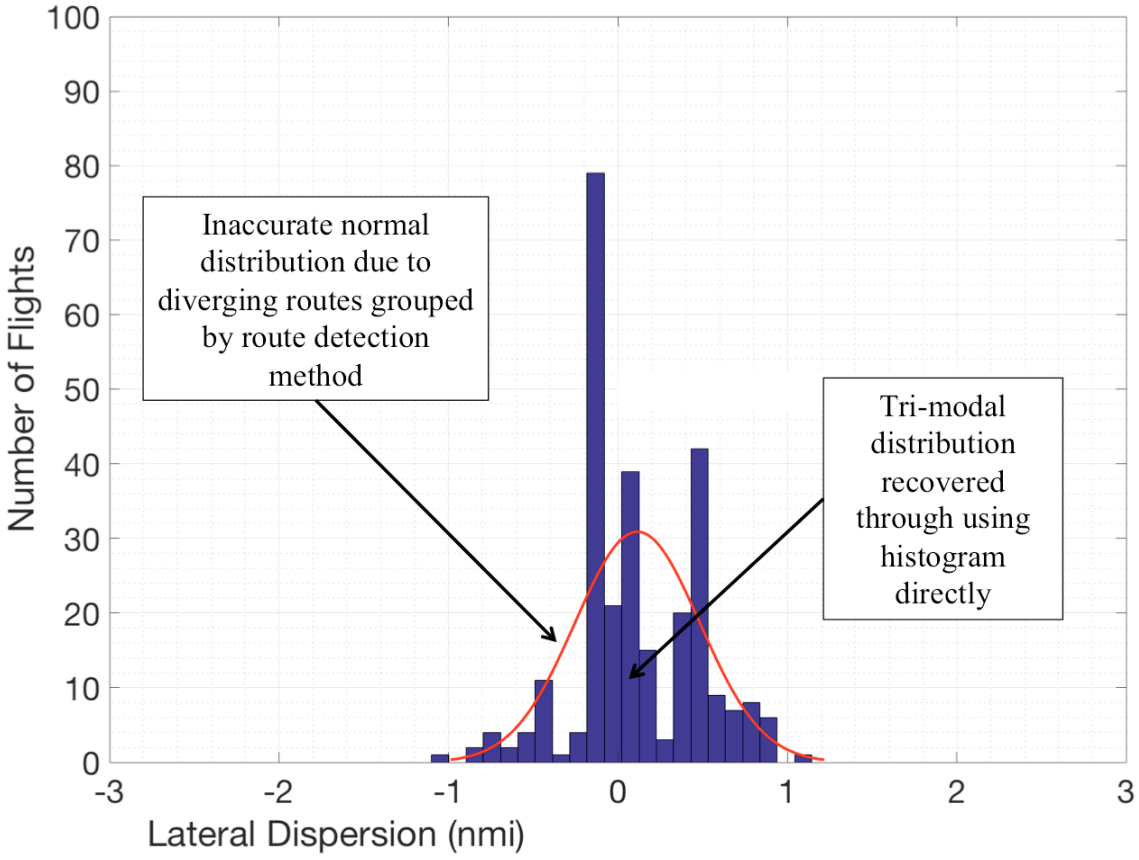

Figure 47. An example of recovering a discrete distribution from real flight track data. Rather than using the fitted probability function (shown in red), this method would use the distribution directly.

One potential advantage of this discretization approach is that it does not require an explicit probability function. While the continuous approach would assume that operations matched the probability distributions of the fitted Gaussian functions in these figures, the discrete approach would use the histogram bins directly. This approach provides a particular benefit when analyzing radar data, because, as stated in Section 3.2.1, due to the difficulties of trajectory classification, assuming a normal distribution may not be accurate farther from the airport. Even if multiple normal distributions could be used to model a multimodal distribution like the one above, it would be difficult to

determine specifically at what along-track distance a route should split from unimodal to multimodal without closely checking the distribution at each point. One potential disadvantage of the discrete approach is that discretization error could be incurred if too few bins are used. This risk was mitigated through the validation efforts shown in Chapter 6, confirming that any discretization error did not significantly compromise results.

Using this discrete distribution, Equation (10) shows the discretized form of Equation (8), which is used to sum SEL noise in the discrete approach. In this equation, N_i is the operation count for each discrete bin.

$$SEL_{eq}(r_x, r_y) = 10 \log_{10}\left(\frac{1}{N_{tot}} \sum_{i=1}^{N_{tot}} N_i * 10^{\frac{SEL_0(r_x - x_i, r_y - y_i)}{10}}\right) \quad (10)$$

Once again, this discrete approach can be used with multiple metrics. Equation (11) shows the discrete form of Equation (9). This is equivalent to Equation (10), but for use with LAMAX and N_{above} instead of SEL.

$$N_{60}(r_x, r_y) = \frac{1}{N_{tot}} \sum_{i=1}^{N_{tot}} N_i * (LAMAX_0(r_x - x_i, r_y - y_i) > 60) \quad (11)$$

Another significant benefit of the discrete approach relative to the continuous approach is that it removes the need to fit the noise data with a surface, since noise is only sampled at discrete points using this approach. This further reduces computational expense. **Figure 48** can be used to visualize this discrete approach, with the total noise calculated through the sum of the three discrete offset values pictured instead of an integration across all possible x values. At each of the three x_i lateral offsets, noise is shifted to that offset, weighted by the probability N_i (represented by the gray bar), and sampled at $x = r$. The result from each station is then summed according to Equation (10).

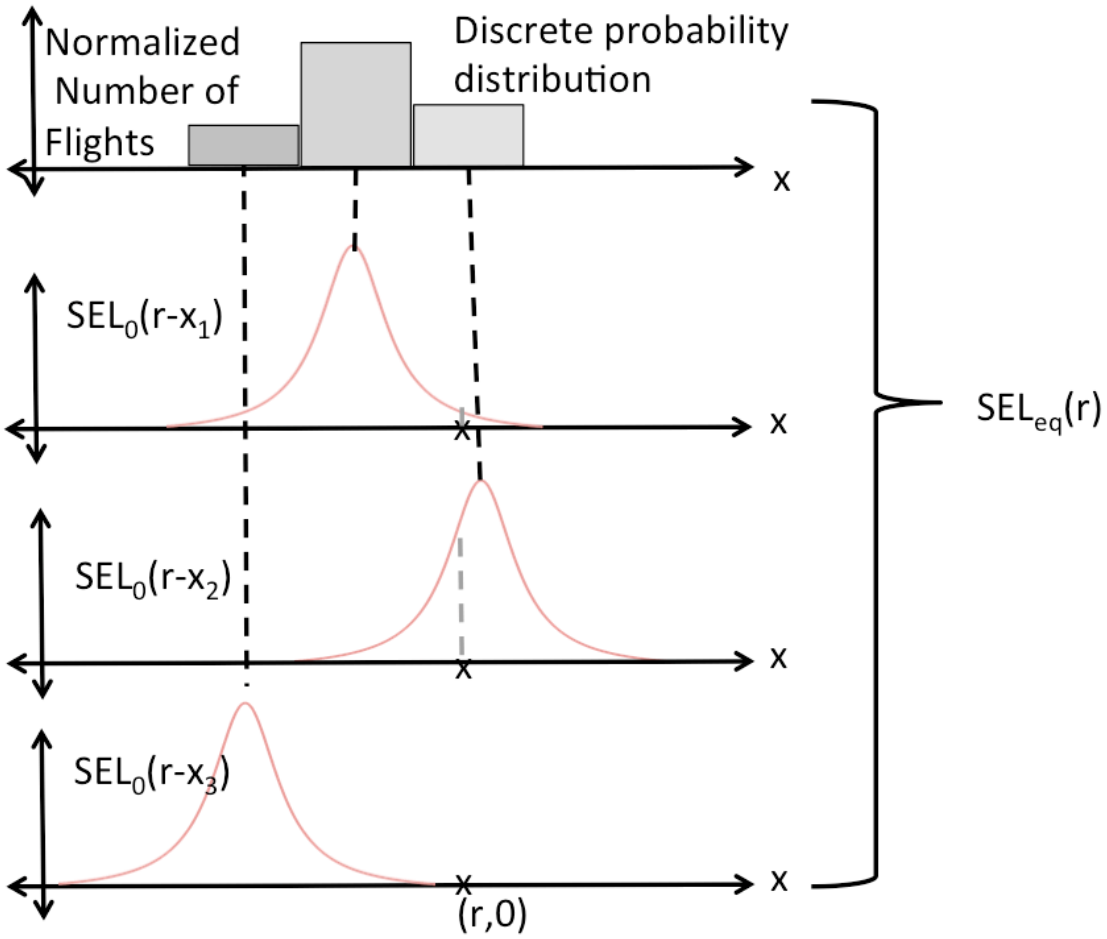

Figure 48. Illustration of discretized dispersion summation method. The gray bars at the top represent discrete probabilities at 3 lateral offset locations, while the 3 red curves show the noise shifted to that position.

5.2 MULTI-SEGMENT DISPERSION MODELING APPROACH

The dispersion summation method presented in Section 5.1 is effective for a single, straight segment, but real flight tracks include curved paths that must be modeled with many segments. To model multi-segment tracks, the model must be able to sum noise from multiple segments while minimizing any discretization error that occurs from segmenting the track. If these multi-segment tracks have curvature, the model must also account for the physical difference in noise propagation of a curved flight track.

5.2.1 SEGMENT SUMMATION

Each flight segment has a unique distribution, and only noise near a segment should be shifted based on that segment's distribution—shifting noise near takeoff due to lateral dispersion 5 miles from the airport would not be desirable, for example. To avoid this problem, the model was designed such that each segment only impacts noise inside a region immediately surrounding that segment, which will be referred to as the "region of impact" of that segment. The region of impact of a given segment controls the lateral dispersion distribution that is modeled in that region. This approximation assumes that dispersion does not jump drastically from one segment to the next, which is a valid assumption so long as segment size is small enough.

Each segment's region of impact must be clearly defined. A simplistic method for defining this region would be to extend perpendicular lines from each endpoint of the segment, with each segment only impacting noise within the region bounded by those lines. This method works for straight segments, as shown in **Figure 49**. In this figure, the thick black line represents the flight track. The thin black rectangles show the region of impact of each segment, and inside each region of impact the noise contours in that region are shown.

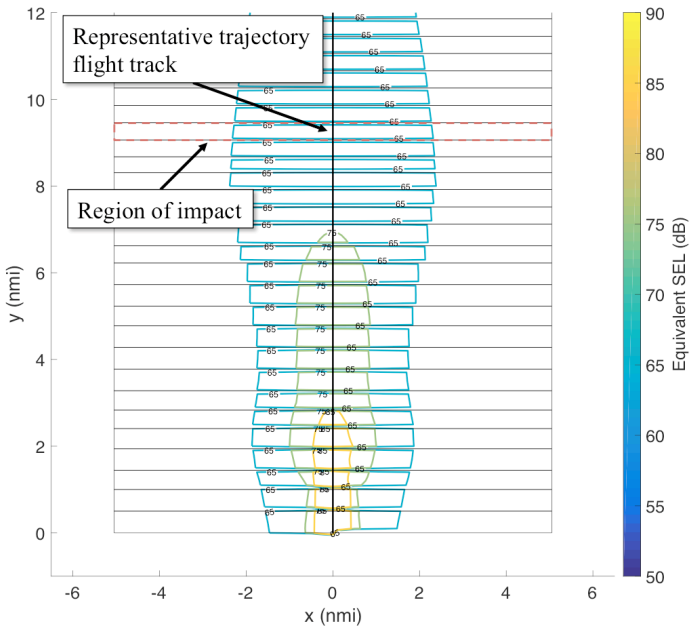

Figure 49. Regions of impact for simple straight-out dispersion case.

With each segment's region of impact defined, the noise from each region must be summed. To do this, first, a distribution must be defined for each segment. **Figure 50** illustrates the definition of a discrete distribution for each flight segment. This distribution is split into bins with a width of 0.1 nautical miles, and the sum of the percentages across all bins is equal to 100% in all cases. This figure shows a simple, straight-out, evenly distributed dispersion case, in which flights begin fanning 4 nautical miles after takeoff and reach a maximum width of 4 nautical miles.

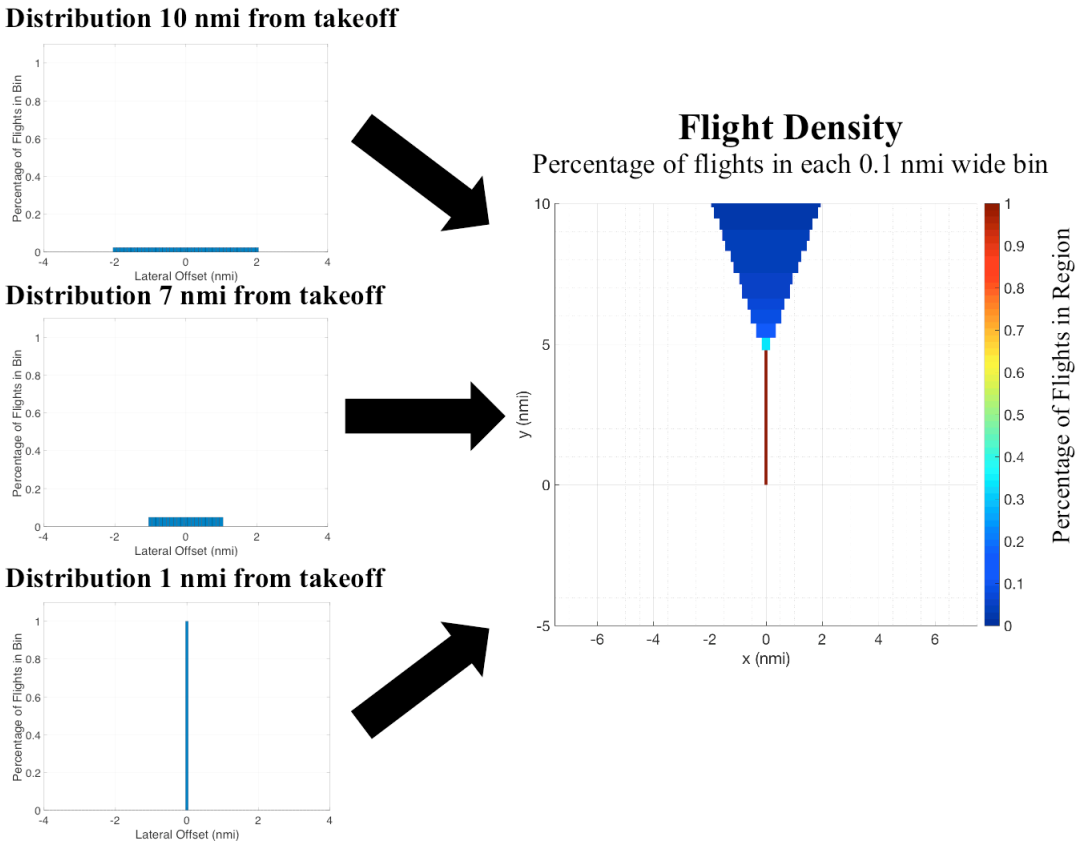

Figure 50. A discretized flight density plot, illustrating evenly distributed flights fanning outwards at each flight segment beginning 4 nmi after takeoff.

In this density plot, each flight segment has a distribution definition. Three example distributions are shown on the left-hand side of the figure. Then, for each segment, each discrete bin of lateral offset is integrated across to determine what percentage of flights fly above that bin. Using these percentages, the noise summation equations presented in Section 5.1 are used. For the discrete approach, Equation (10) is used to calculate equivalent SEL and Equation (11) is used to model N_{above}. The

dispersed noise from each segment impacts noise only in its region of impact, and then Equation (10) or (11) can be used to sum the noise of each segment into a single, overall contour. If there is any discontinuity due to discretization of segments after this summation, a 3-dimensional smoothing filter can be used to smooth noise values at the intersection of each segment's region of impact.

5.2.1 ACCOUNTING FOR TRACK CURVERATURE

The simplistic approach to defining region of impact must be modified to model curved tracks. First, this representation would not be physically representative of noise propagation of a curving flight track. Since noise travels spherically outwards from the source, as an aircraft travels around a curve it impacts a wider region on the outside of the turn than on the inside. Second, for curved segments, defining perpendicular regions of impact will leave the noise in some regions unaffected by any segment, while noise in other regions will be affected by multiple segments, potentially leading to double-counting of noise. These problems are illustrated in **Figure 51**.

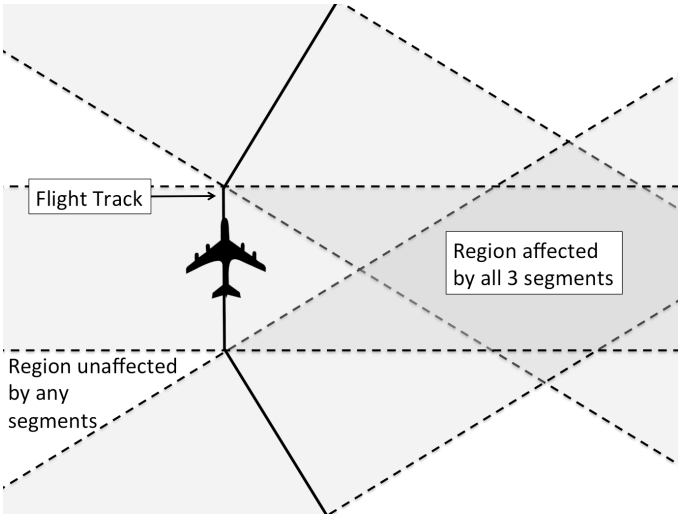

Figure 51. 3 flight segments and the regions that each segment impacts using a simplistic multi-segment approach.

To account for this physical effect and to avoid the issue illustrated in **Figure 51**, rather than being parallel, the edges of each region of impact are defined with a slope that is the mean between the two slopes perpendicular to flight segments on either side of that edge. Using this approach, each flight segment has a region of impact that fans

proportionally with the radius of curvature of the turn present at that segment. This fanning effect accounts for the physical sound propagation effects. The approach also ensures that each segment's region of impact shares an edge with the adjacent segment, and thus do not overlap with adjacent segments' regions of impact or leave gaps between them. This approach is illustrated in **Figure 52**. In this figure, the blue line represents the flight track. The black polygons show the region of impact of each segment, and inside each region of impact the noise contours in that region are shown.

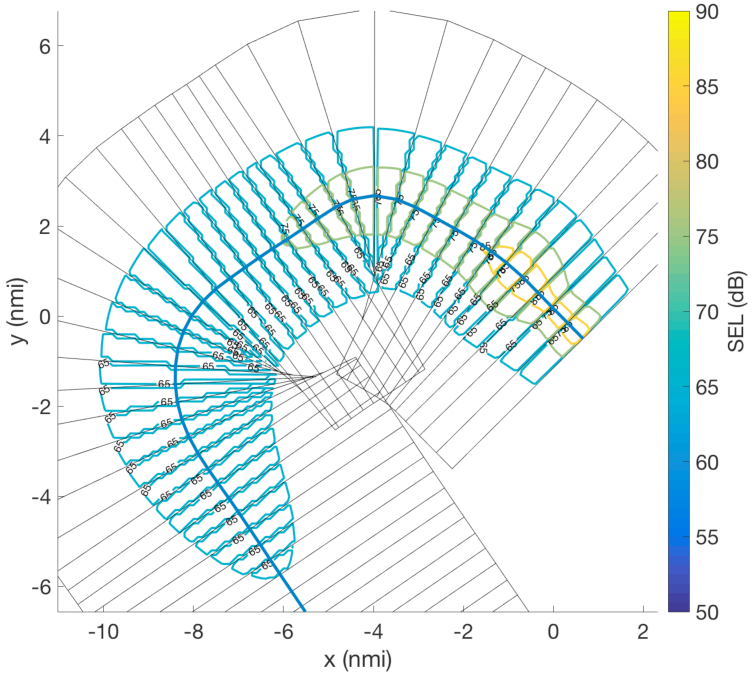

Figure 52. A demonstration of the multi-segment approach used. The flight track is shown in blue, and the regions that each segment impacts are represented with black polygons.

This ensures that all regions on the outside of a turn will be impacted by exactly one segment, as is clear in the figure. It can be seen that multiple segments will have overlapping regions of impact on the inside of a turn, however. To correct for this, a check is performed for each point in the noise grid to ensure that only one segment impacts it. If multiple segments would impact the same grid point, that point is removed from the regions of impact of all segments except the first chronological segment (beginning at takeoff for departures and ending with landing for approaches). This check ensures that each point is only impacted by one segment.

Also, as is shown in the figures, each region of impact has an outer boundary. Without these outer bounds, due to turns in the flight track, regions of impact could include areas directly under a later part of the flight track, which would cause an incorrect lateral dispersion profile to be applied to that region. By bounding the edges of the regions of impact to a user-specified width, this issue can be avoided. The maximum width must be selected to ensure that it contains all relevant noise contours without allowing earlier segments regions of impact to extend under later parts of the flight track. This method has an additional benefit of reducing computational expense by avoiding the calculation of noise in low-noise regions far from the flight track.

5.3 CORRECTING FOR DIFFERENCES IN HEADING

The methods described in Sections 5.1 and 5.2 model lateral dispersion accurately in most cases, but in some special cases some differences in aircraft heading between different flight tracks will cause error if it is not accounted for. One example of such a case is a delayed turn procedure. In this procedure, flights follow the same initial ground track, then turn to a certain heading at different times, with some flights making the turn earlier and some making the turn later. This issue is illustrated in **Figure 53**.

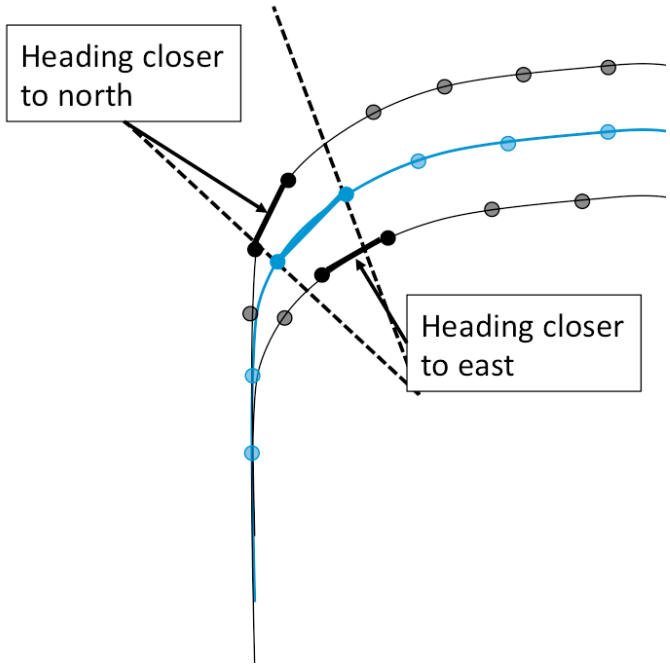

Figure 53. An illustration of the heading differences that arise when modeling delayed turn procedures. The blue track is the representative track, and the two black tracks are other flights in the same flow with some lateral offset. The dotted lines show the region of impact of the bolded blue segment, while the two black bolded segments are the closest segments from the two dispersed routes.

Heading differences can be corrected for by rotating the shifted noise grid based on the heading of each bin. To perform this analysis, first, an average heading is defined or calculated for the representative trajectory and for each bin. Then, in addition to shifting the representative trajectory noise to match the lateral offset of that bin, the grid is rotated by the difference in heading between that bin and the representative trajectory, θ. This rotation is performed by multiplying by the rotation matrix, $R(\theta)$, as shown for SEL in Equation (12).

$$SEL_{eq}(r_x, r_y) = 10\log_{10}\left(\frac{1}{N_{tot}}\sum_{i=1}^{N_{tot}} N_i * 10^{\frac{R(\theta_i)*SEL_0(r_x - x_i, r_y - y_i)}{10}}\right) \quad (12)$$

An example of the shifting and grid rotation performed as part of the heading correction is shown in **Figure 54**.

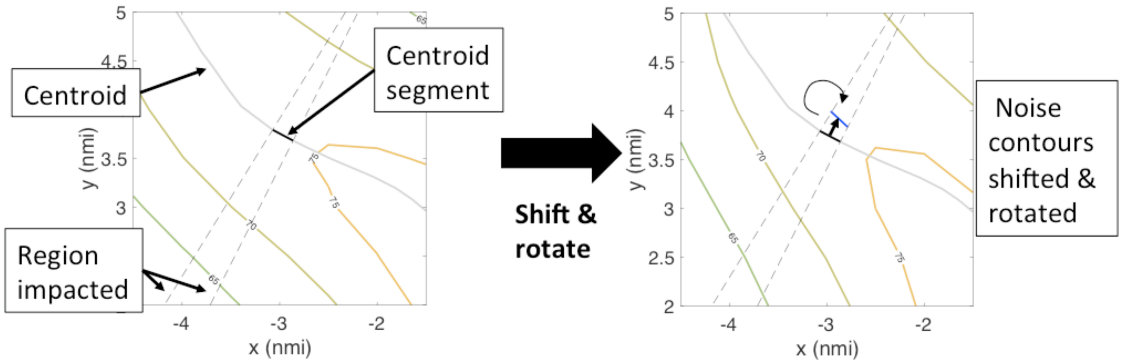

Figure 54. Demonstration of heading correction grid rotation.

CHAPTER 6 EXAMPLE APPLICATIONS

Using the methodology described in Chapter 5, a model was implemented capable of modeling the noise impacts of trajectory variability. This model can be used for applications including procedure design and rapid noise modeling. This chapter first presents some examples of procedure design applications, and shows validation of the model based on these examples, then shows an example of a rapid noise modeling application at KBOS.

6.1 SIMPLE, STRAIGHT-OUT DISPERSION EXAMPLE

The dispersion-modeling tool that was developed can be useful either for designing procedures to intentionally include flight track lateral dispersion or to model the dispersion that occurs naturally on a procedure. To demonstrate the utility of the model in these applications, a series of example procedures were examined. First, a simple, straight-out fanning example was modeled to demonstrate and validate the model. For this case, equivalent SEL was examined, directly comparing single flight equivalent results for single aircraft type.

To model this case, the dispersion model requires three inputs: a representative trajectory flight track, a grid of noise results corresponding to this flight, and a definition of lateral dispersion as a function of along-track distance. Therefore, it was first necessary to define a representative trajectory flight profile and calculate its resulting gridded noise. The representative trajectory was modeled as a Boeing 737-800. To determine the thrust, speed, and altitude profiles of the representative trajectory, the profile matching procedure and example B738 departure profile described in Section 4.3.1 was used. The noise contours of this representative trajectory are shown in **Figure 55**.

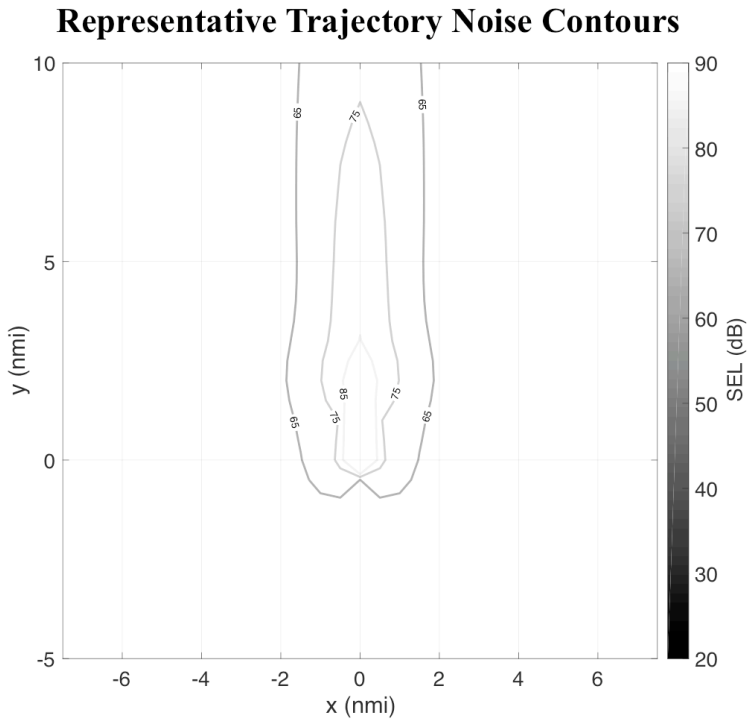

Figure 55. The SEL noise contours for a Boeing 737-800 representative trajectory.

With this input calculated, next, lateral dispersion as a function of along-track distance was defined. The first case examined was evenly distributed lateral dispersion beginning four nautical miles after takeoff and fanning out to a maximum width of four nautical miles. With the noise grid, flight profile, and dispersion as a function of along-track distance defined, the variability model was implemented to calculate equivalent SEL for the procedure. **Figure 56** shows a visualization of this procedure and the equivalent SEL noise contours modeled by the dispersion model.

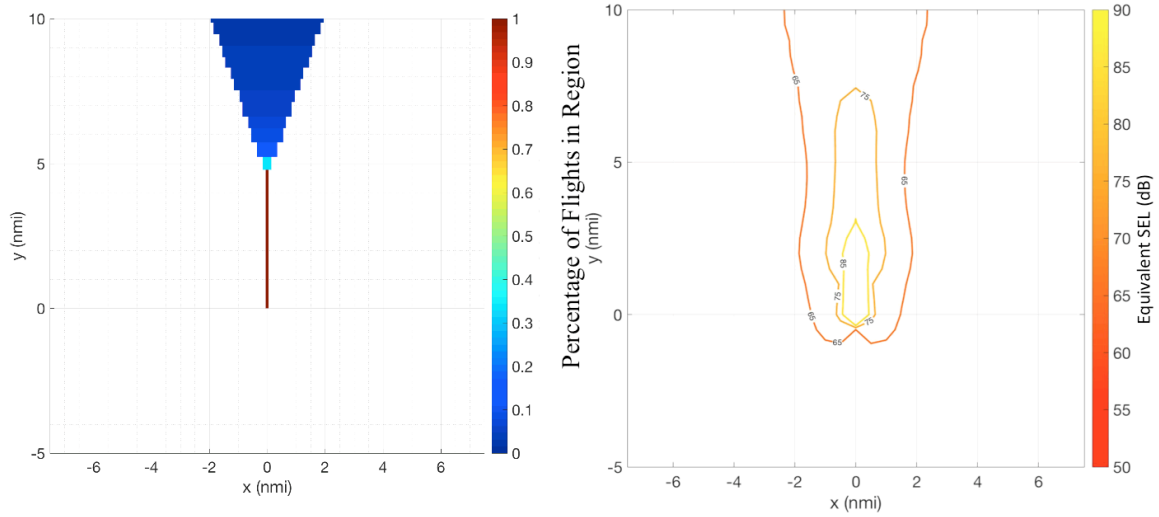

Figure 56. Evenly distributed fanning, beginning at 4 nautical miles and increasing to a maximum lateral dispersion width of 4 nautical miles. On the left, flight density used for noise spreading is shown. On the right, SEL noise contours generated by the dispersion model are shown.

These contours were also overlaid on those of the representative trajectory, and once again this comparison shows a shortening and widening of noise contours. At the 75 dB level, this procedure appears to show a significant benefit, with noise contours only slightly widening but becoming significantly shorter. At the 65 dB level, however, contour width increases significantly. These results are shown in **Figure 57**.

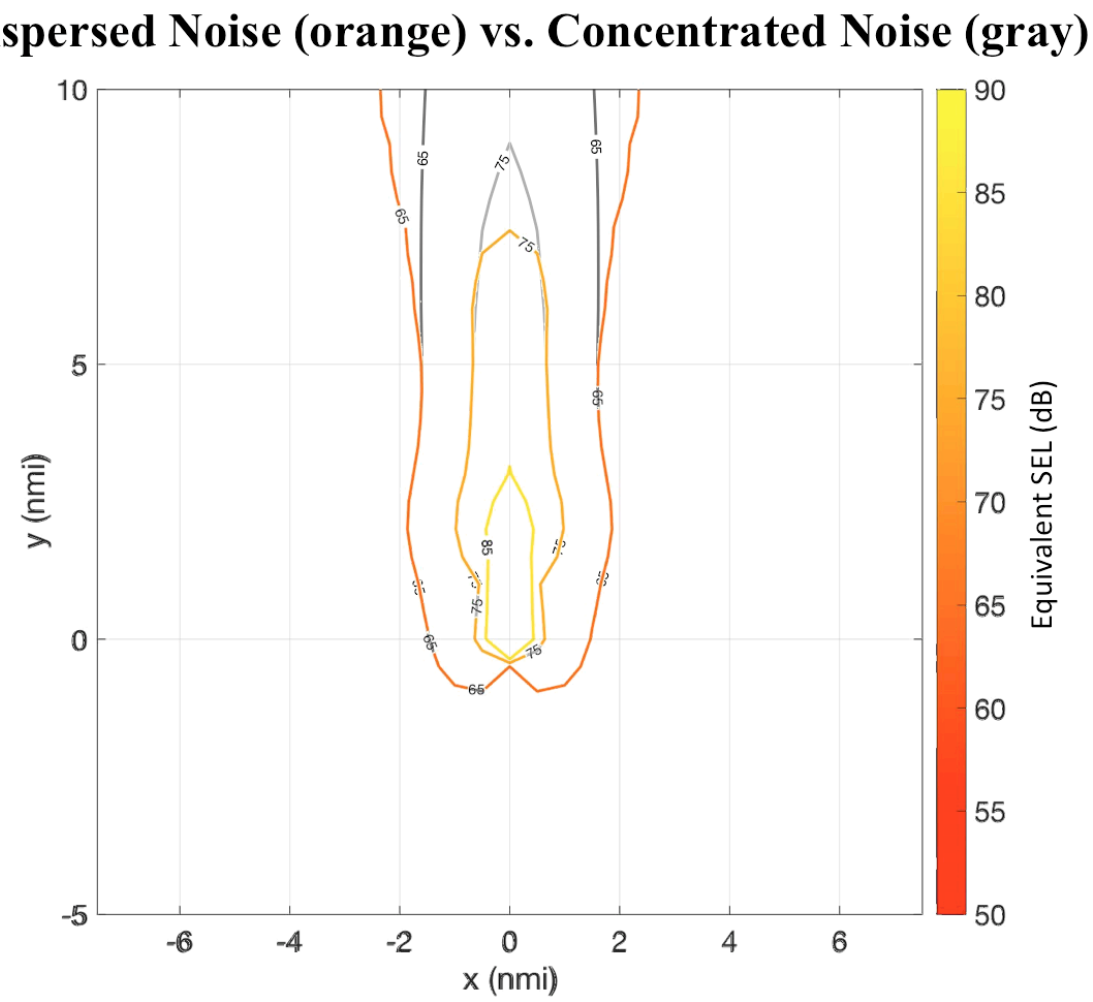

Figure 57. Results from the evenly distributed, straight-out dispersion case also show contours shortening and widening. The yellow and orange contours show the equivalent SEL contours of the dispersed route, while the gray contours show the SEL contours (modeled in AEDT) of the representative trajectory.

These two examples show that lateral dispersion creates a noise tradeoff: it can be an effective way to reduce noise under the representative track, but it will invariably spread noise impacts to a wider region. The 75 dB contour pulls in from about 9 nautical miles to about 7.5, while only widening very slightly (a few tenths of a mile)—this is a significant benefit. The 65 dB contour, however, increases in width by nearly 1 nautical mile by 10 nautical miles from takeoff. By tuning parameters such as when dispersion begins, what type of distribution dispersion has (e.g. normal distribution, even distribution), and how widely dispersed tracks are, it is possible to shift noise impacts to different regions; this allows lateral dispersion to be used as a tool to create procedures beneficial to locally specific population distributions.

One benefit of the variability model is its speed. Using 60 by 60 nautical mile noise grids with points spaced every half nautical mile, AEDT typically takes approximately 30 seconds to calculate the noise of a single flight. The examples modeled above represent smooth distributions of flights in a traffic flow, which could be representative of hundreds or thousands of flights the procedure. To model each of these flights individually could be quite time consuming—and this is assuming that flight profiles (speed, thrust, and altitude) are already calculated, which could be quite a difficult task in and of itself given that this data is often not widely available. The variability model took an average of about 120 seconds to model the noise of these routes, providing significant savings in computational expense. As examples, a direct calculation in AEDT of 100 flights would take 25 times longer, and 1,000 flights would take 250 times longer.

While the model's speed provides orders of magnitude savings in computational expense, it must be validated. To verify that the results from this model are correct, the second example modeled above was calculated using both the model and a direct calculation of the noise of many trajectories. 148 Boeing 737-800 trajectories fanning in the same pattern as **Figure 56** were generated, and AEDT was used to model the SEL noise due to each. Then, the overall noise was summed into an equivalent SEL, which was overlaid with the contours from the variability model. The results of this comparison are shown in **Figure 58**.

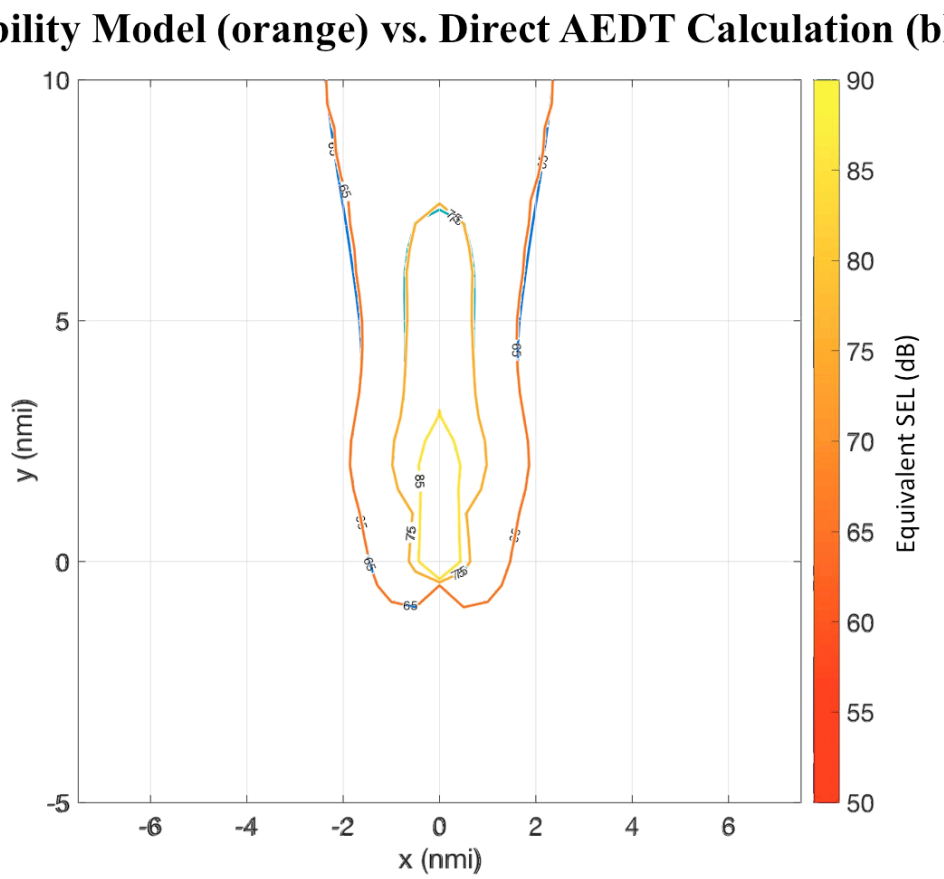

Figure 58. Comparison of the variability model to a direct calculation in AEDT. The yellow and orange contours show the output from the variability model, while the barely visible blue and green contours show the results from a direct calculation of 148 trajectories in AEDT.

This comparison shows that the model's results are accurate, validating its results. In **Figure 58**, the underlying contours from the direct calculation are barely visible because the yellow and orange contours from the variability model are nearly identical. Where there is some difference, it is likely due to discretization; both in discretizing the flight profile into segments and within a segment discretizing the lateral offset distribution. This error, however, is very small, and computation time is drastically reduced.

6.1.3 More Realistic Dispersion Example

Once the model was implemented and validated on simple case, it was tested using a more realistic lateral dispersion profile generated from historical radar data. This example is still reasonably simple, however, and only for a single aircraft type; thus, once again, equivalent SEL was used to compare contours. First, the noise due to this lateral dispersion profile was modeled on a straight-out departure track, and then the same

dispersion profile was modeled on the real flight track that it was calculated from. The lateral dispersion profiles from the analysis in Chapter 3 for KBOS Runway 33L departures in 2010 and 2015 (shown in **Figure 24**) were used for this example. Dispersion in each case was modeled with a normal distribution. The representative trajectory flight profile was once again modeled using the radar matched Boeing 737-800 departure profile.

First, these lateral dispersion profiles were modeled for straight-out departures. The results of this analysis for both the 2010 case and the 2015 case are shown in **Figure 59**.

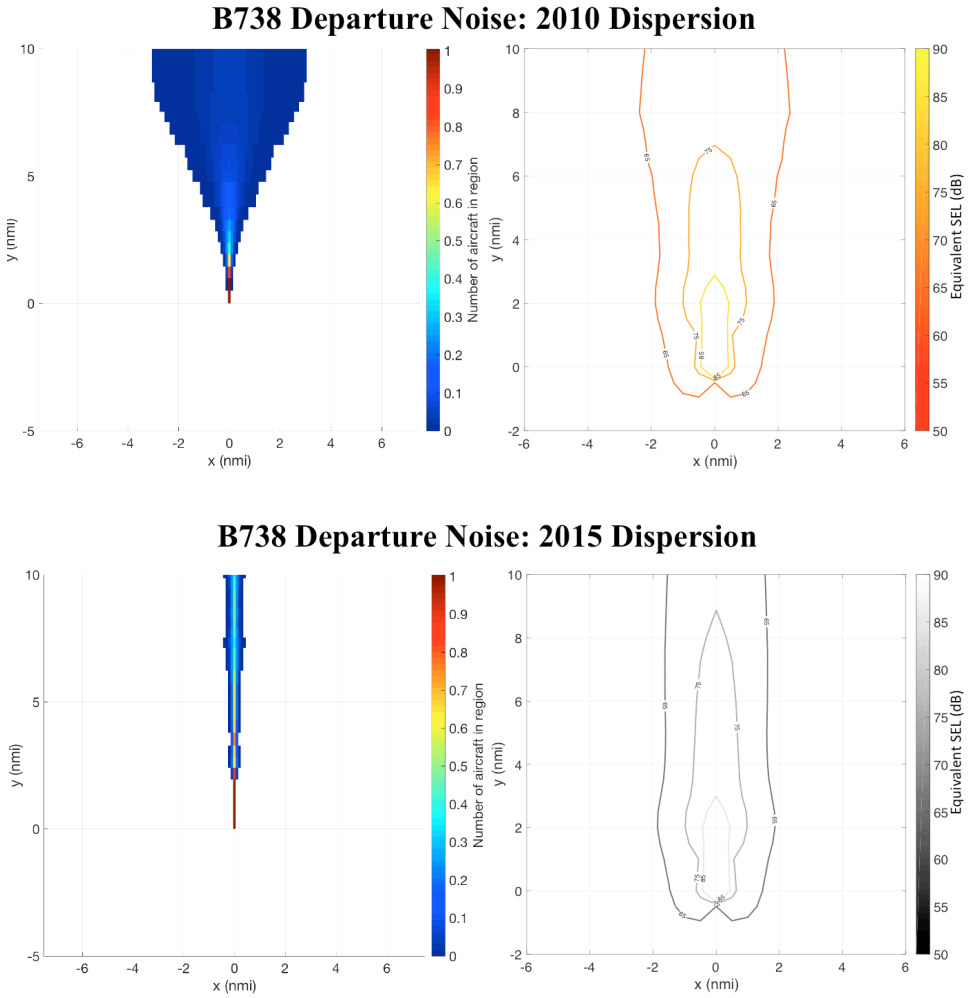

Figure 59. Lateral dispersion profiles from KBOS Runway 33L in 2010 (top) and 2015 (bottom) applied to straight-out departures.

This example is useful to look at because it allows for the impact of pre- and post-RNAV levels of lateral dispersion to be compared for a simple, straight-out case, making the noise difference clear. To better examine this difference, the two contours are overlaid in **Figure 60**.

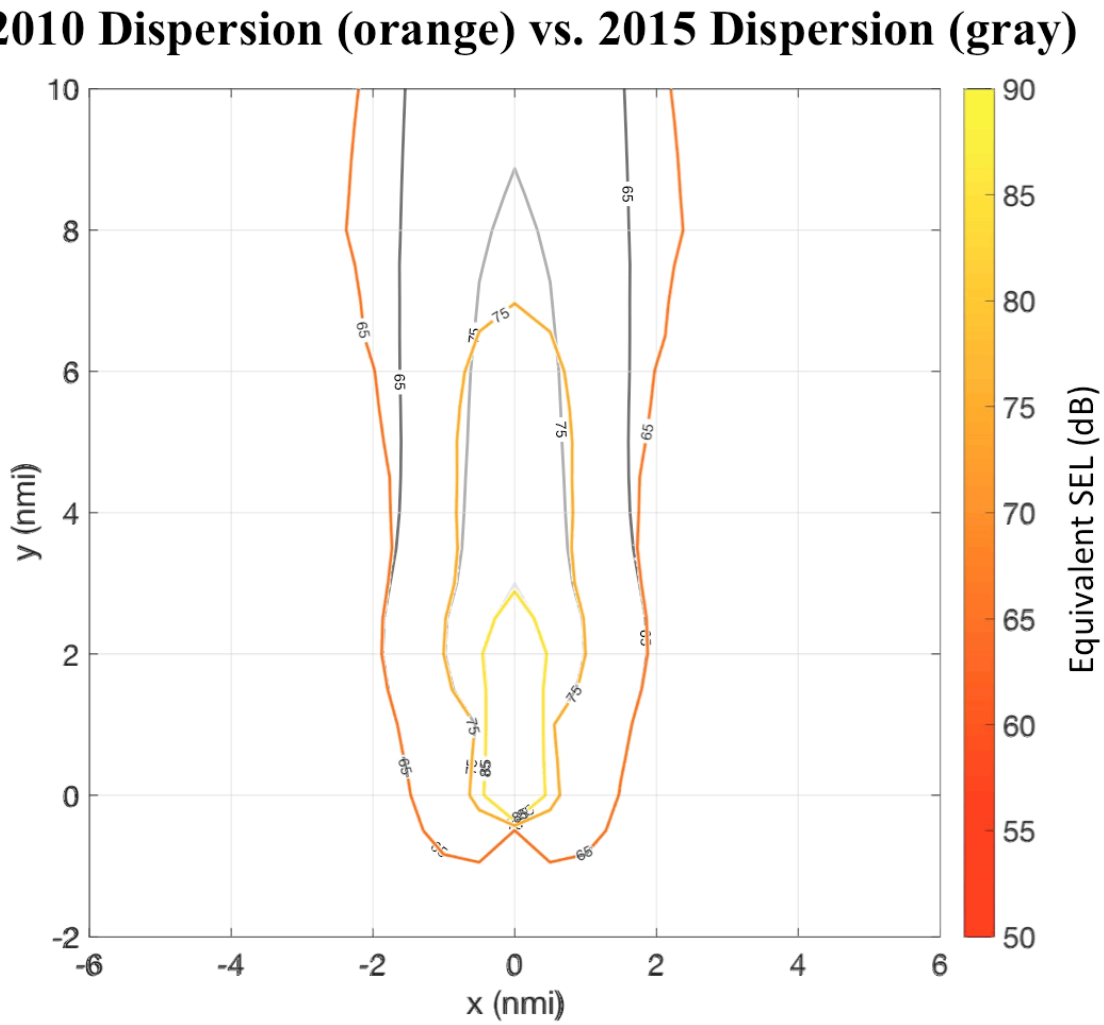

Figure 60. Comparison of Boeing 737-800 equivalent SEL for 2010-level lateral dispersion (orange) and 2015-level lateral dispersion (gray) on a straight-out departure.

This comparison demonstrates that the concentration effects of RNAV caused contours to slightly narrow and significantly extend directly under the track. Particularly at the 75 dB equivalent SEL level, the contour is about 1.75 nautical miles shorter and only about 0.2 nautical miles wider on each side, which shows a significant noise savings below the track with a relatively minor cost to the side at this noise level. Once again, though, at slightly lower noise levels, the 65 dB contour increases in width by about 0.75

nautical miles in width on each side, making the contour significantly wider. This shows that lateral dispersion can be a good way to reduce higher noise levels below the track, but will potentially expose more people to lower noise levels, depending on local population distribution.

Next, the same lateral dispersion profiles were modeled, but now the flight track was modeled as a departure from KBOS Runway 33L. This track was found using the clustering representative trajectory identification method described in Appendix A applied to the 2015/2016 KBOS ASDE-X dataset. It corresponds to the BRUWN 4 departure, shown in magenta in **Figure 61**.

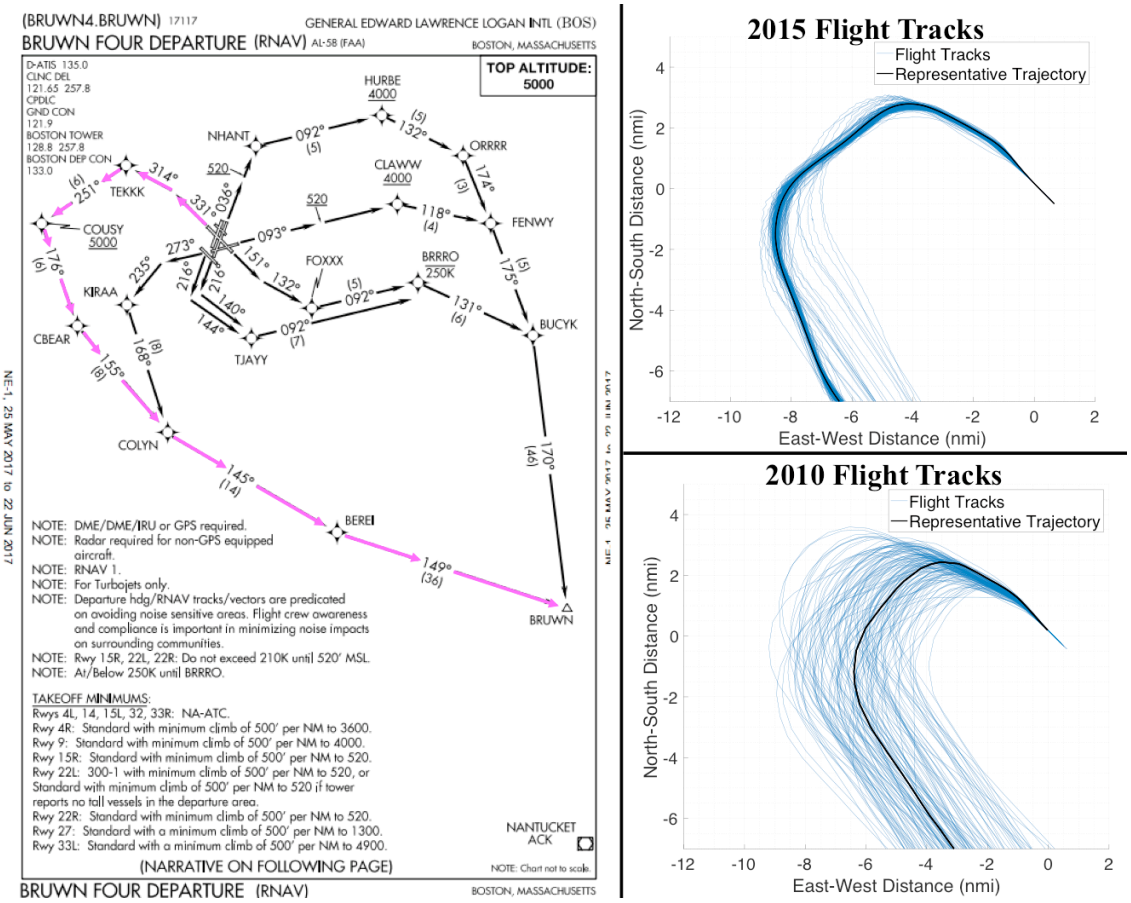

Figure 61. On the left, the official route definition for the BRUWN 4 departure at KBOS with the 33L departure route shown in magenta. On the right the corresponding KBOS flight tracks detected via clustering analysis are shown.

Lateral dispersion profiles from both 2010 and 2015 were applied to the BRUWN 4 departure track from 2015 so that they could be directly compared. Applying the 2010 dispersion profile to the 2015 ground track will slightly shift the 2010 impacts, because

the representative trajectory ground track in 2010 is not identical to the one from 2015. This difference is small, however, and this method allows a more direct comparison of the impacts of lateral dispersion since both profiles are applied to the same ground track. Given this representative ground track and the lateral dispersion profiles for the 2010 case and 2015 case, noise was modeled for both cases. These results are shown in **Figure 62**.

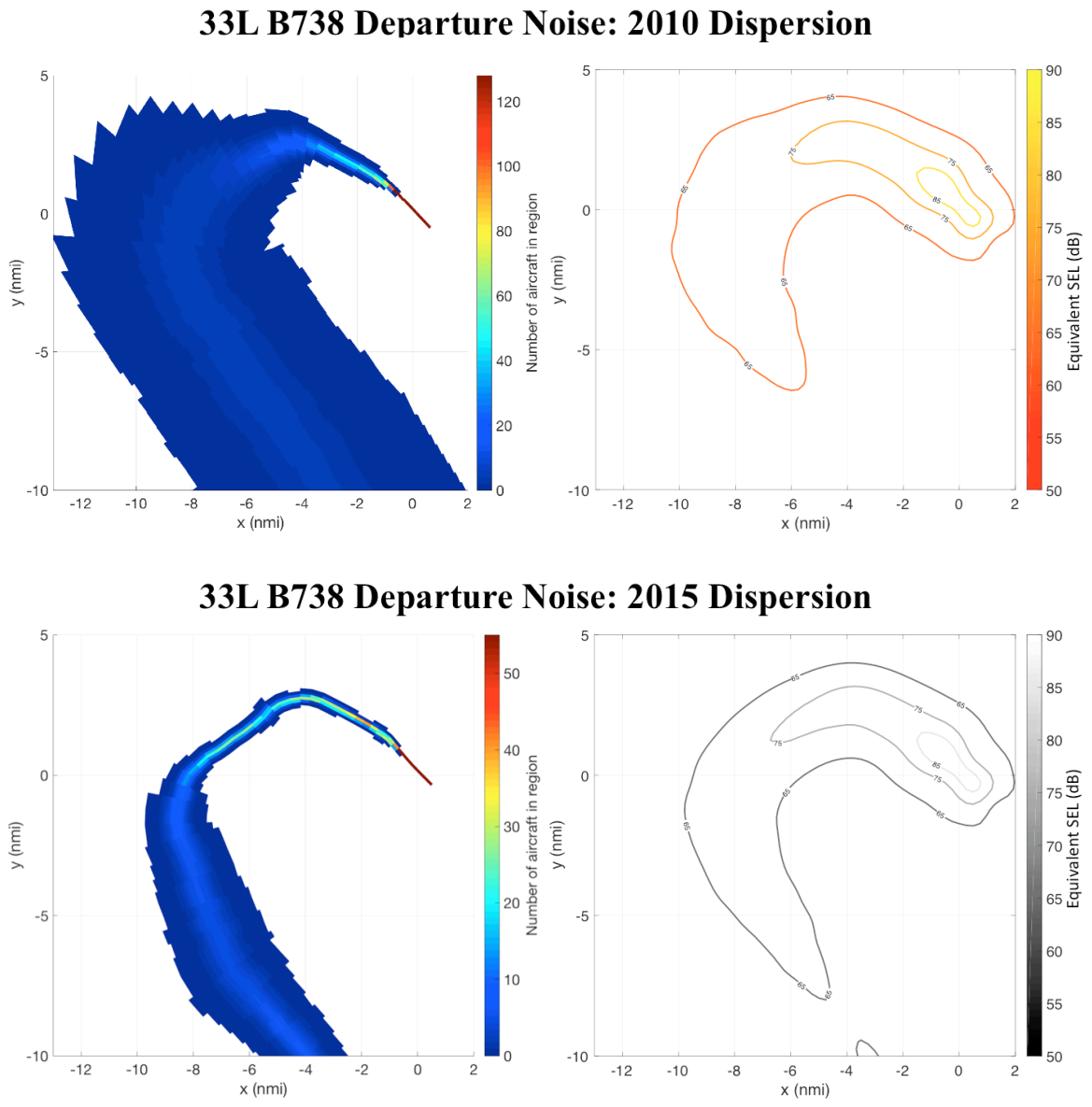

Figure 62. Lateral dispersion profiles from KBOS Runway 33L in 2010 (top) and 2015 (bottom) applied to 2015 radar detected Runway 33L representative ground track.

With noise calculated for both cases, the contours of these two analyses were overlaid to compare noise impacts with 2010 levels of lateral dispersion to the impacts with dispersion due to the existing RNAV route. This comparison is shown in **Figure 63**. It is clear from this analysis that the concentration due to the RNAV route caused noise to increase under the flight track and decrease for locations offset from the track—that is, contours for the 2015 case are longer and narrower.

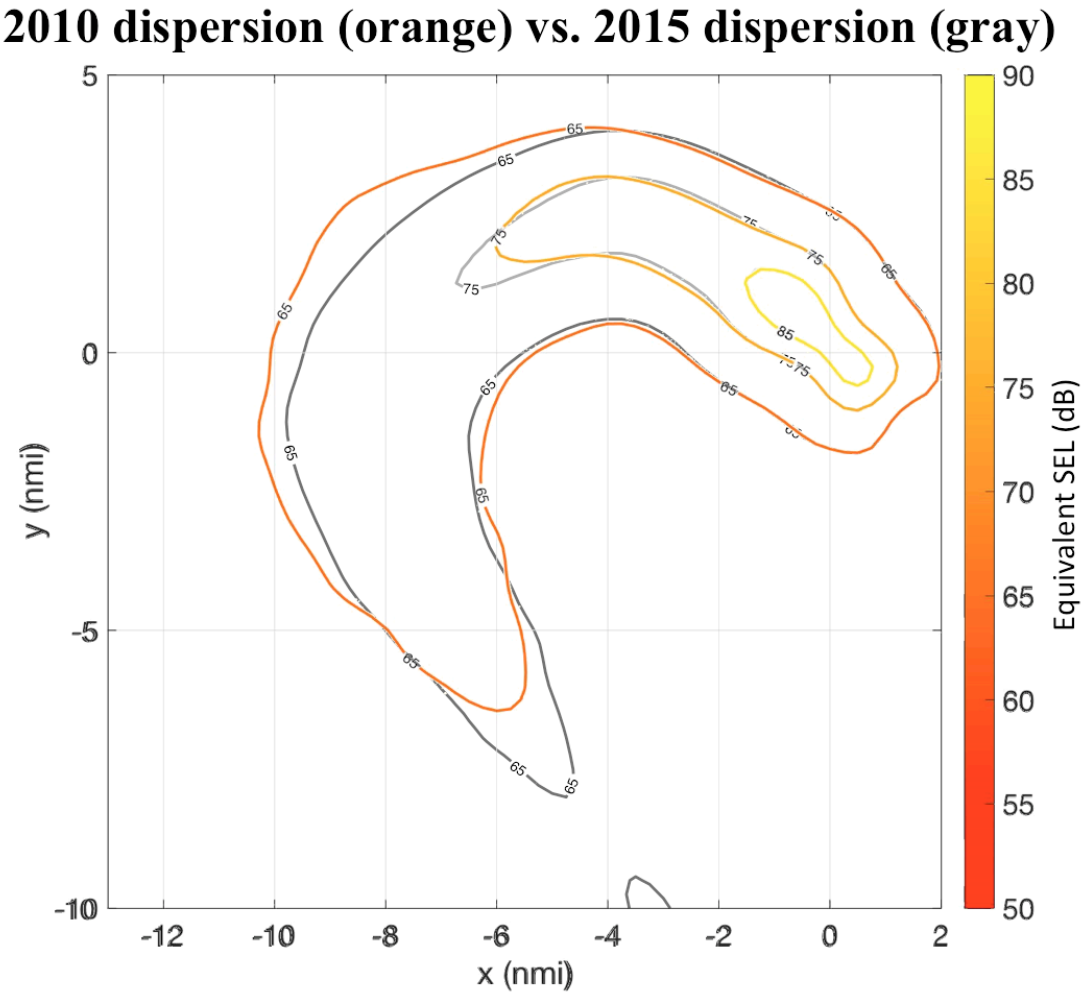

Figure 63. Boeing 737-800 equivalent SEL noise results for 2010-level lateral dispersion (orange) and 2015-level lateral dispersion (gray) on KBOS Runway 33L BRUWN 4 departure.

As was discussed for the straight-out case, the 75 dB contour reduces in length significantly without widening very much, but the lower, 65 dB contour does show clear widening in addition to its shorter length. This example shows that the dispersion-modeling tool that was created is useful for realistic analysis, and provides a useful way

to quantify noise differences due to different levels of lateral dispersion. This can be used to compare the noise impacts of procedures before and after RNAV, as shown in this example, or for procedure design or rapid noise modeling applications, as will be shown in the following sections.

5.2 BOSTON RUNWAY CONCEPTUAL 33L OPEN SID

Once the model was demonstrated and validated on the simple case and used to analyze a real departure flow, it was used to perform analysis for design of a realistic flight procedure to demonstrate its practical utility. This procedure was designed using the Open SID framework described in Section 2.3.2.

6.2.1 OPEN SID DESIGN

Two variations of a conceptual Open SID procedure were designed. Both were based on the same concept: aircraft flying the Open SID would fly the standard RNAV procedure until reaching a specified altitude, at which point ATC would issue a direct-to command towards a specified waypoint. A 4,000-foot turn and a 2,000-foot turn scenario were analyzed. Because there is a good deal of natural variation in aircraft climb rate due to different aircraft types, weights, and thrusts, this would result in the creation of natural flight track lateral dispersion. **Figure 64** shows the altitude profiles of all jet departures from KBOS Runway 33L over 20 days in 2015 and 2016.

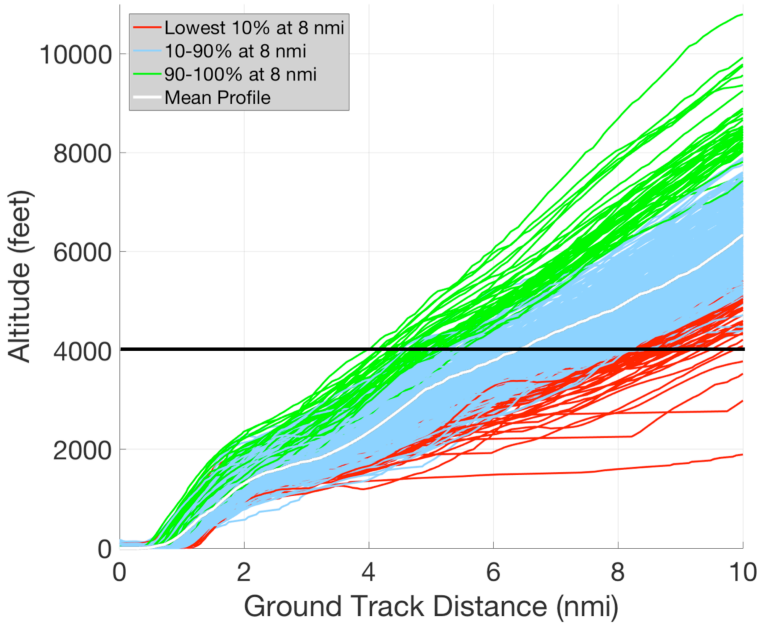

Figure 64. Altitude vs. along-track distance for all Runway 33L jet departures at KBOS over 20 days in 2015 and 2016. The black line shows 4,000 feet, making it apparent how much natural variability in climb rate exists.

The turn altitudes chosen for this analysis was 2,000 feet and 4,000 feet, but this threshold could be changed depending on the desired noise profile and procedure design criteria. Given these thresholds, however, many flight tracks were generated based on the altitude profiles shown in **Figure 64**. These tracks are shown for the 4,000-foot case in **Figure 65**. In this figure, the white line shows the current RNAV route, connecting the TEKKK waypoint to the COUSY waypoint. Implementing the Open SID procedure would create lateral dispersion through this turn, and the variability model developed is able to capture the noise impacts of this dispersion.

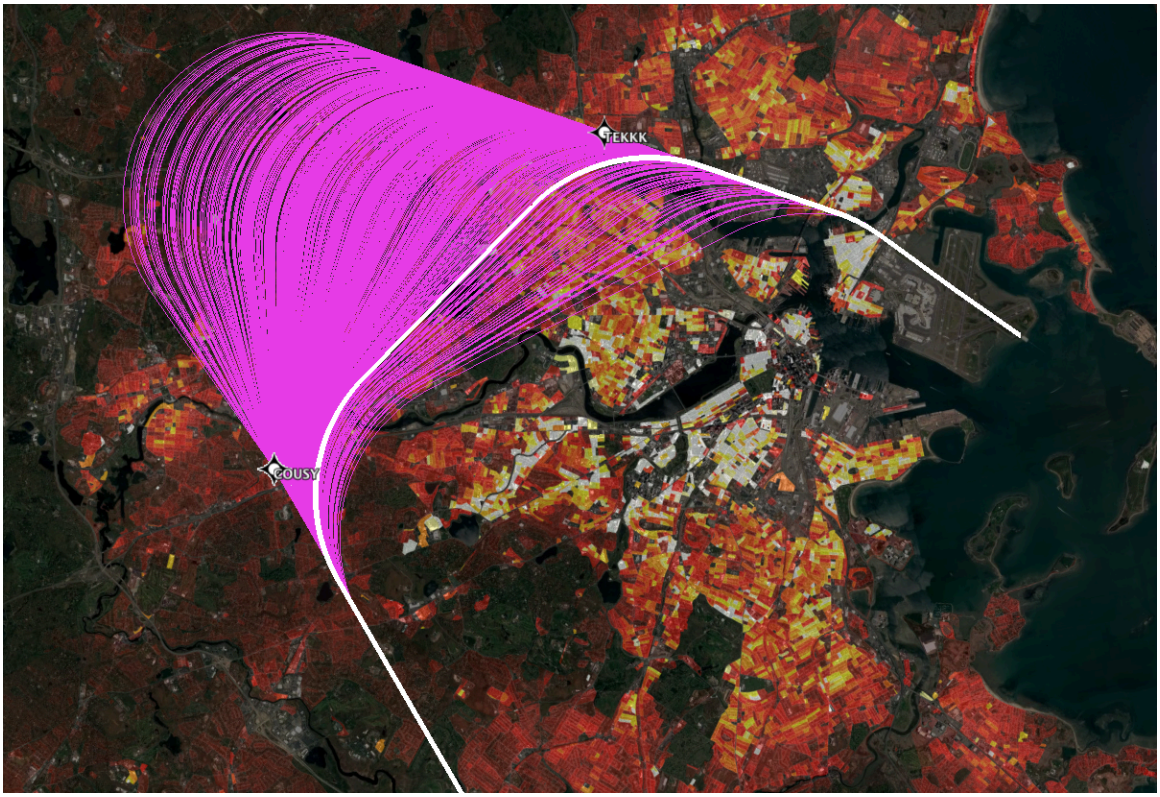

Figure 65. Ground tracks for the 4,000-foot turn Open SID procedure are shown in magenta.[1] The white track shows the nominal RNAV procedures as it exists today, and the heat map below the tracks shows population density.

Next, a similar process was undertaken for the 2,000-foot case, but aircraft were issued a heading directly to the CBEAR waypoint instead of first turning towards COUSY. This is for two reasons: first, it decreases path length, and thus saves fuel. Second, it allows aircraft to initiate a sharper turn, creating more dispersion near the TEKKK waypoint relative to the 4,000-foot case. Because the current RNAV procedure has caused a spike in noise complaints near TEKKK, this could be a benefit. The ground tracks generated based on this procedure are shown in **Figure 66**.

[1] Both the flight tracks shown and this figure were generated by Luke Jensen.

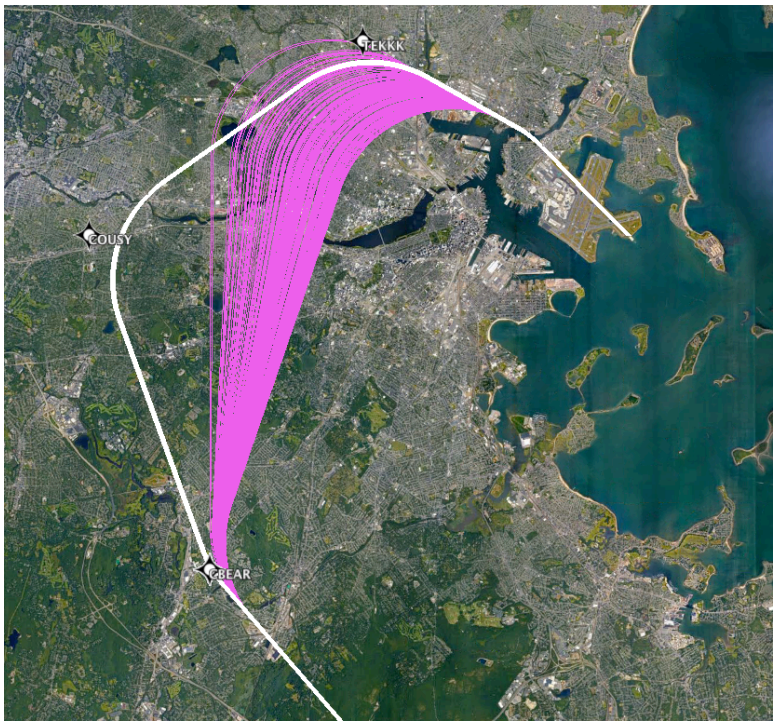

Figure 66. Ground tracks for the 2,000-foot turn Open SID procedure are shown in magenta. The white track shows the nominal RNAV procedures as it exists today.[1]

It is clear from this figure that this procedure creates less dispersion than the 4,000-foot turn procedure, which makes sense when inspecting the altitude profiles shown in **Figure 64**. Because aircraft altitudes diverge more as along-track distance increases, dispersion will be greater for a higher turn altitude. It is also apparent from these ground tracks that the 2,000-foot turn creates a much sharper turn, which should shift noise farther to the south.

6.2.2 OPEN SID NOISE MODELING

Lateral dispersion distributions were detected directly from the flight tracks to ensure that the distribution matched that created by the natural altitude variability. Using these lateral dispersion profiles, the dispersion model was first used to calculate equivalent SEL contours for this procedure. These contours and the associated flight density plot are shown for a Boeing 737-800 for both Open SID cases in **Figure 67**.

[1] The ground tracks and this figure were both generated by Luke Jensen.

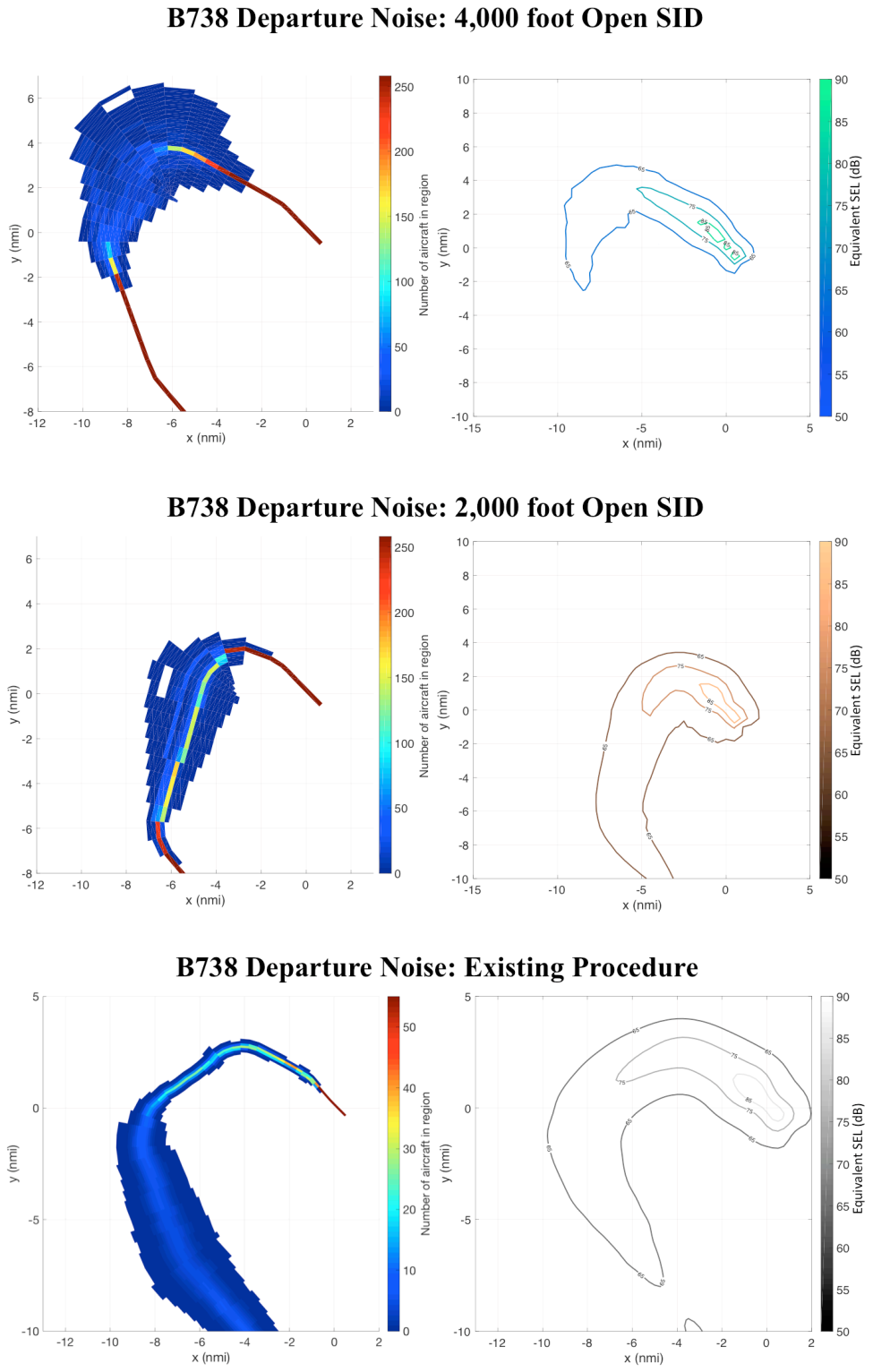

Figure 67. Flight density plot and equivalent SEL noise contours for a B738 for the 4,000 foot Open SID (top), 2,000 foot Open SID (middle), and the existing procedure (bottom).

For this more complex use of the dispersion model, however, instead of just comparing equivalent SEL contours, these equivalent SEL contours were calculated for the seven representative aircraft types described in Section 4.3.2. Then the equivalent SEL contours were summed proportionally to calculate DNL contours for the procedure. This analysis is shown in the following section.

6.2.3 OPEN SID DNL CALCULATION

To model noise from this procedure, first, a flight schedule representative of one day of operations was determined by analyzing the ASDE-X radar trajectories used to generate the ground tracks shown in **Figure 65**. This analysis found 258 flights with a wide variety of aircraft types. Given the representative aircraft types assignment described in Section 4.3.2, each flight was assigned to one of the 7 representative types. The number of flights in each category was calculated based on the ASDE-X data. The number of flights for each representative aircraft type for the representative day is shown in **Figure 68**.

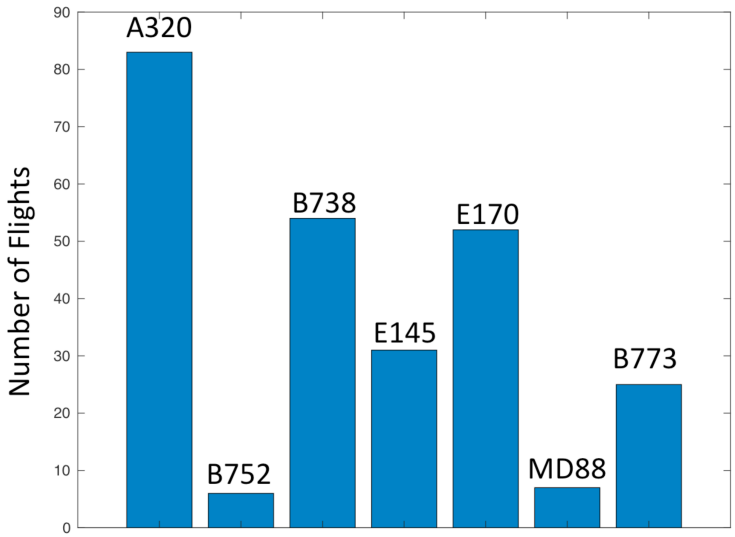

Figure 68. Number of flights for each representative aircraft type for the representative day on the 33L Open procedure.

Once ground tracks and flight schedule were defined for the procedure, it was necessary to define flight profiles for each representative aircraft type. Each ground track was matched to an aircraft type based on the aircraft type of the altitude profile that was used to define that track. Then, each flight of the same aircraft type was assumed to use

the same standard flight profile; thus, only one flight profile was needed for each of the seven aircraft types. These profiles were calculated to match observed radar data for all flights of the same type at KBOS using the profile matching procedure described in Section 4.3.1.

With ground tracks, flight profiles, and flight scheduled all determined, and with the equivalent SEL contours calculated for each aircraft type, DNL contours were calculated. The DNL contours of the 4,000 foot Open SID are overlaid on those of the existing procedure RNAV procedure in **Figure 69**.

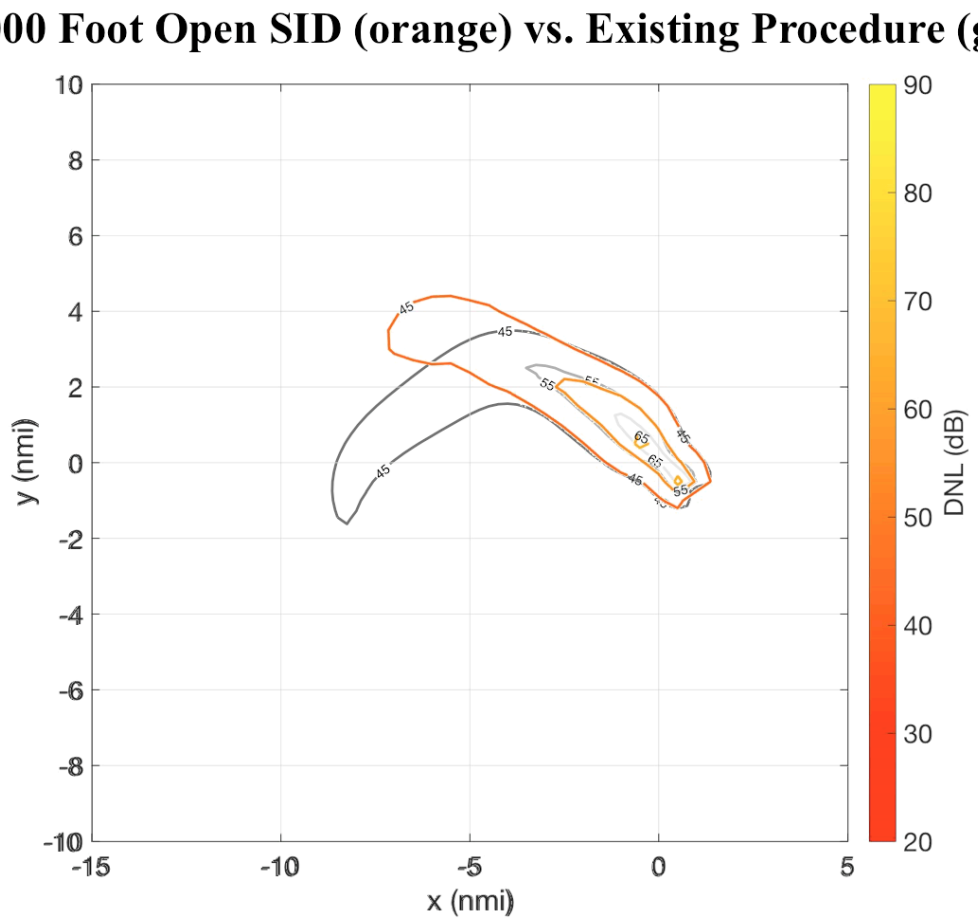

Figure 69. DNL contours of the 33L 4,000 foot turn Open SID procedure (orange) overlaid on those of existing 33L procedure (gray).

This shows the complex tradeoffs in noise that must be considered when designing a new procedure. The increased lateral dispersion present in this procedure does shorten and widen the contours, as expected. Once again, this appears to be a significant benefit at higher noise levels like 55 dB DNL. At lower noise levels, like 45

dB, however, the comparison is made more difficult because in this Open SID variation, many aircraft turn later than they currently do. This causes the 45 dB contour to extend about 2 nautical miles farther to the northwest, and to remain quite wide, while noise contours of the existing procedure extend down to the southwest are nearly 5 nautical miles.

Next, the DNL contours of the 2,000-foot Open SID case were calculated then overlaid on those of the existing procedure, and results of this calculation are shown in **Figure 70**.

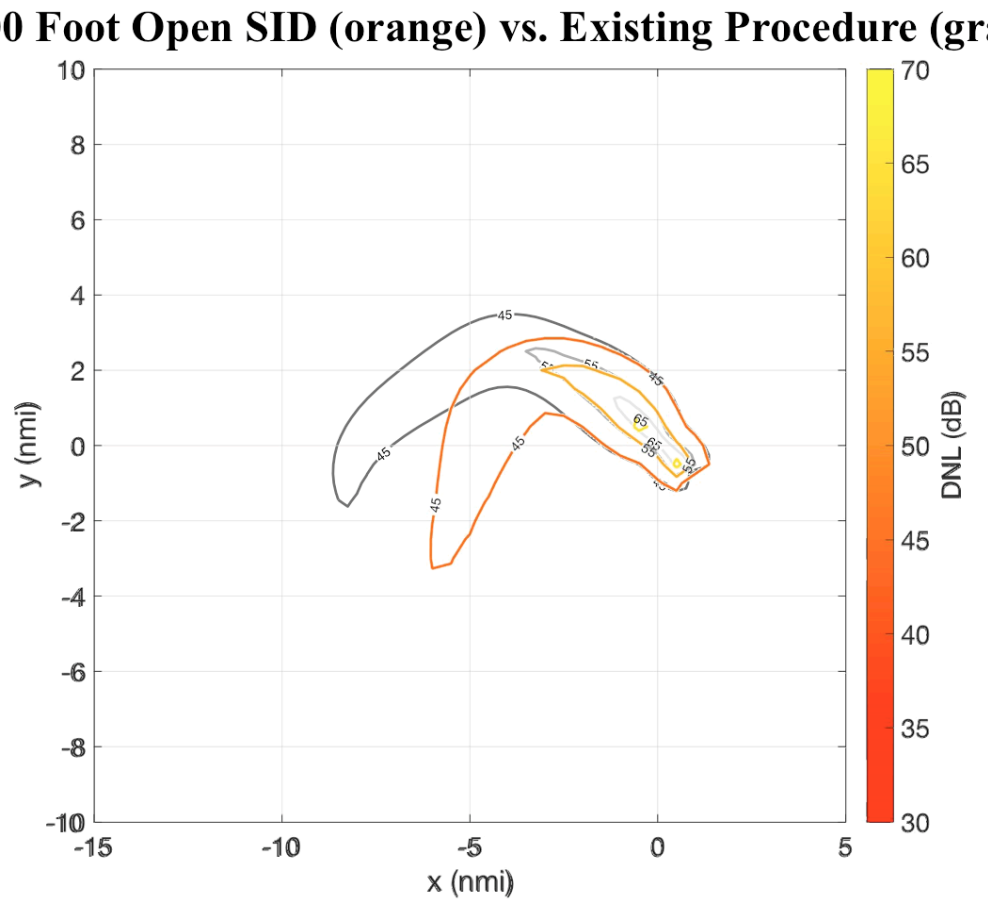

Figure 70. DNL contours of the 33L 2,000 foot turn Open SID procedure (orange) overlaid on those of existing 33L procedure (gray).

As expected, noise is shifted to the south due to the increased turn, and contours are slightly shorter and wider—particularly at 55 DNL, where there again appears to be more benefit than harm. Because this procedure exhibits less lateral dispersion than the 4,000-foot turn case, however, the shortening and widening of contours is notably less

extreme, with the 45 dB contour exhibiting a length that is not much less than that of the existing procedure.

It is difficult to say exactly which of these procedures gives the most desirable result in terms of noise impact. For each procedure—the existing, the 4,000-foot turn, and the 2,000-foot turn—noise burden is shifted to different locations. Selecting one of these procedures to implement raises interesting but difficult questions regarding environmental justice, equity, and politics—who should bear the burden of noise? In practice, this must be determined on a case-by-case analysis, accounting for factors such as population density, and the model developed for this thesis provides one crucial piece of the tools necessary for this type of analysis.

6.2.4 OPEN SID N_{ABOVE} CALCULATION

The model is also capable of calculating the noise impacts of procedures in terms of N_{above}. To demonstrate this capability, the impact of the 4,000-foot turn Open SID procedure was also modeled in terms of N60 (for a given observer location, N60 is the number of events with an LAMAX value greater than 60 dB). These results are shown in **Figure 71**.

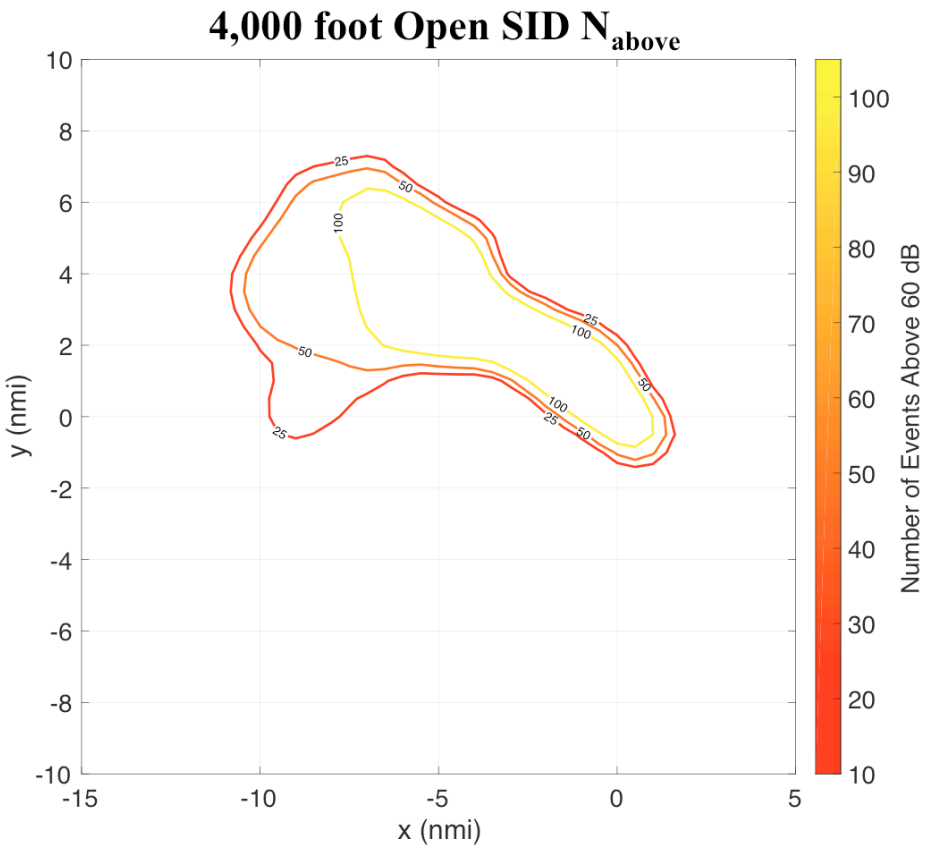

Figure 71. N60 contours due to the 4,000 foot Open SID procedure.

It is apparent that these contours show a much more significant increase in width around the turn—where flights are most dispersed—showing that N_{above} metrics could be a useful tool for evaluating the noise impacts of dispersion and concentration. This difference in contour shape is likely due in part to the difference between the linear scaling of N_{above} and the logarithmic scaling of DNL. Another difference, however, could simply be the chosen thresholds—looking at low noise thresholds will create larger contours that show lateral dispersion more clearly, but if a threshold is too low, it will not be representative of a significant noise impact on the surrounding community. Although N_{above} analysis could be a useful tool for procedure design, because federal aircraft noise regulations are currently based on DNL values, at this time N_{above} analysis is a useful supplement to DNL rather than a replacement.

6.2 BOSTON LOGAN ALL RUNWAY NOISE COMPUTATION

Next, to demonstrate the ability of the model to rapidly calculate noise impacts for all flight operations across all runways at an airport, an example computation was performed KBOS in 2015. DNL contours of a representative, annually averaged day were calculated using a method intended to be consistent with the environmental analyses performed at airports across the nation to ensure compliance with FAA noise regulations. This approach is different from examining a single day of use, as was done for the Open SID case. Instead, operations across a year are averaged to create a "representative day", which may not be consistent with of any real day, since in reality a runway often sees heavy use on some days and no use on others. For comparison, this analysis was performed both with the dispersion model and assuming that all flights flew exactly along the representative ground track—that is, assuming no dispersion. The representative day DNL contours with and without dispersion were compared to determine the impacts of dispersion on noise impacts of all operation from all runways for the airport.

6.2.1 Representative Trajectory and Schedule Definition

This analysis was based on the 20-day 2015/2016 ASDE-X dataset described in Chapter 3. Representative ground tracks were found from this dataset using the methods described in Section 3.1.2. These routes are shown in **Figure 72**.

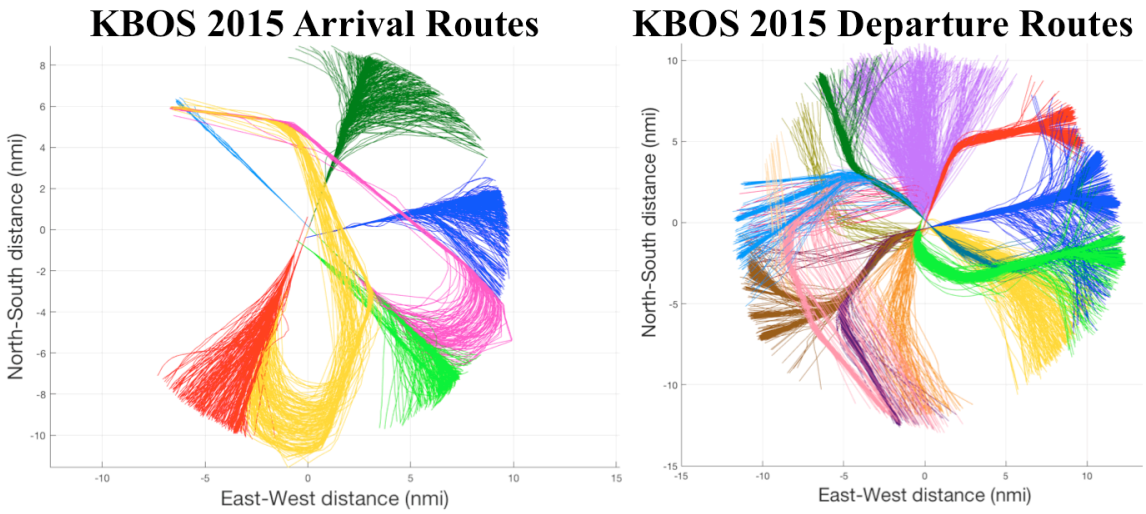

Figure 72. Arrival and departure routes used for KBOS noise analysis.

Next, each flow was analyzed to create lateral dispersion distribution profiles to be used as inputs to the variability model. For this application, distributions were detected

directly from radar data rather than assuming a particular distribution, because this method is faster and has ability to model non-normal distributions. The results of this distribution analysis for example arrival and departure flows are shown in **Figure 73**.

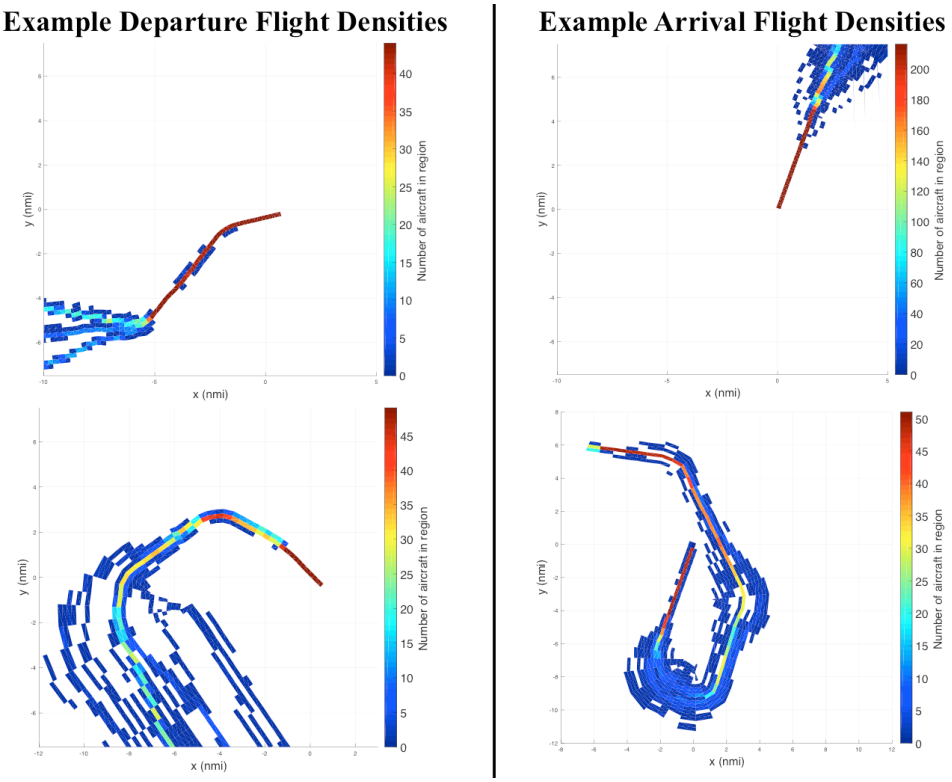

Figure 73. Dispersion model visualization of flight density for two arrival flows at KBOS (left) and two departure flows (right).

These flows show a much higher concentration close to the centerline, as expected for RNAV procedures. There was, however, some presence of lateral dispersion, particularly around the downwind turning leg for the arrival on the bottom right of the figure, and as the aircraft got farther from the airport for all other cases. Also, the departure example shown in the top left corner of the figure splits into a tri-modal distribution after several miles. These examples further demonstrate that fitting a normal distribution to lateral dispersion is not always a valid assumption as aircraft are farther from the airport; thus, in this case, the discretized distribution was detected directly from radar data, rather than through an assumed distribution function.

Next, a representative fleet and schedule were defined for the analysis. The representative fleet was defined according to the method discussed in Section 4.3.2, using

7 representative aircraft types. Flight profiles for the representative fleet were defined as described in Section 4.3.1, and the example flight profiles shown in that section—along with comparable ones for each of the representative aircraft types—were used for this analysis.

Finally, the flight schedule used for this analysis was generated from a combination of NOMS and ASPM data; the details of this schedule are shown in Appendix B.[1] Note that this schedule uses an average annual day, with operations averaged out over the year, rather than a single day of use like the Open SID case discussed above.

6.2.2 NOISE COMPUTATION RESULTS

With these inputs defined, gridded SEL noise was calculated in AEDT for each representative trajectory. Then, two methods were compared: first, DNL contours were calculated according to the schedule and assuming no lateral dispersion. Next, the variability model was used to account for the trajectory variability on each route, and DNL contours were calculated from these results. The resulting two sets of contours are overlaid in **Figure 74**.

[1] The flight schedule analysis was conducted by Morrisa Brenner for her thesis. [30]

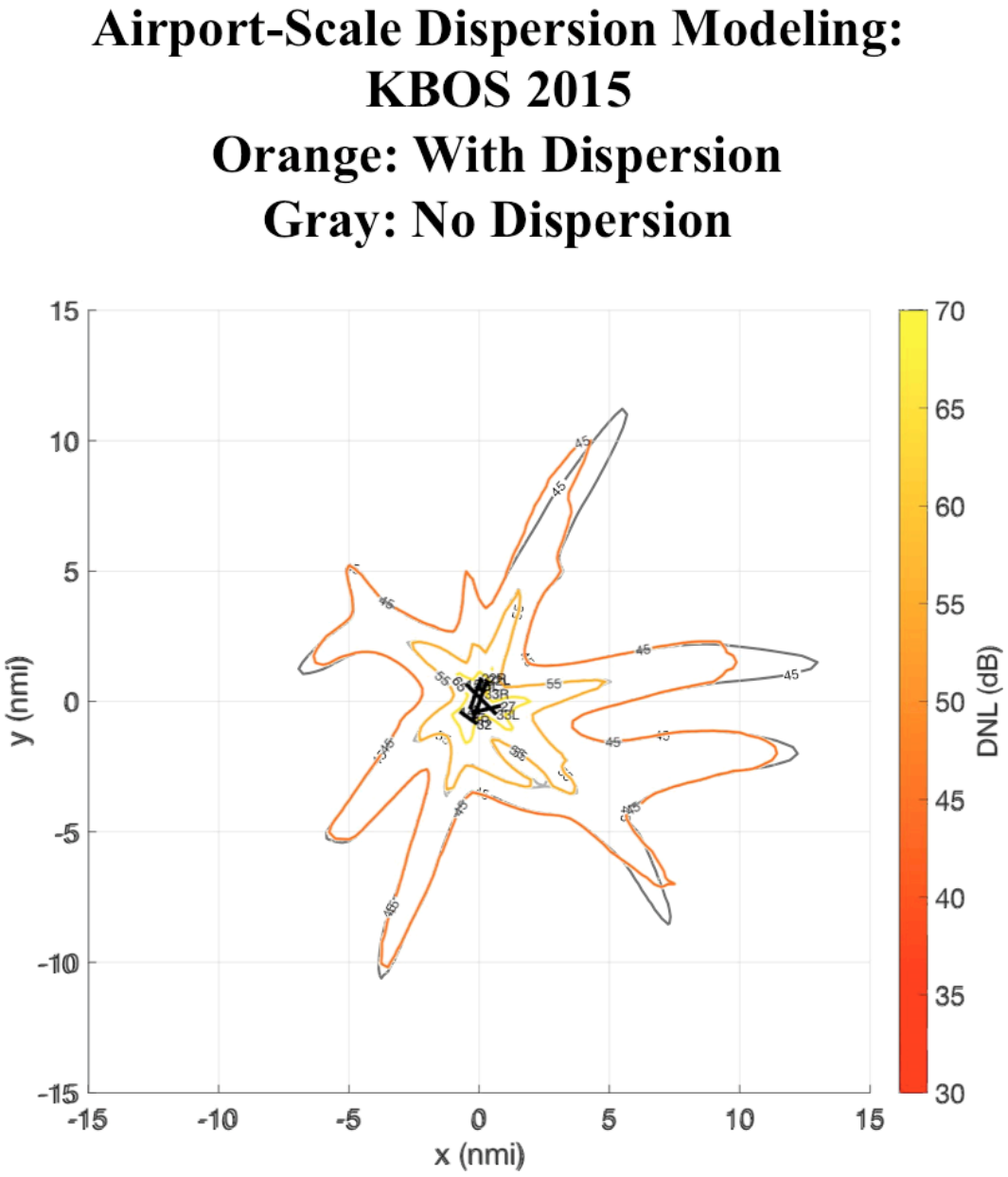

Figure 74. DNL contours at KBOS using the rapid noise modeling architecture. Gray shows the contours using only representative trajectories with no lateral dispersion, orange shows the contours using the variability model.

This figure shows that, because RNAV routes ensure very little lateral dispersion, the method with no variability modeling is quite accurate, particularly at higher noise levels such as the DNL 65 level. As the aircraft get farther from the airport and lateral dispersion increases, however, a clear shortening and slight widening of many parts of the contour occur at the 45 DNL level. In some cases, there is also some lateral shifting

farther from the airport, as the trajectory that was highly representative of the flow closer to the airport is less centered in the flow as the distribution of flights changes father from the airport. This shows that accounting for trajectory variability in airport-scale noise analysis could prove important to reduce error. To calculate the 65 DNL contour at an airport that primarily uses RNAV routes, variability modeling is largely unnecessary. To calculate the 45 DNL contour accurately, however, it is clearly necessary. Further, analysis at an airport with flows that include more lateral dispersion than present-day KBOS does could show even larger noise differences. For pre-RNAV analysis, for example, results calculated without accounting for dispersion would not be accurate.

This analysis also shows that some lateral dispersion as aircraft get farther from the airport could be beneficial for noise. The 45 dB DNL contour below several procedures shrinks significantly when dispersion is modeled. This shows that, as aircraft get farther from the airport and turn in different directions, causing lateral dispersion, the widening of the contours is, in most cases, less extreme than the shortening of the contours. It is also important to note, however, that this calculation relies on an average annual day. This method of averaging operations over a year is the industry standard practice for calculating DNL impacts, but this averaging process makes contours less sensitive to small changes, and reduces the amount of noise complaints that are captured by noise contours. [30] This could be part of the reason that the increased width of the noise contours is not clearly visible.

Dispersion effects are only obviously present for some procedures, however. In particular, the routes to the east, which extend over the ocean, show the largest effect. This is likely because those routes have more lateral dispersion due to more aircraft turning in diverging directions as they head to their destination. This demonstrates that using dispersion effectively as a tool, perhaps mimicking the dispersion seen as aircraft turn onto or off of the ocean routes above, could provide noise benefits—particularly at the 45 dB level, which has been shown to be an effective noise level for capturing a high percentage of noise complaints. [30]

CHAPTER 7 CONCLUSIONS

The advent of PBN has made the noise impacts of flight track variability highly relevant. Most PBN tracks create significant flight track concentration, and therefore, modeling and understanding the noise impacts due to lateral flight track dispersion or concentration is essential. In addition, the tools available as part of PBN unlock a new set of possible procedure designs that can be used to mitigate noise impacts. Some of these procedures—such as Open SID procedures—could intentionally introduce lateral dispersion, creating a further need to be able to model the noise impacts of lateral dispersion. While some existing tools could be used for this purpose, current options are either very computationally expensive or are inaccurate. To address this need, this thesis developed a fast, accurate tool capable of modeling the noise impacts of lateral dispersion.

First, speed, altitude, and lateral trajectory variability were examined and quantified to determine what kinds of distributions could be used to model the various different types of trajectory variability. It was discovered that speed and altitude variability, a normal distribution modeled the distributions well. For lateral dispersion, a normal distribution could be used accurately near the airport, but, due to difficulties with trajectory classification, could not always be used farther from the airport. Given these understandings of different forms of trajectory variability, it was shown that the noise impacts of speed and altitude could be captured fairly accurately by assuming that all flights flying the same procedure flew at the mean altitude and speed. It was also shown that lateral dispersion could not be modeled in this manor, and that dispersion effects had to be modeled explicitly.

Given this analysis, a model was developed to calculate the noise impacts of flight track lateral dispersion along an arrival or departure flow based on the noise of a single representative trajectory. This model was then demonstrated and validated on several examples. First, a simple, straight-out case with fanning lateral dispersion was modeled, and the model was validated against a direct calculation of many flights in AEDT. Next, the model was used to show the impacts of RNAV flight track concentration on KBOS

Runway 33L Departures for a single aircraft type. As expected, the model showed that noise contours grew narrower and longer due to the concentration effects of the RNAV route. At higher noise levels (75 dB equivalent SEL), the contours shrank significantly, shortening by about 1.75 nautical miles and widening by only a few tenths of a nautical mile on each side. At lower noise levels (65 dB equivalent SEL), however, the contours broadened more significantly— up to nearly a full nautical mile on each side.

The model was also used to examine more complex, realistic use cases. First, two variants of Open SID procedures were analyzed for KBOS Runway 33L departures. This analysis showed the complex tradeoffs present in procedure design—particularly when examining lateral dispersion, which inherently entails shifting noise burdens from one location to another. Once again, there were some noise savings under the track and an increase to the side of the central flight track, but the procedures examined also shifted position of the noise contours significantly, changing the location of the peak noise by several miles. Finally, the model was used as part of a rapid noise modeling method to quickly calculate the noise due to flights across all of Boston Logan International Airport. This analysis showed that lateral dispersion could perhaps be a useful tool to reduce DNL impacts, but the results were generated using average annual day methods, which could reduce their sensitivity to the widening of noise contours at slightly lower noise levels.

The examples analyzed showed that, in general, lateral dispersion can be useful to significantly reduce high noise levels directly below the flight track and approximately 5-10 nautical miles away from the airport. Noise contours below a flight track can be reduced in length by several miles—a significant savings—while only increasing the width of the contour at that level slightly. This comes at a cost, however, of having significantly wider contours at slightly lower noise levels. For certain population distributions or flight procedure geometries, this effect could be desirable, while for others it might be harmful for noise exposure. Each procedure must be analyzed on a case-by-case basis to determine how lateral dispersion would impact noise exposure.

This modeling tool could be useful in a broad range of procedure design and analysis applications. Because the model saves 1-2 orders of magnitude of computational expense relative to direct calculation, it is easier to examine a wide range of possible

procedures and select one that best achieves design criteria, or to quickly model the noise impacts of all flight procedures at an airport. As air traffic control and flight procedure design are brought into the modern era through NextGen and other modernization efforts, a new set of noise modeling tools becomes necessary to both understand changes to noise impacts and to utilize technology to design better flight procedures. Flight track variability has seen substantial changes as part of these new procedures, and this thesis helps quantify how this variability impacts aircraft noise. This work should allow for a better understanding of these impacts in future noise analysis.

APPENDICES

APPENDIX A

REPRESENTATIVE TRAJECTORY IDENTIFICATION METHODS

This appendix discusses the methodology for detecting representative trajectories from radar flight trajectory data. Two methods exist, the RNAV filtering method and the Clustering method.

RNAV Filtering Method

One simple method to find representative trajectories from radar data is to take advantage of the clear route definitions that are easily accessible for all flights that follow RNAV routes. To take advantage of this, another method was created to filter radar data and detect which flights were flying on published RNAV routes. This simple method requires the RNAV waypoints for all routes as an input. Any radar trajectory that passes within 0.5 nautical miles of every waypoint on a given route is determined to be flying on that route. Then, as in the clustering method, the trajectory with the minimum RMS distance from the mean is selected as the representative trajectory of the specified route. An example of this analysis at KDCA is shown in **Figure 75**. In this example, 80% of all flights were determined to be flying RNAV routes.

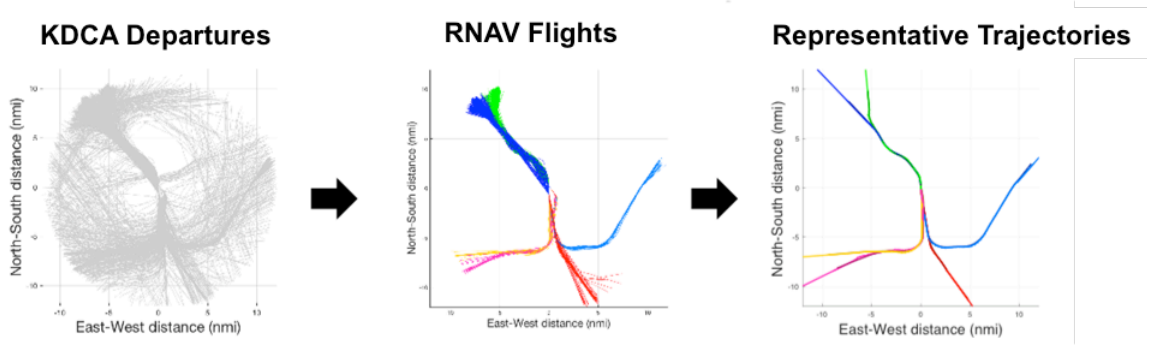

Figure 75. An example of route detection analysis performed using the RNAV filter method on 20 days of departures at Ronald Reagan National Airport (KDCA).

Clustering Method

The second technique for representative trajectory identification uses a method based on the DBSCAN clustering algorithm.[1] One advantage of this technique is that it does not require any *a priori* information about the routes. Separate clusters were generated for each operation type (arrival or departure) and aircraft type. This algorithm compares trajectories based on distance between the trajectories in hyper-dimensional space as shown in **Figure 76**.

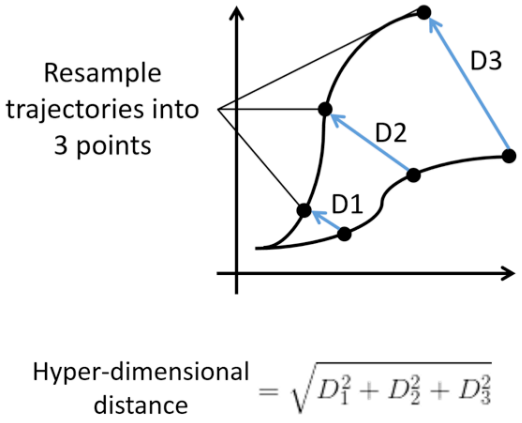

Figure 76. Graphical depiction of resampling of trajectories and hyper-dimensional distances

In order to compare trajectories, each trajectory must be resampled to have the same number of points, *n*, and for a 3-dimensional trajectory, this results in a 3*n*-dimensional hyperspace. For any trajectory, then, the hyper-dimensional distance between it and every other trajectory can be calculated. If a trajectory is within a certain distance, ε, of a specified number, *MinPts*, of other trajectories, a cluster is formed as shown in Figure 77.

[1] The clustering method used in this thesis was adapted from a method originally developed by Mayara Murca. [32]

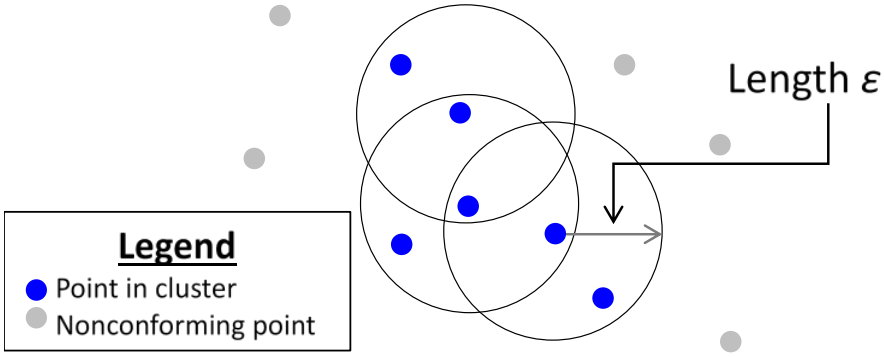

Figure 77. 2-dimensional cluster definition example

By tuning MinPts and ε, clusters, or routes, of spatially similar flights can be determined. The parameters were tuned such that all major routes seemed to be captured as a cluster and relatively few flights (<10%) were categorized as nonconforming. Then, for each cluster, an n-point centroid was calculated by taking the spatial average of each of the n points of all the trajectories in the cluster. Because this centroid is not a real flight, however, the centroid itself was not used to represent the cluster. Instead, the real trajectory that was closest to the centroid based on root-mean-square (RMS) distance was selected as the representative trajectory of that cluster. Given this central trajectory closest to the mean of the route, variability could be defined as deviation from this representative trajectory.

APPENDIX B

KBOS RAPID NOISE SCHEDULE DEFINITION

This schedule and these tables were generated by Morrisa Brenner. The tables show the number of operations for each aircraft type on each runway for both arrivals and departures and separated by day and night operations.

Table 3. Annual average day departures – day operations per runway by representative aircraft type

Representative Aircraft Type	15R	04R	04L	09	14	15L	33L	22L	22R	27	32	33R
B773	2.37	1.89		1.82			3.05	1.53	3.38	0.47		
A320	3.35	5.52		28.15			16.68	3.19	31.64	11.38		
B738	2.75	6.35		18.02			11.65	3.43	21.42	6.65		
B752	0.54	0.84		4.46			2.63	0.25	5.17	1.48		
MD88	0.35	0.31		6.59			2.66	0.07	6.65	3.00		
E170	1.68	1.09		37.02			14.29	0.10	37.26	14.65		
E145	0.64	1.54	5.95	16.72			9.80	0.06	22.72	5.47	0.01	0.01

Table 4. Annual average day departures – night operations per runway by representative aircraft type

Representative Aircraft Type	15R	04R	04L	09	14	15L	33L	22L	22R	27	32	33R
B773	2.35	0.44		0.73			2.20	0.32	1.91	0.08		
A320	2.90	0.55		2.56			2.07	0.24	3.61	2.68		
B738	3.35	0.83		2.16			2.00	0.41	3.25	2.58		
B752	0.45	0.13		0.51			0.44	0.06	0.86	0.41		
MD88	0.53	0.09		0.85			0.70	0.02	1.31	0.59		
E170	1.37	0.23		3.11			0.96	0.02	4.01	3.25		
E145	0.69	0.10	0.21	0.49			0.78	0.02	1.03	0.33		

Table 5. Annual average day arrivals – day operations per runway by representative aircraft type

Representative Aircraft Type	15R	04R	04L	09	14	15L	33L	22L	22R	27	32	33R
B773	0.39	8.10	0.06				3.57	6.07		3.09		
A320	1.22	28.48	3.29				12.06	21.45	0.02	22.20		
B738	0.88	21.62	1.67				7.13	11.32	0.01	20.03		
B752	0.24	5.37	0.22				1.62	3.18		4.02		
MD88	0.28	6.39	0.73				3.01	3.60		6.08		
E170	1.52	32.61	6.46				16.24	24.24	0.04	27.05	2.67	0.01
E145	0.75	10.94	12.51				7.94	16.85	0.53	10.33	4.34	0.14

Table 6. Annual average day arrivals – night operations per runway by representative aircraft type

Representative Aircraft Type	15R	04R	04L	09	14	15L	33L	22L	22R	27	32	33R
B773	0.02	0.48					0.68	0.79		0.08		
A320	0.58	5.26	0.06				7.81	9.93		3.35		
B738	0.48	4.21	0.03				7.85	7.85		2.77		
B752	0.08	0.67	0.01				1.14	1.29		0.43		
MD88	0.07	0.90	0.01				1.57	1.31		0.48		
E170	0.33	2.48	0.06				2.36	4.48		1.89		
E145	0.08	0.80	0.08				1.11	1.42		0.45	0.01	0.01

WORKS CITED

[1] Federal Aviation Administration, "Next Generation Air Transportation System (NextGen)," 2017.

[2] Lori Aratani, "Advances in airport technology mean sleepless nights for some - The Washington Post," *The Washington Post*, 04-Mar-2016.

[3] Federal Aviation Administration, *FAR Part 150 - Airport Noise Compatibility Planning*. eCFR — Code of Federal Regulations.

[4] Federal Aviation Administration, "Aircraft Noise Issues," 2016.

[5] M. Brenner, "New Approaches for Visualizing Spatially-Distributed Aviation Environmental Impacts," in *Joint University Program*.

[6] Massachusetts Port Authority, "Boston-Logan International Airport 2015 Environmental Data Report," Boston, MA, 2015.

[7] Federal Aviation Administration, *Noise, Fuel Burn, and Emissions Modeling Using the Aviation Environmental Design Tool Version 2b*. 2015.

[8] M. J. T. Smith, *Aircraft Noise*. Cambridge, UK: Cambridge University Press, 1989.

[9] L. L. Beranek, T. J. Mellow, L. L. Beranek, and T. J. Mellow, "Chapter 1 – Introduction and terminology," in *Acoustics: Sound Fields and Transducers*, 2012, pp. 1–19.

[10] R. R. Riesz, "Differential Intensity Sensitivity of the Ear for Pure Tones," *Phys. Rev.*, vol. 31, 1928.

[11] United States Environmental Protection Agency, "Noise and its Measurement," 1981.

[12] G. G. Fleming, "Aviation Environmental Design Tool (AEDT) Technical Manual, Version 2c," 2016.

[13] T. J. Schultz, "Synthesis of social surveys on noise annoyance," *J. Acoust. Soc.*

Am., vol. 64, no. 377, 1978.

[14] M. Basner *et al.*, “Auditory and non-auditory eff ects of noise on health,” *Lancet*, vol. 383, no. 9925, pp. 1325–1332, 2014.

[15] A. L. Hansell *et al.*, “Aircraft noise and cardiovascular disease near Heathrow airport in London: small area study,” *Bmj*, vol. 347, no. oct08 3, pp. f5432–f5432, 2013.

[16] D. Federal Aviation Administration, “Establishment of Area Navigation Routes (RNAV),” *Fed. Regist.*, vol. 68, no. 90, 2003.

[17] ICAO, *Performance-Based Navigation Manual - Advance fourth edition (unedited)*. 2012.

[18] B. DeCleene, “Criteria for RNAV SIDs that contain RADAR Vector Segments,” 2015.

[19] M. Bradley, “PBN Departure Procedures: Open SID Implementation & Utilization Guidelines,” 2015.

[20] S. Harrison, “FAA dispersing Charlotte Douglas departures to scatter jet noise,” *The Charlotte Observer*, 14-Jul-2016.

[21] FAA, “Airport Surface Detection Equipment, Model X (ASDE-X),” *www.faa.gov*, 2017. [Online]. Available: https://www.faa.gov/air_traffic/technology/asde-x/. [Accessed: 10-May-2017].

[22] Amber Goodspeed, “Hanscomfield 2015 Annual Noise Report,” Bedford, MA, 2015.

[23] M. Ester, H. Kriegel, J. Sander, and X. Xu, “A density-based algorithm for discovering clusters in large spatial databases with noise.,” *AIAA KDD-96 Proc.*, 1996.

[24] D. Forsyth, J. GuIding, and J. DiPardo, “Review of Integrated Noise Model (INM) Equations and Processes,” 2003.

[25] Society of Automotive Engineers, “SAE AIR 1845: Procedure for the Calculation of Airplane Noise in the Vicinity of Airports,” 1986.

[26] J. Thomas, L. L. Jensen, C. Brooks, and M. Brenner, “Investigation of Aircraft Approach and Departure Velocity Profiles on Community Noise,” *AIAA Aviat. Forum*, pp. 1–12, 2017.

[27] L. L. Jensen, J. Thomas, C. Brooks, M. Brenner, and R. J. Hansman, “Development of Rapid Fleet-Wide Environmental Assessment Capability,” *AIAA Aviat. Forum*, pp. 1–14, 2017.

[28] P. Boone, “Noise Abatement Departure Procedures,” 2006.

[29] W. E. Zorumski, “Airframe Noise Module (FNKAFM),” in *ANOPP Theoretical Manual*, NASA Langley Research Center, 2009.

[30] M. Brenner, “Comparison of Methods for Evaluating Impacts of Aviation Noise on Communities,” Massachusetts Institute of Technology, 2017.

[31] J. L. Thomas and R. J. Hansman, “Modeling Performance and Noise of Advanced Operational Procedures For Current and Future Aircraft,” Massachusetts Institute of Technology, 2017.

[32] E. Clemons *et al.*, “Multi-Scale Data Mining for Air Transportation System Diagnostics.”